Quantitative ^{1}H N.M.R. Chemical Shift Imaging of Neuronal Content

by

Alexander Savio Ramos Guimaraes

Submitted to the Department of Nuclear Engineering in
Partial Fulfillment of the Requirements for the Degree of

DOCTOR OF PHILOSOPHY
in Radiological Sciences

at the
Massachusetts Institute of Technology

August 12, 1994

Signature of Author_____
Massachusetts Institute of Technology
Department of Nuclear Engineering, Radiological Sciences Program
August 12, 1994

Certified by_____
R. Gilberto González, M.D., Ph.D.
Harvard Medical School
Thesis Supervisor

Certified by_____
Sow-Hsin Chen, Ph.D.
Massachusetts Institute of Technology
Thesis Committee Chairman

Certified by_____
Bruce R. Rosen, M.D., Ph.D.
Harvard Medical School & Massachusetts Institute of Technology
Thesis Committee Member

Certified by_____
Robert M. Weisskoff, Ph.D.
Harvard Medical School & Massachusetts Institute of Technology
Thesis Committee Member

Accepted by_____
Allan F. Henry, Ph.D.
Massachusetts Institute of Technology
Chairman, Nuclear Engineering Departmental Graduate Committee

Abstract

Quantitative ^{1}H N.M.R. Chemical Shift Imaging of Neuronal Content

by

Alexander Savio Ramos Guimaraes

Submitted to the MIT Department of Nuclear Engineering on August 12, 1994 in partial fulfillment of the requirements for the degree of Doctor of Philosophy in Radiological Sciences

This thesis describes the design and implementation of experiments to verify the utility of N-acetyl aspartate (NAA), a neuron specific brain metabolite, as a Nuclear Magnetic Resonance (NMR) neuronal marker and the development of novel chemical shift imaging (CSI) techniques for determining neuronal content volumetrically in humans. The data presented in this thesis demonstrate the ability of CSI to provide quantitative, spatially resolved images of neuronal loss in a striatal lesion rat model. By providing a comparison of the percentage of neuronal survival measured by *in vivo* NMR with established enzymatic measures of neuronal loss, these data indicate that NAA provides an excellent marker for neuronal content. They also support the claim that *in vivo* CSI provides an index of neuronal loss that may be more sensitive than classical biochemical assays. These facts have served as the foundation for the successful development of novel, volumetric CSI techniques (EP CSI). EP CSI exploits the rapid traversal of k-space inherent in EPI to allow a slight decrease in spectral resolution in order to improve spatial (and possibly temporal) resolution. Data presented in this thesis demonstrate that EP CSI can produce chemical shift images of NAA in phantoms and humans with spatial resolution that is superior to both existing CSI techniques and signal-to-noise ratio that is concordant with theoretical results from analytical simulations. Future optimizations that decrease imaging times to 10 minutes or less will make it feasible to acquire high resolution, volumetric maps of neuronal content routinely, as part of a comprehensive functional imaging examination. The implementation of EP CSI techniques that utilize NAA as a neuronal marker is therefore expected to provide the means for a volumetric, periodic assessment of the progression of neurodegeneration in patients suffering from neurodegenerative diseases.

Thesis Supervisor: R. Gilberto González M.D., Ph.D.; Division of Neuroradiology, Department of Radiology, Massachusetts General Hospital, Harvard Medical School.

Acknowledgments

I would like first of all to express my sincere gratitude to Dr. Gil González for being a patient, wise and thoughtful mentor these last five years. It is rare when the advisor-student relationship becomes one of friend and colleague, but during these years we have been fortunate to maintain this unique relationship. I look forward to many years of close collaboration and friendship.

I am also extremely grateful to Dr. Thomas Brady, who has provided me with the resources to perform this research in addition to the good fortune of working in the best of all possible environments to foster my education. I only wish I could beat him in racquetball. My heartiest congratulations go to Dr. Brady and Dr. Bruce Rosen for their ability to create a unique, cheerful laboratory that maintains rigorous standards of excellence within an atmosphere of cooperation.

During these years I have also had the good fortune of working with scientists whose intellectual caliber is unmatched. Topping that list is Dr. Robert Weisskoff. Robert has served as one of the principle forces behind the development of EP CSI, while contributing scientific insight at all levels of my research. I am deeply indebted to him. I know that we will continue to be friends, and that he will continue to be a damn fine pool player, though I doubt that he will ever beat me. Dr. Bruce Jenkins and Dr. John Baker have also served in similar capacities throughout my research. I am fortunate to call them friends, in addition to being sincerely grateful for their scientific contributions to this work and Bruce's assistance in my golf game. I am also grateful to Dr. Sow-Hsin Chen for 6 years of excellent education within the Nuclear Engineering Department as well as 4 years of patient mentorship.

My friends and family have served as my emotional foundation during this experience. Among the many friends that I have made these last few years, I would like to thank most of all Cindy Carr, Paul Schwarz, Urs Berger, Larry White, Craig Miller, Charlie Hultgren, Chantal Stern, Jill Kosewski and Michael Brandstein for their assistance in my work in addition to many memorable experiences. Their are three lifelong, special friends that I need to thank because their friendship and love has been integral to my existence. These are Maureen Walton, Matt Casselton, and Marshall Kleven.

Lastly, my deepest gratitude goes to two people without which this research and my eventual career in medicine would not have occurred. These are Jo Anne Fordham and Dr. Bruce Rosen. It is rare when one encounters the love of a sibling in a friend, but Jo Anne and Bruce are the siblings that I have been fortunate to find at the age of 28. Jo Anne has served as a psychologist, editor, English mentor, and dear, patient friend. I thank her from the bottom of my heart for all of her assistance in this endeavor. Likewise, Bruce has served as a personal and scientific mentor as well as a soul brother through these years. I thank him for the unlimited encouragement he has bestowed upon me, as well as for opening his home and family to me during a very critical time of my life. I look forward to lifelong friendship with Joanne and Bruce.

I thank God, most of all, who has provided me with unfailing support through this entire experience.

Dedication

I dedicate this thesis to my loving parents

Moises and Iolanda Margarida

for their inspiration and wisdom, and for instilling in me
the importance of familial love
and the quotidian faith in God that have guided
me through the travails of my life while
serving as the foundation of a cheerful existence.

Table of Contents

List of Figures

Chapter 1

Neurodegenerative diseases range from acute insults such as stroke, hypoglycemia, trauma, and epilepsy to chronic neurodegenerative states such as Huntington's disease, acquired immunodeficiency syndrome (AIDS) dementia complex, amyotrophic lateral sclerosis, and Alzheimer's disease (1). The morbity and mortality associated with these clinical manifestations have served as the rationale for the development of quantitative methods with which to study neurodegenerative progression. In addition, animal models of neurodegeneration have been used to investigate the role of excitatory amino acids as a source of neurotoxicity. These models, however, are hampered by the inability of extant biochemical and morphological techniques to characterize the temporal evolution of neuronal loss. Non-invasive, quantitative nuclear magnetic resonance (NMR)

methods have the potential to provide a temporal index of this loss that can be applied to both *in vivo* models and studies of patients suffering from neurodegenerative diseases.

NAA Background

To date, NMR spectroscopic methods have utilized the neuron-specific metabolite N-acetyl aspartate to study concordant decreases in neuronal loss that occur subsequent to neurodegenerative diseases. N-acetyl aspartate (NAA) has been demonstrated to be a neuron-specific brain metabolite by evidence gained through biochemical, immunocytochemical and spectroscopic studies. In 1956, Tallan *et al.*, utilizing a cat model, first described the discovery of this bound aspartate (NAA), located exclusively in nervous tissue (2). In 1972, Nadler confirmed that NAA is localized to neuronal tissue by demonstrating its absence in bovine tumor tissue (3). In further efforts to characterize the cellular localization of NAA, Simmons *et al.* used immunocytochemical staining with monoclonal antibodies against the metabolite to demonstrate that NAA-like immunoreactivity is specific to neurons and distributed throughout the brain (4). These findings indicate that NAA is indeed a valid neuronal marker.

Many theories have arisen regarding the role of NAA in the nervous system. Early evidence supports the hypothesis that NAA may serve as a storage form for aspartate, since it has no effect on amino acid receptors and is in general not incorporated into peptides (5). Other researchers have proposed that NAA is involved in lipid synthesis in the production of myelin (6), because their results had

demonstrated that the acetyl group of NAA is incorporated into brain lipids three times more effectively than acetate alone (6). Further studies by this group demonstrated that the immature rat incorporates the acetyl moeity from NAA maximally, in the time period immediately before or during myelination, approximately 8 days after birth, which supports the hypothesis that NAA may be involved in *de novo* fatty acid synthesis in the nervous system (6, 7). Subsequent investigators then suggested that NAA may act as a regulator of protein synthesis because enzymatic incorporation of ^{14}C-acetate into the t-RNA fraction that contains N-[1-^{14}C] acetylaspartic acid had been observed (8). Although each of these theories is supported by credible data, no definitive result has clarified the true function of NAA.

Study of the processes of synthesis and catabolosis of NAA has not produced any further understanding of NAA's role within the nervous system. The metabolite is synthesized solely within nervous tissue by one of two reactions: the acetylation of L-aspartate from acetyl-CoA, which is catalyzed by L-aspartate N-acetyltransferase (ANAT) within the mitochondria (9); or the catabolosis of N-acetyl-aspartyl-glutamate (NAAG), a putative neurotransmitter that may possess neuromodulator qualities, into NAA and glutamate (10). Evidence for the ANAT catalyzed reaction is suggested by the synthesis of NAA in the presence of metabolic conditions that are likely to cause an increase in the concentration of acetyl-CoA (11). However, evidence obtained by Truckenmiller *et al.* found ANAT present in rat brain and spinal cord homogenates that had a high affinity for L-aspartate (12). These data

demonstrated a tenfold variation in enzyme activity within CNS tissues. In the samples studied, brain stem and spinal cord tissues showed the highest activity, and retinal tissue the lowest, in a strikingly similar distribution to that of NAAG (13). This suggests that NAA may act as a precursor for NAAG. Recent *in vitro* evidence that demonstrates the cleavage of NAAG into NAA and glutamate by a Cl-dependent N-acetylated-α-linked acidic dipeptidase (NAA-LADase)(10) support this hypothesis and reinforce the dual synthesis of this neuronal specific metabolite.

NAA is metabolized within the CNS by enzymes called amino acylases or amidohydrolases. In the 1950's, Birnbaum *et al.* postulated the existence of two distinct enzymes, Acylase I and II, and suggested that Acylase II hydrolyzes acetyl-aspartate (14). Further work by Goldstein *et al.* (15) confirmed that brain amidohydrolase activity predominately was of the aspartate acylase type II. D'Adamo *et al.* elaborated on this work by demonstrating that the activity of N-acetyl-L-aspartate amidohydrolase (NAA AH) increases most rapidly between the ages of 15 and 18 days in rats, during which time these animals are experiencing elevated myelin production. Further, amidohydrolase activity was found to be three times higher in white than in grey matter, although the concentration of NAA is twice as high in grey as in white matter (16). Given the distribution and temporal activity of NAA AH, along with previous findings about the incorporation of the acetyl group of NAA into brain lipids, this evidence supports the hypothesis that NAA may be involved in the *de novo* production of

brain lipids incorporated into myelin. More recent evidence has demonstrated the preferential incorporation of the aspartyl moiety of NAA into NAAG (17), supported the hypothesis that NAA may serve as a precursor for NAAG and reinforced the dual function this metabolite may exert within the CNS.

The details concerning the synthesis, breakdown, function, and distribution of NAA provided by these investigations reinforce the uncertainty that exists concerning the role of NAA within the nervous system. Conflicting reports also exist concerning the distribution of this neuron-specific metabolite. Some suggest that NAA exists in a concentration gradient in the central nervous system, increasing rostrally (18). Other studies have not been able to verify this, and have demonstrated a more homogeneous distribution of NAA (13, 19). Despite this discrepancy, NAA has been found to be present in lesser amounts within peripheral, rather than central, nervous tissue (20), and it is not found outside the nervous system at all (2, 3, 21). The only certainty that exists concerning NAA is its neuronal specificity.

The advent of proton NMR spectrosocopy has lent a different importance to these biochemical findings. The structure of NAA is shown in Figure 1.1, alongside a high resolution proton spectrum of the metabolite. The methyl group in bold possesses three NMR visible protons that resonate in a large singlet at 2.0 ppm, as shown in Figure 1.1. This peak is quite prominent in both the *in vitro* and *in vivo* proton spectrum because of the high concentration of NAA, second

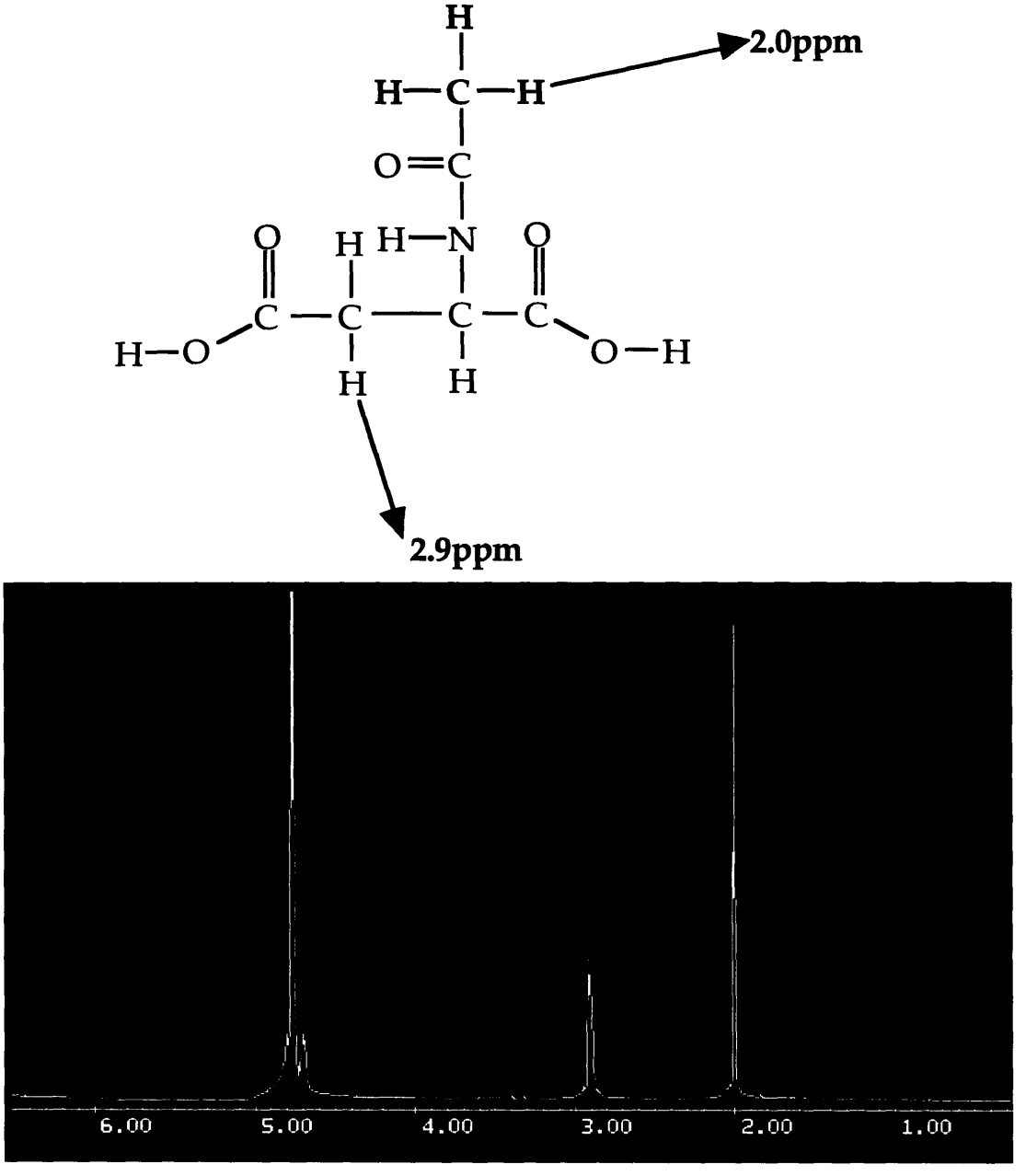

Figure 1.1 The chemical structure of N-acetyl-L-aspartic acid (NAA) and its high resolution NMR spectrum. The group in bold is part of the acetyl group whose moiety resonates at 2.0 ppm.

only to glutamate, in the adult mammalian nervous system. This prominence, in conjunction with evidence for the metabolite's neuronal specificity, has served as the rationale behind the use of NAA as an *in vivo* NMR neuronal marker. Quantitative NMR spectroscopic studies of the putative, concordant decrease of NAA in neurodegenerative disease are expected to provide *in vivo* measures of neuronal loss; this hypothesis has already been incorporated in several useful, recent patient studies of neurodegenerative disease (22-26).

Although significant data concerning the validity of NAA as a neuronal marker in NMR spectroscopic studies have been obtained, the core of this work has remained *in vitro* (27), and the ability of NAA to provide quantitative measures of neuronal loss has not yet been validated. Moreover, the NAA peak, although demonstrating a prominent peak at 2.0ppm, may be contaminated by other resonances that resonate in the 2.0ppm±.25ppm range. Michaelis *et al.* have demonstrated that the glutamate and glutamine possess complex resonance patterns that overlap with NAA at 2.0ppm (28). By analyzing 1:1 solutions of glutamate with NAA, Michaelis demonstrated that the low visibility of the glutamate signal relative to the single methyl resonance of NAA at 2.0ppm may be entirely attributed to a distribution of its intensities into a large number of multiplet resonances. Moreover, he observed similarities in these solutions' spectra to *in vivo* spectra, which demonstrated that the relative intensity of the NAA resonances (those observed at 2.0 and 2.5 ppm) were the same; this finding supports the lack of glutamate

contamination occurring in the NAA peak observed at 2.0ppm. The level of cerebral glutamine in the brain is low, approximately 5 times lower than NAA by measurements made with NMR spectrosocpy (28). This fact makes the probability of contamination of the NAA peak almost negligible. This fact and the fact that glutamate possesses little to no level of contamination of the NAA peak at 2.0 ppm does not preclude the accurate quantification of neuronal content using NAA as a neuronal marker. An initial specific aim of this research was therefore to verify the utility and assess the sensitivity of NAA as an *in vivo* NMR spectroscopic marker for neuronal loss in animal models of neurodegeneration utilizing glutamatergic neurotoxins.

Animal model

Glutamate is the neurotransmitter of many neuronal pathways, but it also possesses excitotoxic properties which can produce lesions reminiscent of neurodegenerative disorders. The excitatory effects of glutamate and other acidic amino acids are mediated by three receptor types named for the specific agonist compounds at each of the receptors (29). These are the NMDA, the Kainate, and the AMPA receptors. Abnormal activation of the excitatory amino acid transmitter receptors, in particular the N-methyl-D-aspartate (NMDA) receptor, is believed to be a pathway by which a variety of injuries result in neuronal damage. This excitotoxic mechanism is thought to play a fundamental pathogenetic role in a variety of neurological diseases, including acute stroke, neurodegenerative diseases and AIDS-related dementia (30).

Kainic acid, an analogue of glutamate, produces well characterized and NMR visible lesions in the rat brain (31-35). Injection of kainic acid into the striatum causes a profound degeneration of neurons intrinsic to the region, accompanied by a marked reduction in the presynaptic markers for cholinergic and GABAergic neurons (36). By contrast, the presynaptic markers for the dopaminergic and serotonergic terminals innervating the region are not reduced (33). A measure of GABAergic and cholinergic presynaptic activity comparing hemispheres with and without lesions could thus serve as a viable marker for the neuronal loss accompanying striatal injection of kainic acid.

We tested the hypothesis that NAA may serve as a NMR spectroscopic measure of neuronal content by modifying extant chemical shift imaging (CSI) techniques for the purpose of quantifying NAA in a neurodegenerative rat model that utilized unilateral injection of kainic acid into the rat brain corpus striatum. These NMR spectroscopic measurements of NAA loss were then compared with enzymatic measures to verify the utility of NAA as a NMR spectroscopic measure of neuronal loss. In the first set of experiments, we examined rats lesioned with kainic acid to determine whether a significant difference exists in the amount of NAA between the brain hemispheres of rats with unilateral kainic acid lesions, and to assess the correlation of any such differences between enzymatic and *in vitro* NMR spectroscopic measurements. The existence of a correlation between these *in vivo* and *in vitro* measures of NAA within the same

animal, with measures obtained by GAD and ChAT activites, would further support the hypothesis that NAA can provide a quantitative *in vivo* index of neuronal loss.

To assess the sensitivity of NAA in determining subtle modulations of neuronal loss and protection, methods developed on a kainic acid model were applied to an excitotoxic system able to demonstrate evidence of excitotoxicity (through NMDA) and of neuroprotection (through the action of antagonists, in particular MK-801). NMDA, a synthetic analogue of glutamate, produces selective lesions upon unilateral instillation into the rat corpus striatum (37). Since first recognized as a specific receptor type, the NMDA receptor has become among the best characterized of all receptor types in the central nervous system (38). Studies carried out both *in vivo* and *in vitro* demonstrate that competitive and noncompetitive antagonists of NMDA receptors protect against neuronal injury produced by NMDA (37, 39, 40). These observations have raised considerable interest in the potential therapeutic applications of NMDA antagonists. Rapid and sensitive methods to quantify the *in vivo* neuroprotective effects of such compounds are needed. Most *in vivo* models of brain injury have relied on morphological or biochemical approaches to quantify the severity of injury and efficacy of neuroprotective agents. Cell counts, histopathologic cross-sectional area measurements, activity of specific neuronal markers such as ChAT activity, measurement of disparities between NMDA injected and contralateral cerebral hemisphere weights, and neuron-specific immunoreactivity are often

used to assess of neuronal injury (32, 39, 41, 42). Although these methods provide an accurate measure of neuronal loss, the measures obtained are acute, and thus limit dynamic assessment of neuronal degeneration and the long term potentiation of antagonists.

CSI techniques which had been modified and applied to the kainic acid rat model were used in the present work to obtain a quantitative, non-invasive *in vivo* assessment of neuronal injury. The aim of these investigations was to address the issue of NAA's sensitivity as a NMR spectroscopic index of neuronal loss. Our CSI techniques were applied in a NMDA rat model that made use of a non-competitive, NMDA antagonist, MK-801 (43). NMR spectroscopy was applied *in vivo* and *in vitro* to Sprague-Dawley rats, some treated with MK-801 and NMDA, and some with NMDA alone, to determine the sensitivity of NMR spectroscopic measurements of NAA as a quantitative indicator of neuronal loss. The measurements obtained were then compared with those determined through GAD and ChAT activity.

Echo Planar Chemical Shift Imaging

Assuming that NAA measurements are indicative of neuronal content, we proceeded to develop a method whereby we might make NAA measurements in humans. These involved the development of a novel approach to chemical shift imaging (CSI) that exploited echo planar imaging's (EPI) capability to traverse k-space rapidly for improvements in spatial resolution and volume coverage. This new approach is here termed echo planar chemical shift imaging (EP CSI).

Conventional phase-encoded chemical shift imaging (CSI) (44, 45) methods produce metabolic images with superior spectral resolution, but are hindered in their ability to achieve high spatial resolution by the need for multidimensional phase encoding. This limitation becomes more pronounced when volumetric information is required, necessitating increased time to encode three spatial dimensions.

Recently, however, metabolite images covering three to five slices of the brain have been produced by using multi-slice imaging in combination with with either conventional phase-encoded CSI or multi-echo CSI (46). Yet, saturation effects and volume encoding time prevents CSI from providing contiguous slice, volumetric, metabolic information about the brain. The advent of EP CSI promises to redefine spectroscopic imaging significantly by exploiting potential tradeoffs between spatial resolution and volumetric coverage. That is, metabolite maps of superior spatial resolution (<500μl voxel volumes) can be achieved at the sacrifice of some spectral resolution through the ability of EP CSI to sample k-space rapidly. Unlike other conventional techniques, this approach lends itself easily to full 3D spatial encoding without a loss in temporal resolution because of the multiple excitations (NEX) required to obtain useful SNR.

We have placed particular emphasis on volumetric mapping of neuronal content by using N-acetyl aspartate (NAA) as a neuronal marker. Although MRS has demonstrated decreased NAA in neurodegenerative diseases (22-24, 26, 47, 48), the majority of these

measurements remain focal and limit the ability to assess global patterns of degeneration that occur in many disease states, such as Alzheimer's disease (AD) (22) and the AIDS dementia complex (ADC) (49). The development of EP CSI would allow such global measures to be obtained through the production of high resolution, volumetric maps of neuronal content. These maps would be capable of supplying information about both focal patterns of degeneration and global patterns of neuronal loss that could aid in the assessment of neurodegenerative diseases. A specific aim in the present study was to implement EP CSI on an *in vivo* GE Signa 1.5T human imager, to evaluate this technique on phantoms of different millimolar concentration brain metabolites, and to assess its capability to produce high spatial resolution ($\leq$ 6x6 mm) metabolite maps in normal humans within reasonable imaging times.

The primary objectives of the investigations described in this thesis were to design and implement experiments, verify the utility of NAA as a NMR neuronal marker and to develop novel CSI techniques for determining neuronal content by employing this marker. This provided a foundation for the development of novel approaches to map volumetrically the neuronal distribution of the human brain. These techniques offer a non-invasive, quantitative means of measuring the progression of neurodegeneration in patients. This information, which presently is impossible to acquire by other means, may be of benefit in assessing patient prognosis and as a guide for therapy.

References

1. Lipton S, Rosenberg P. Excitatory amino acids as a final common pathway for neurologic disorders. New England Journal of Medicine 1994;330(9):613-622.

2. Tallan H, Moore S, Stein W. N-acetyl-L-aspartic acid in brain. Journal of Biological Chemistry 1956;219:257-264.

3. Nadler J, Cooper J. N-acetyl-L-aspartic acid content of human neural tumours and bovine peripheral nervous tissues. Journal of neurochemistry 1972;14:551-554.

4. Simmons ML, Frondoza CG, Coyle JT. Immunocytochemical localization of N-acetyl-aspartate with monoclonal antibodies. Neuroscience 1991;45(1):37-45.

5. Curtis D, Watkins J. The excitation and depression of spinal neurones by structurally related amino acids. Journal of Neurochemistry 1960;6:117-141.

6. D'Adamo Jr. AF, Gidez LI, Yatsu FM. Acetyl transport mechanisms. Involvement of N-acetyl aspartic acid in de novo fatty acid biosynthesis in the developing rat brain. Experimental Brain Research 1968;5:267-273.

7. D'Adamo Jr. A, Yatsu F. Acetate metabolism in the nervous system. N-acetyl-L-aspartic acid and the biosynthesis of brain lipids. Journal of Neurochemistry 1966;13:961-965.

8. Clarke D, Greenfield S, Dicker E, Tirri L, Ronan E. A relationship of N-acetylaspartate biosynthesis to neuronal protein synthesis. Journal of Neurochemistry 1975;24(479-485).

9. Knizley H. The enzymatic synthesis of N-acetyl-L-aspartic acid by a water-insoluble preparation of a cat brain acetone powder. Journal of Biological Chemistry 1967;242:4619-4622.

10. Blakely R, Robinson M, Thompson R, Coyle J. Hydrolysis of the brain dipeptide N-acetyl-L-aspartyl-L-glutamate: subcellular and regional distribution, ontogeny, and the effect of lesions on N-acetylated-a-linked acidic dipeptidase activity. Journal of Neurochemistry 1988;50:1200-1209.

11. Berlinguet L, Laliberte M. Metabolism of N-acetyl-L-aspartic acid in mice. Canadian Journal of Biochemistry 1966;44:783-789.

12. Truckenmiller M, Namboodiri M, Brownstein M, Neale J. N-acetylation of L-aspartate in the nervous system: differential

distribution of a specific enzyme. Journal of Neurochemistry 1985;45:1658-1662.

13. Miyake M, Kakimoto Y. N-acetyl-L-aspartic acid, N-acetyl-α-aspartylglutamic acid and β-citryl-l-glutamic acid in different brain regions and spinal cords of rat and guinea pig. Journal of Neurochemistry 1981;37:1064-1067.

14. Birnbaum S, Levintow L, Kingsley R, Greenstein J. Specificity of amino acid acylases. Journal of Biological Chemistry 1952;194:455-470.

15. Goldstein FB. Amidohydrolases of brain; enzymatic hydrolysis of N-acetyl-L-aspartate and other N-acyl-L-amino acids. J. Neurochem. 1976;26:45 - 49.

16. D'Adamo A, Smith J, Woiler C. The occurrence of N-acetylaspartate amidohydrolase (aminoacylase II) in the developing rat. Journal of Neurochemistry 1973;20:1275-1278.

17. Cangro C, Namboodiri M, Sklar L, Corigliano-Murphy A, Neale J. Immunohistochemistry and biosynthesis of N-acetylaspartylglutamate in spinal sensory ganglia. Journal of Neurochemistry 1987;49:1579-1588.

18. Curatolo A, D'Arcangelo P, Lino A, Brancati A. Distribution of N-acetyl-aspartic and N-acetyl-aspartyl-glutamic acids in nervous tissue. Journal of Neurochemistry 1965;12:339-342.

19. Marcucci F, Mussini E, Valzelli L, Garattini S. Distribution of N-acetyl-L-aspartic acid in rat brain. Journal of Neurochemistry 1966;25:11-14.

20. Fleming M, Lowry O. The measurement of free and N-acetylated aspartic acids in the nervous sytem. Journal of Neurochemistry 1966;13:779-783.

21. Koller K, Zaczek R, Coyle J. N-acetyl-aspartyl-glutamate: regional levels in rat brain and the effects of brain lesions as determined by a new HPLC method. Journal of Neurochemistry 1984;43:1136-1142.

22. Miller B, Moats R, Shonk T, Ernst R, Woolley S, Ross B. In vivo abnormalities of cerebral myo-inositol and n-acetyl residues in Alzheimer disease. Radiology 1992;.

23. Kreis R, Ernst T, Ross B. Development of the human brain: in vivo quantification of metabolite and water content with proton magnetic resonance spectroscopy. Magn Reson Med 1993;30(4):424-437.

24. Jarvik J, Lenkinski R, Grossman R, Gomori J, Schnall M, Frank I. Proton MR spectroscopy of HIV-infected patients: characterization of abnormalities with imaging and clinical correlation. Radiology 1993;186:739-744.

25. Gideon P, Henriksen O. In vivo relaxation of N-acetyl-aspartate, creatine plus phosphocreatine, and choline containing compounds during the course of brain infarction: a proton MRS study. Magn Reson Imaging 1992;10:983-988.

26. Chong W, Paley M, Wilkinson I, *et al.* Localised Cerebral Proton MR Spectroscopy in HIV infection and AIDS. AJNR 1994;15:21-25.

27. Urenjak J, Williams SR, Gadian DG, Noble M. Proton nuclear magnetic resonance spectroscopy unambiguously identifies different neural cell types. J. Neurosci. 1993;13(3):981-989.

28. Michaelis T, Merboldt K, Hanicke W, Gyngell M, Bruhn H, Frahm J. On the identification of cerebral metabolites in localized 1H NMR spectra of human brain *in vivo*. NMR in Biomedicine 1991;4:90-98.

29. Greenamyre J. The role of glutamate in neurotransmission and in neurologic disease. Archives of Neurology 1986;43(10):1058-63.

30. Cotman C, Iverson L. Excitatory amino acids in the brain - focus on NMDA receptors. TINS 1987;10(7):263-272.

31. Olney J, Rhee V, Ho O. Kainic acid: a powerful neurotoxic analogue of glutamate. Brain Res 1974;77:507-512.

32. Coyle J, Schwarcz R. Lesion of striatal neurones with kainic acid provides a model for Huntington's chorea. Nature 1976;263(5574):244-246.

33. Schwarcz R, Coyle J. Striatal lesions with kainic acid: neurochemical characteristics. Brain Res 1977;127:235-249.

34. King M, van Bruggen N, Ahier R, *et al.* Diffusion-weighted imaging of kainic acid lesions in the rat brain. Magn Reson Med 1991;20(1):158-164.

35. Guimaraes A, Nguyen T, Kennedy D, Hyman S, Gonzalez R. Quantitative Magnetic Resonance Imaging of Experimental Neurotoxicity. Proceedings of the Society of Magnetic Resonance in Medicine. San Francisco: , 1991: .

36. Zaczek R, Schwarcz R, Coyle J. Long-term sequelae of striatal kainate lesion. Brain Res 1978;152:626-632.

37. McDonald J, Silverstein F, Johnston M. Neurotoxicity of N-methyl-D-aspartate is markedly enhanced in the developing rat central nervous system. Brain Research 1988;459:200-203.

38. Watkins J. Excitatory amino acids. In: McGeer E, Olney J, McGeer P, ed. Kainic Acid as a Tool in Neurobiology. New York: Raven Press, 1978:

39. Foster A, Gill R, Kemp J, Woodruff G. Systemic administration of MK-801 prevents N-methyl-D-aspartate induced neuronal degeneration in rat brain. Neuroscience Letters 1987;76:307-311.

40. Choi D, Koh J, Peters S. Pharmacology of glutamate neurotoxicity in cortical cell culture: Attenuation by NMDA antagonists. Journal of Neuroscience 1988;8:185-196.

41. Beal M, Kowall N, Swartz K, Ferrante R, Martin J. Systemic approaches to modifying quinolinic acid striatal lesions in rats. Journal of Neuroscience 1988;8:3901-3908.

42. McDonald J, Roeser N, Silverstein F, Johnston M. Quantitative assessment of neuroprotection against NMDA-induced brain injury. Experimental Neurology 1989;106:289-296.

43. Wong E, Kemp J, Priestley T, Knight A, Woodruff G, Iversen L. The anticonvulsant MK-801 is a potent N-methyl-D-aspartate antagonist. Proceedings of the National Academy of Sciences 1986;83:7104-7108.

44. Brown T, Kincaid B, Ugurbil K. NMR chemical shift imaging in three dimensions. Proc Natl Acad Sci USA 1982;79:3523-3526.

45. Pykett I, Rosen B. Nuclear magnetic resonance: in-vivo proton chemical shift imaging. Radiology 1983;149:197-201.

46. Duyn J, Moonen C. Fast proton spectroscopic imaging of human brain using multiple spin-echoes. Magn. Reson. Med. 1993;30:409-414.

47. Menon D, Ainsworth J, Cox I, *et al.* Proton MR spectroscopy of the brain in AIDS dementia complex. J Comput Assist Tomogr 1992;16:538-42.

48. Miller B, Moats R, Shonk T, Ernst T, Woolley S, Ross B. Alzheimer disease: depiction of increased cerebral myo-inositol with proton MR spectroscopy. Radiology 1993;187(2):433-437.

49. Menon D, Baudouin C, Tomlinson D, Hoyle C. Proton MR spectroscopy and imaging of the brain in AIDS: evidence of neuronal

loss in regions that appear normal with imaging. J Comput Assist Tomogr 1990;14:882-885.

Chapter 2

Neurodegeneration: Hypothesis of Cause

Glutamate Neurotoxicity

Glutamate is the neurotransmitter for many critical neuronal pathways, including cognition, memory, movement, and sensation (1). However, glutamate also possesses excitotoxic properties able to produce lesions similar to those found in a number of neurodegenerative disorders. The first observation of the neurotoxic effects of glutamate was reported in 1957 by Lucas and Newhouse, after their study of the cytotoxic effects of systemically adminstered glutamic acid on the retina of neonatal mice (2). This work was expanded by Curtis and Watkins, who in 1960 provided neurophysiologic evidence to support the hypothesis that acidic amino acids such as glutamate produce excitatory effects on central neurons (3). A fundamental understanding of the relationship between the excitatory effects produced by the acidic amino acids and neurotoxicity was achieved through the electron-microscope investigations of Olney. He reported that the neurotoxic effects of excitatory amino acids result from

their depolarizing action. The influx of sodium and water into the dendrites of receptors specific to these neurotransmitters subsequent to depolarization has a deleterious effect on the neuron, while axons and non-neuronal elements that do not possess excitatory receptors are not vulnerable. That is, excitatory amino acids, in sufficiently high concentrations within the extracellular matrix, destroy neurons by their depolarizing effects. For this reason, Olney termed these amino acids "excitotoxins" (4).

In recent work, excitatory amino acids, including glutamate and aspartate, have been implicated to some degree in the degenerative processes associated with many neurologic disorders, ranging from such acute insults as stroke, hypoglycemia, trauma, and epilepsy, to chronic neurodegenerative states, such as Huntington's disease, acquired immunodeficiency syndrome (AIDS) dementia complex, amyotrophic lateral sclerosis, and Alzheimer's disease (5). The clinical manifestations produced by these excitotoxic agents have continued to provide the rationale for developing non-invasive, quantitative methods of investigating neurotoxic efficacy in animal models of neurologic disorders and the progression of chronic neuronal loss in patients who suffer from neurodegenerative disease.

Glutamate agonists

The clinical importance of excitotoxic amino acids and their efficacy in destroying neurons necessitates a differentiation between the types of glutamate receptors and ion channels that may be directly or indirectly

affected. Although 20 different genes encode the subunits of these receptors, increasing receptor differences, two types can be separated on the basis of molecular, pharmacologic, and electrophysiologic properties. These two are the ionotropic receptors, which are coupled directly to membrane ion channels, and the metabotropic receptors, which are coupled to G proteins and modulate such intracellular second messengers as inositol trisphosphate, calcium, and cyclic nucleotides (5). We have concentrated our efforts on the former of these subtypes, the ionotropic subclass of glutamate and its acidic amino acids, which are mediated by three receptor types named for the specific agonist compounds located at each of the receptors. These include the NMDA, the kainate, and the AMPA receptors (6). The structures of glutamate, NMDA, and kainate are shown in Figure 2.1.

Kainic acid, a conformationally restricted analogue of L-glutamate, is a potent neuroexcitant in the central nervous system of mammals (7). Neurophysiologic studies indicate that it is 30- to 100-fold more potent than glutamic acid as a neuronal excitant (7). Intrastriatal injection of kainic acid produces a rapid and selective degeneration of those neurons whose cell bodies are located in the striatum, but spares the axons that innervate the region directly affected by the toxin (8). This selectivity of action has been demonstrated by extensive neurochemical studies. In these, marked reductions in presynaptic markers for cholinergic and GABAergic neurons

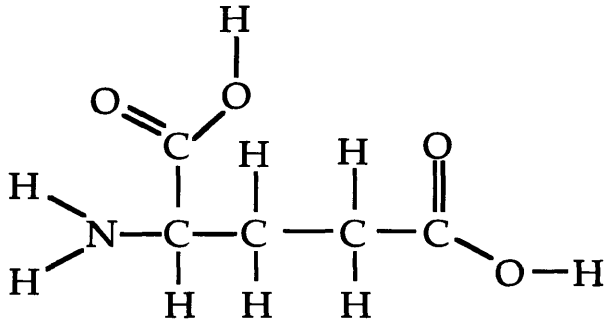

Glutamic Acid

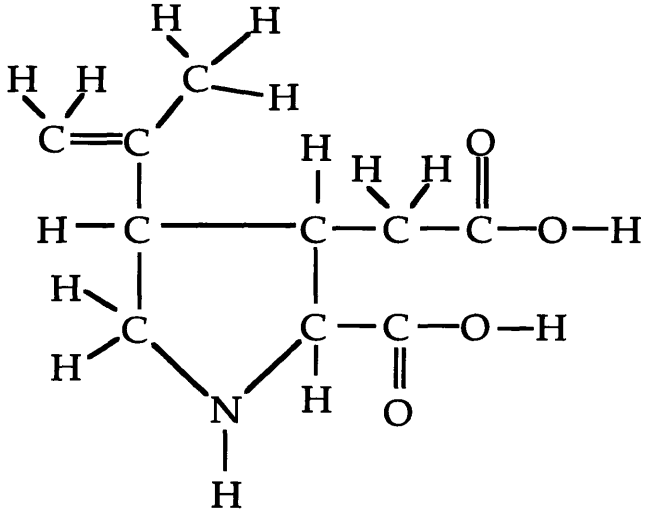

Kainic Acid

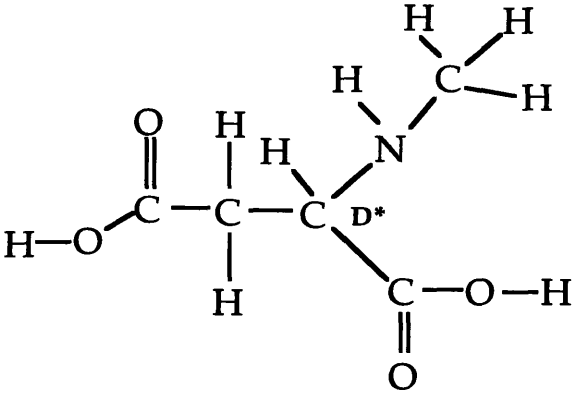

N-Methyl-D-Aspartic Acid (NMDA)

Figure 2.1 Chemical structure of glutamate and its agonists: N-methyl-D-Aspartatic acid, Kainic acid.

intrinsic to the striatum were observed, while presynaptic markers for the dopaminergic terminals innervating the region were maintained (9). In fact, unilateral injection of 2.5μg of kainic acid into the rat striatum caused a 70% reduction in the striatum of the cholinergic parameter, choline acetyltransferase (ChAT), and a similar reduction in the GABAergic parameter, glutamic acid decarboxylase (GAD) (9). Although the degeneration of the intrinsic neurons takes place within 48-72h, secondary changes, including axonal atrophy, caused by the loss of postsynaptic sites, axonal sprouting and alterations of the neurochemical characteristics of the remaining neuronal processes, would presumably occur much more gradually (10).

Although less potent than kainic acid, NMDA, another structural analogue of glutamate, exhibits similar morphologic and neurochemical characteristics to kainic acid when injected unilaterally in the rat brain corpus striatum. The same anatomical and enzymatic tools for assessing neurotoxic efficacy that were used on kainic acid, in particular ChAT and GAD, may be employed for the study of NMDA. Recently, the study of antagonists to the NMDA receptor have been studied in the hope of possible therapeutic intervention prior to NMDA neurotoxicity. To elucidate other possible interventional strategies, a more complete understanding of the mechanisms involved in glutamate neurotoxicity is necessary.

Mechanism of acute glutamate toxicity

The effects of glutamate-induced neurotoxicity may be separated into two distinct forms, acute and delayed, on the basis of the time course and ionic dependence of the neuronal degeneration (11). Within minutes after exposure to glutamate or one of its agonist forms, excessive amounts of sodium and chloride ions, together with water, enter the cell. This causes neuronal swelling, that sometimes, but not always, leads to cell death. Removing extracellular sodium and chloride attenuates the effects of acute glutamate toxicity, but does not ameliorate the effects of delayed toxicity (5).

A credible hypothesis can be made that glutamatergic excitotoxicity is an initial event in the metabolic cascade involved in neuronal degeneration. However, further evidence suggests a delayed response to glutamate. The inverse correlation that exists between glutamate receptor density and neuronal excitotoxic sensitivity (12), concomitant with evidence suggesting delayed glutamate excitotoxicity in axons (generally spared from direct excitotoxic effects) (13, 14), supports the hypothesis of delayed glutamatergic response. The temporal characteristics of neurodegeneration further supports this hypothesis, since some neurons die several hours after excitotoxic instillation. All of these factors have motivated further investigations of the causal relationship of glutamate in delayed neurotoxicity.

Delayed glutamate toxicity

Delayed neurotoxicity, in which neurons die several hours after exposure to glutamate, has been linked at least partially to an extracellular influx of calcium into the neurons through ionic channels. Although Ca^{2+} is integral to the maintenance of many physiologic processes, excessive concentrations may contribute to overstimulation of neurons and indirectly death. The coupling of glutamatergic stimulation with an increase in the extracellular influx of calcium ions mediates neuronal death by activating a series of enzymes, including proteinkinase C, phospholipases, proteases, protein phosphatases, and nitric oxide synthase. The series of events leading to possible neuronal death begins with the activation of phospholipase A_2 (PLA_2), which subsequently activates arachidonic acid, its metabolites, and platelet-activating factor. Platelet-activating factor in turn stimulates the release of glutamate, while arachidonic acid inhibits the re-uptake of glutamate. This increase in glutamate exacerbates the situation by increasing the neuronal calcium levels representing negative feedback. Further, arachidonic acid metabolism produces oxygen free radicals which have the combined deleterious effect of increasing PLA_2 production and introducing oxidative stress (discussed below). The increased production of PLA_2 continues the cascade of events that eventually leads the neuron to effectively digest itself by protein breakdown, free radical formation and lipid peroxidation.

The activation of peptidases, such as calpain I, caused by increased intraneuronal Ca^{2+}, can have similar delayed neurotoxic effects by

catalyzing the enzymatic conversion of xanthine dehydrogenase to xanthine oxidase, which metabolizes purine bases and yields free radicals such as $\bullet O_2^-$(15). Other evidence suggests that nitric oxide (NO) causes the neurons that are in close proximity to neurons activated by NMDA to degenerate through the concomitant increase in Ca^{2+}, which activates nitric oxide synthetase (NOS) (16). Dawson et al. have demonstrated that by increasing the concentration of NOS inhibitors or decreasing the amount of hemoglobin that binds NO, protection against NMDA neurotoxicity can be effected in tissue culture (16). Further work has demonstrated that NO contributes to delayed neuronal death via oxidative stress in the production of free radicals. That is, NO reacts with $\bullet O_2^-$ to form the peroxynitrite anion, which decomposes to •OH. Free radicals have been shown to have a deleterious effect on neurons through an oxidative stress mechanism (17).

Oxidative stress

Oxygen is integral to the maintenance of life. The brain utilizes more oxygen than any other organ because its metabolism is governed almost completely by the aerobic metabolism of the central nervous system's mitochondrial respiratory cycle. For this reason, neuronal mitochondrial respiration is governed by the need to produce the requisite number of ATP molecules for adequate neuronal firing. The rate of mitochondrial respiration, combined with the effects of Kreb's tri-carboxylic acid cycle and oxidative phosphorylation, varies linearly with neuronal firing. By reducing O_2 to H_2O, oxidative phosphorylation

generates the requisite number of ATP to maintain neuronal firing, but the addition of e^- to H^+ within the mitochondrial electron transport chain, the last phase of oxidative phosphorylation, often leads to e^- leakage. This leads to the formation of $\bullet O_2$ and H_2O_2 (18).

Stimulation of glutamate ionotropic receptors activates a variety of processes putatively leading to oxidative stress. Oxidative stress can be summarized as the destructive consequence of free radical production within the cytoplasm. Superoxide anion ($\bullet O_2^-$), hydroxy radical ($\bullet OH$), and hydrogen peroxide (H_2O_2) may be produced either as byproducts of increased Ca^{2+} production after glutamatergic activation or through normal and aberrant metabolic processes that utilize molecular oxygen (O_2). Oxygen radicals can attack locations on DNA, proteins, and lipid membranes that are particularly vulnerable to reduction reactions (11). Polyunsaturated fatty acids, which contain double bonds within their molecular structure, are particularly vulnerable to attack by peroxy radicals ($\bullet OH$) (19). When the hydrogen atom is abstracted by the peroxy radical, a carbon radical is formed that stabilizes to a conjugated diene. This conjugated diene doubles the number of double bonds, thus increasing the number of points vulnerable to peroxy radical attack and altering the integrity of the cellular membrane through the action of cross-linked fatty acids. Because the brain primarily metabolizes aerobically, the concentration of molecular oxygen, O_2, is high. Under these conditions, the double bonds of the conjugated dienes favor the formation of additional organic peroxy radicals. The number of conjugated dienes and cross-links continues to rise, disrupting membrane integrity. In

addition, the peroxy radicals can combine with an abstracted hydrogen atom to form lipid hydroperoxides which, in the presence of Fe^{2+}, decomposes to alkoxy radicals and aldehydes (11). A single •OH can thus initiate a chain reaction that generates numerous toxic reactants: they disrupt membrane integrity through cross-linking mechanisms and alter membrane proteins (11).

Cells protect themselves from the consequences of free radical destruction through enzymes that catalyze the degradation of $•O_2^-$ and H_2O_2 (11). These enzymes include superoxide dismutase, catalase, and glutathione peroxidase. Superoxide dismutase is commonly found in cells in three forms. Copper-zinc superoxide dismutase (CuZnSOD) is cytosolic, whereas manganese-containing superoxide dismutase (MnSOD) is localized within the mitochondrial matrix (20). All three forms of SOD catalyze the formation of H_2O_2 from $•O_2^-$, thereby reducing the risk of •OH formation. Furthermore, H_2O_2 is produced within the brain by the enzymes monoamine oxidase, tyrosine hydroxylase, and L-amino oxidase as a normal byproduct of their normal activity (see Figure 2.2) (11). The action of catalase and glutathione peroxidase remove H_2O_2 from the intracellular environment by reducing it to H_2O and O_2.

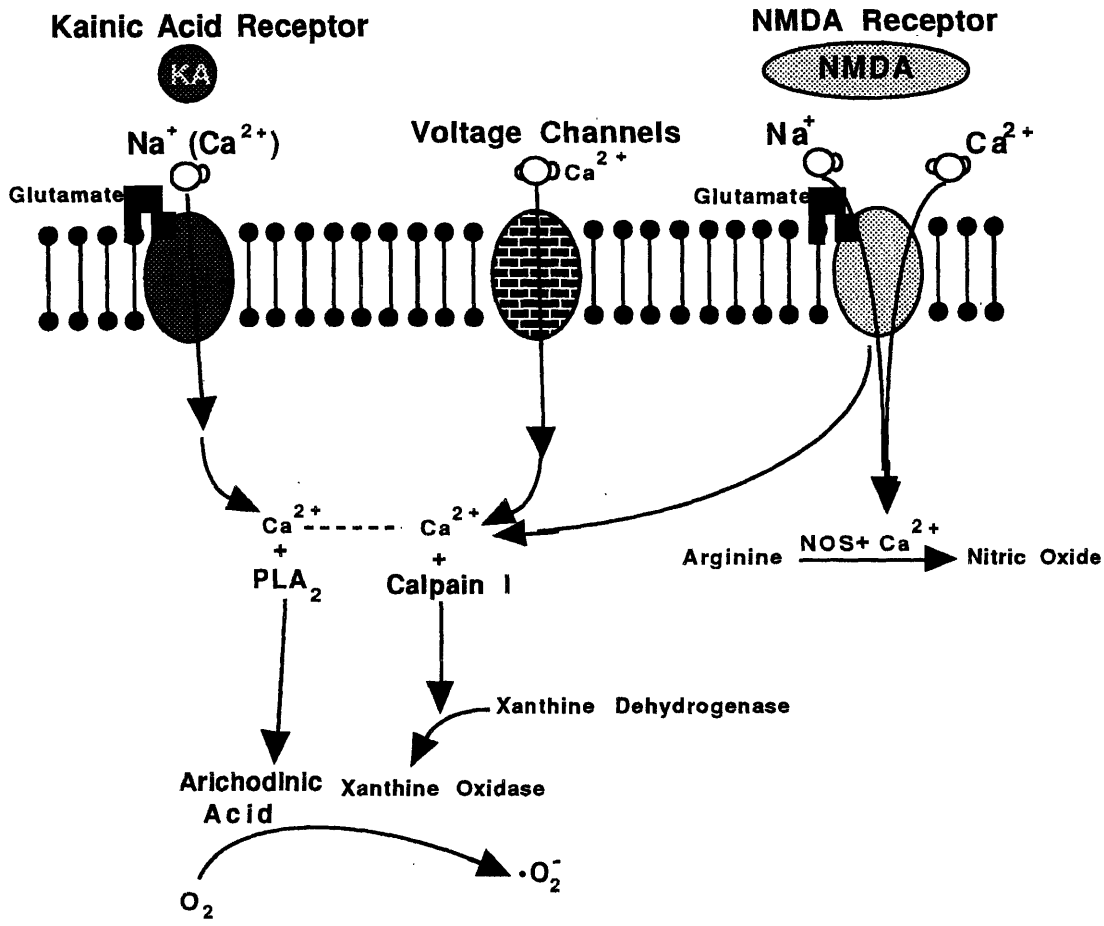

Figure 2.2 Figure demonstrating the coupling of glutamatergic neurotoxicity with oxidative stress putatively leading to neuronal death. Adapted from (11) with permission of JT Coyle.

Although the brain is able to prevent the initiation of destructive free radical chain reactions, mutations in the genes that encode superoxide dismutase may occur. Where lowered superoxide dismutase levels exist, neuronal destruction might be occasioned through oxidative stress. The temporal characteristics of neuronal destruction mediated through oxidative stress suggest an underlying mechanism for the delayed onset and progressive nature of neurodegenerative diseases (11, 21).

Clinical manifestations

Recently, much evidence has surfaced that relates the coupling of glutamate neurotransmission and oxidative stress to many neurodegenerative disorders. Parkinson's disease (PD) is a chronic, progressive disorder of later life that is characterized by rigidity, unintentional tremor, and bradykinesia (11). The neuropathological characteristics of PD primarily involve the degeneration of neurons within the substantia nigra that project to the caudate-putamen. These two structures comprise a majority of the corpus striatum, which possibly explains the symptomology associated with PD. The discovery of chemically induced Parkinsonism in humans caused by MPTP (1-methyl-4-phenyl -1,2,3,6-tetrahydropyridine) (22) has provided extremely strong evidence for a mitochondrial origin to PD. The active metabolite of MPTP, MPP^+ (*N*-methyl-4-phenylpyridinium), is a potent blocker of Complex I (NADH Dehydrogenase) in the mitochondrial electron transport chain (23). Recent evidence demonstrating that mice transgenic for and overexpressing CuZnSOD are resistant to the neurotoxic action of MPTP (24) also supports this hypothesis. Moreover, treatment with NMDA

receptor antagonists protect against the dopaminergic degeneration induced by both amphetamine and MPP^+ (25, 26), indicating a critical link between oxidative stress and glutamate neurotransmission in this system.

Amyotrophic lateral sclerosis (ALS) is a neurodegenerative disorder that exhibits a select degeneration of the lower motor neurons within the spinal cord and the upper motor neurons within the cerebral cortex. Evidence has suggested that this degenerative process may be mediated through the action of excitotoxins because of results demonstrating increased concentrations of glutamate, aspartate and their putative neuronal storage form, N-acetyl-aspartyl-glutamate, within the cerebral spinal fluid of these patients (27). More recent evidence has demonstrated mutations in the CuZnSOD gene of patients who present with a familial history of ALS, lending further support to the hypothesis of a coupling between oxidative stress and excitotoxicity in this disorder.

Where neurodegeneration is caused by glutamatergic neurotoxicity, it occurs in one of two forms: acute or delayed. Although acute excitotoxicity is well understood and occurs through a neuronal swelling mechanism, a troubling conundrum exists in understanding the temporal dynamics that relate the neurotoxic action of glutamate to age-related neurodegenerative disorders. The dynamics of glutamate-gated ion channels occur in milliseconds, while neurodegenerative diseases usually occur gradually. Compelling evidence has been demonstrated in a number of neurodegenerative disorders that suggests a coupling between glutamatergic neurotoxicity and oxidative stress, linked by a host of ionic and/or enzymatic mediators. However, current techniques for

investigating and quantifying the neuronal loss observed after induced neurochemical insult in animal models and accompanying neurodegenerative disorders in patients remains *in vitro*. The development of novel methodologies with which to index chronic neuronal loss quantitatively and non-invasively may provide important information concerning *in vivo* mechanisms of neuronal loss that is presently unavailable.

References

1. Gasic G, Hollmann M. Molecular neurobiology of glutamate receptors. Annual Review of Physiology 1992;54:507-536.

2. Lucas D, Newhouse J. The toxic effect of sodium L-glutamate on the inner layers of the retina. Archives of Ophthalmology 1957;58:193-204.

3. Curtis D, Watkins J. The excitation and depression of spinal neurones by structurally related amino acids. Journal of Neurochemistry 1960;6:117-141.

4. Olney J. Toxic effects of glutamate and related amino acids on the developing central nervous system. In: Nyhan W, ed. Heritable Disorders of Amino Acid Metabolism. New York: John Wiley and Sons, 1974: 501-512.

5. Lipton S, Rosenberg P. Excitatory amino acids as a final common pathway for neurologic disorders. New England Journal of Medicine 1994;330(9):613-622.

6. Greenamyre J. The role of glutamate in neurotransmission and in neurologic disease. Archives of Neurology 1986;43(10):1058-63.

7. Biscoe T, Evans R, Headley P, Martin M, Watkins J. Structure-activity relations of excitatory amino acids on frog and rat spinal neurons. British Joural of Pharmacology 1976;58:373-382.

8. Coyle J, Schwarcz R. Lesion of striatal neurones with kainic acid provides a model for Huntington's chorea. Nature 1976;263(5574):244-246.

9. Schwarcz R, Coyle J. Striatal lesions with kainic acid: neurochemical characteristics. Brain Res 1977;127:235-249.

10. Zaczek R, Schwarcz R, Coyle J. Long-term sequelae of striatal kainate lesion. Brain Res 1978;152:626-632.

11. Coyle J, Puttfarcken P. Oxidative stress, glutamate, and neurodegenerative disorders. Science 1993;262:689-695.

12. Kato K, Puttfarcken PS, Lyons WE, Coyle JT. Developmental time course and ionic dependence of kainate-mediated toxicity in rat cerebellar granule cell cultures. J. Pharmacol. Exp. Ther. 1991;256(1):402-11.

13. Schwarcz R, Scholz D, Coyle JT. Structure-activity relations for the neurotoxicity of kainic acid derivatives and glutamate analogues. Neuropharmacology 1978;17(2):145-51.

14. Coyle JT, Molliver ME, Kuhar MJ. In situ injection of kainic acid: a new method for selectively lesioning neural cell bodies while sparing axons of passage. J. Comp. Neurol. 1978;180(2):301-323.

15. McCord JM. Oxygen-derived free radicals in postischemic tissue injury. N-Engl-J-Med. 1985;312(3):159-63.

16. Dawson T, Dawson V, Snyder S. A novel neuronal messenger molecule in brain: the free radical, nitric oxide. Annals of Neurology 1992;32:297-311.

17. Beckman JS, Beckman TW, Chen J, Marshall PA, Freeman BA. Apparent hydroxyl radical production by peroxynitrite: implications for endothelial injury from nitric oxide and superoxide. Proc. Natl. Acad. Sci. U.S.A 1990;87(4):1620-1624.

18. Moncada S, Palme RM, Higgs EA. Nitric oxide: physiology, pathophysiology, and pharmacology. Pharmacol-Rev. 1991;43(2):109-42.

19. Halliwell B. Oxidants and the central nervous system: some fundamental questions. Is oxidant damage relevant to Parkinson's disease, Alzheimer's disease, traumatic injury or stroke? Acta Neurol. Scand. Suppl 1989;126:23-33.

20. Fridovich I. Superoxide dismutases. An adaptation to a paramagnetic gas. J. Biol. Chem. 1989;264(14):7761-7764.

21. Haliwell B, Gutteridge JMC. Free Radicals in Biology and Medicine.Oxford: Clarendon Press, 1989

22. Langston JW, Ballard P, Tetrud JW, Irwin I. Chronic Parkinsonism in Humans Due to a Product of Mepiridine Analog Synthesis. Science 1983;219:979-980.

23. Ramsay RR, Kowal AT, Johnson MK, Salach JI, Singer TP. The inhibition site of MPP+, the neurotoxic bioactivation product of 1-methyl-4-phenyl-1,2,3,6-tetrahydropyridine, is near the Q-binding site of NADH dehydrogenase. Arch. Biochem. Biophys. 1987;259:645-649.

24. Przedborski S, Kostic V, Jackson-Lewis V, et al. Transgenic mice with increased Cu/Zn-superoxide dismutase activity are resistant to N-methyl-4-phenyl-1,2,3,6-tetrahydropyridine-induced neurotoxicity. J. Neurosci. 1992;12(5):1658-67.

25. Sonsalla PK, Nicklas WJ, Heikkila RE. Role for excitatory amino acids in methamphetamine-induced nigrostriatal dopaminergic toxicity. Science 1989;243(4889):398-400.

26. Turski L, Bressler K, Rettig KJ, Loschmann PA, Wachtel H. Protection of substantia nigra from MPP+ neurotoxicity by N-methyl-D-aspartate antagonists. Nature 1991;349(6308):414-418.

27. Rothstein JD, Tsai G, Kuncl RW, et al. Abnormal excitatory amino acid metabolism in amyotrophic lateral sclerosis. Ann. Neurol. 1990;28(1):18-25.

Chapter 3

Animal Model of Excitotoxicity

The purpose of this research was to verify that *in vivo* nuclear magnetic resonance (NMR) spectroscopic measurements of N-acetyl aspartate (NAA) provide a quantitative index of neuronal loss. Extant methods of chemical shift imaging (CSI) were modified and applied to rats injected unilaterally with kainic acid, an analogue of glutamate that exhibits potent excitotoxic properties. Measurements of NAA were determined *in vivo* and compared to *post mortem* NMR spectroscopic measures of NAA and measures of GABAergic (glutamate decarboxylase (GAD)) and cholinergic (choline acetyl transferase (ChAT)) presynaptic activity. Hemispheres with lesions were compared hemispheres without lesions to obtain measures of the percent neuronal survival. Five rats that had lesions created with kainic acid were examined to answer the

following questions: 1) Is there a significant difference in the amount of NAA between the brain hemispheres of rats with a lesion produced unilaterally with kainic acid; and 2) if a difference exists, how does it correlate with high resolution *in vitro* NMR and enzymatic measurements. If measures of NAA *in vivo* and *in vitro* correlated highly with GAD and ChAT activites within the same animal, the hypothesis that NAA provides a quantitative *in vivo* measure of neuronal loss would be supported. This method would thereby noninvasively furnish information that might otherwise be impossible to acquire.

METHODS

Animal Model

Five 150-250 g Sprague-Dawley male rats (Charles River Farms) were anesthetized with 42 mg/kg pentobarbitol and injected into the right corpus striatum (stereotactic coordinates: AP=Bregma, 3.0mm lateral, and 5mm ventral to the surface of the dura mater) with a dose of 2μg of kainic acid(Sigma) in 1μl of phosphate buffer in saline (pH 7.4). This dose has been shown to produce lesions of moderate sizes by histological and biochemical methods (1). The rats were kept warm (~37°C) by using a water heating blanket (Gaymar, Inc.) until they awakened. They were then given 1ml of lactate ringers and 5% dextrose subcutaneously each day for the first six days following injection.

Animal preparation and imaging

Prior to imaging, the rats were anesthetized using pentobarbital (50 mg/kg) and positioned horizontally in an air-tight, perspex cradle with

gas lines; this apparatus encloses the radiofrequency coil. Anesthesia was maintained with a 1.5% halothane/1:1 oxygen:nitrous oxide mixture during imaging. All *in vivo* experiments were performed on a GE 4.7T Omega system with a home-built, transmit/receive, bird-cage design ^{1}H coil tuned to 200.17MHz. Figure 3.1 is a schematic of the probe used in the investigations. The rat brain was positioned in the magnet isocenter by using high resolution, sagittal, T1-weighted imaging, while B_0 compensation was done with an automated OMEGA Compushim routine (generally the linewidths obtained from water are between 80-110 Hz across the entire rat cerebrum). Proton density and T2 weighted images (TR:TE=3000:40,80) were acquired of the rat brain to obtain 8 contiguous, 2mm slices.

In vivo NMR spectroscopic measurements

Figure 3.2 illustrates the pulse sequence that is used to obtain chemical shift images of excitotoxic damage. This sequence is a modified version of a previously described sequence (2). An inversion-recovery technique was used to null intense lipid peaks by incorporating a Levitt-Ernst type composite pulse. Water suppression was provided by a binomial 2662 pulse whose supression bandwidth was optimized for maximum excitation of the NAA methyl moiety. Typical parameters included the following: fov = 35mm; TR:TE =2000:272; averages = 8; matrix = 16x16; slice thickness = 7mm; inversion time = 210ms; spectral width = 4000Hz; and block size = 512. These resulted in complete acquisition times of approximately 90min.

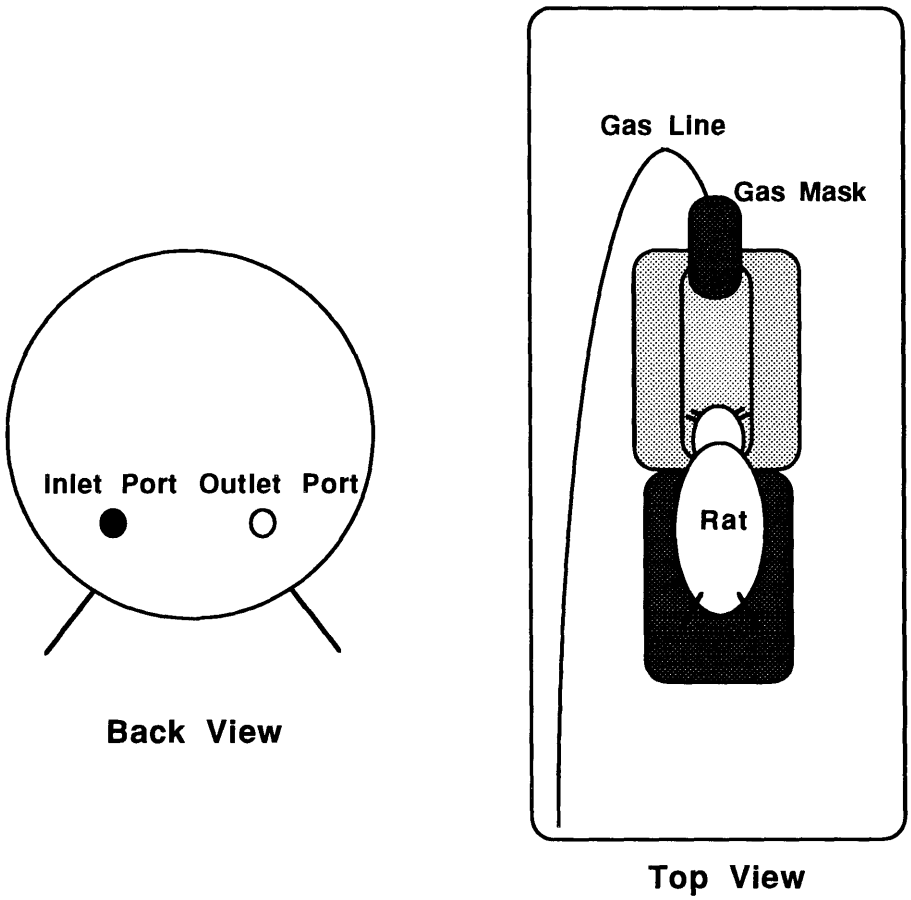

Figure 3.1 Picture of probe used for *in vivo* investigation of the kainic acid lesioned rats. The supporting structure of the probe has inlet and outlet ports for anesthesia.

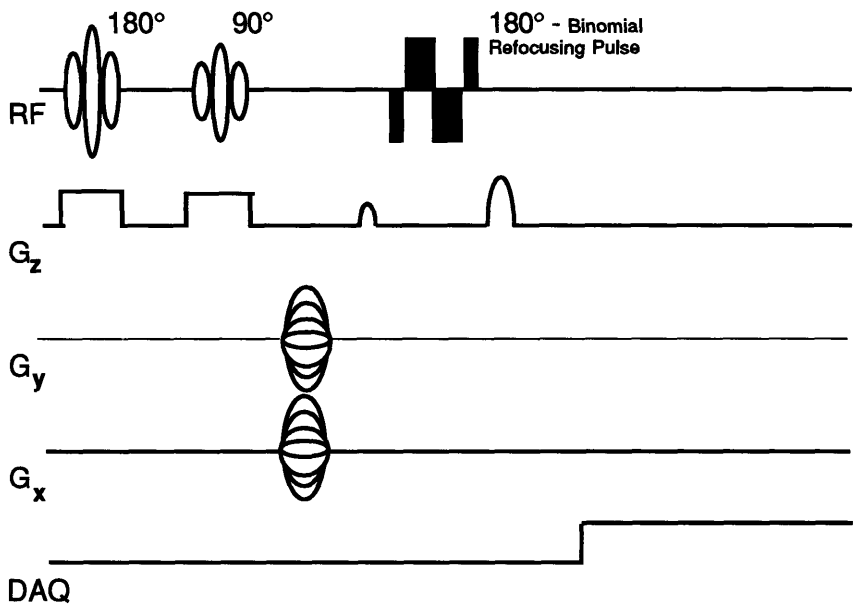

Figure 3.2 Chemical shift imaging sequence for *in vivo* assessment of neuronal loss.

Prior to Fourier transformation, the data was zero filled to 32 steps in each spatial phase encoding dimension. This resulted in metabolite maps with a 32x32 matrix and a voxel volume of 8.4 mm^3. The data were processed by apodization with a sine multiplication in each dimension and subsequent 3D Fourier transformation. Metabolite images were constructed by extracting x and y planes from the 3D data sets. Data reduction for the *in vivo* studies included masking the NAA image onto an outline of a T2-weighted water image for anatomical reference, thereby using the higher resolution of the water image to discriminate between the hemispheres. Signal intensities representing the total NAA signal in each hemispheric slice were then divided (hemisphere with lesion divided by contralateral hemisphere), resulting in an estimate of neuronal survival.

Morphometric analysis was performed on the T2-weighted images using an automated image segmentation program (3). Ventricular volumes were determined and subtracted from hemispheric volumes to obtain a measure of atrophic progression and thus of residual brain parenchyma.

In vitro NMR spectroscopic investigations

After imaging, the rats were sacrificed, the brain rapidly removed, and a slice of brain corresponding to the slice investigated *in vivo* was dissected. Each brain slice was divided into two hemispheres and pulverized under liquid nitrogen. Approximately 50 mg of each pulverized hemisphere was removed for enzymatic activity measurements. The remainder was extracted by using a

methanol/chloroform extraction procedure (4) that entailed the addition of 2 ml of methanol to the tissue followed by thorough homogenization. Chloroform (4 ml.) was then added, followed by brief homogenization and the addition of 4 ml. of 50/50 methanol/chloroform. After centrifuging at 3000 rpm for 10 minutes, the three layers (aqueous, protein, and organic) were separated. The aqueous extract was lyophilized, dissolved in D_2O, and lyophilized again. The extract was then dissolved in D_2O for NMR spectroscopic investigation.

NMR spectra were obtained at 9.4 T using a Bruker MSL 400MHz spectrometer. NMR spectral acquisition parameters included a one pulse experiment, a repetition rate of 15 sec (allowing full recovery of all longitudinal magnetization), a spectral bandwidth of 6 Khz and 8K data points, and 120 averages. For quantification, a coaxial insert with 1:1 CHCL3:CDCL3 was used in each NMR investigation. A calibration curve was constructed using spectra from standards containing 2.5, 5, and 10 mM N-acetyl aspartate. NAA concentrations were determined by obtaining relative integrals comparing NAA peak integrals to $CHCl_3$, the external standard peak integrals.

Spectral analysis was performed with software written by New Methods Research (East Syracuse, NY). NAA concentrations for each hemisphere were obtained by integrating the NAA resonance relative to the external standard and comparing these results with the calibration curve. After correcting for dilution and sample weight, absolute concentrations of NAA were determined for each hemispheric slice.

Glutamic acid decarboxylase (GAD) activity

GAD activity was determined by trapping radioactive carbon dioxide, a product of the decarboxylation of 14C-glutamic acid, as carbonate by using a strong base. Tissue was diluted 1:10(w/v) and sonicated in 0.05M tris (pH 7.4) 0.02% Triton X-100, then centrifuged at 10,000 x g for 10 minutes at 4° C. The supernatant was removed to a fresh test tube, diluted 1:5 in tris-Triton, and kept at 4°C until ready to use. Assay vessels were prepared by inserting 0.5 cm x 2 cm strips of glass fiber filter into a 16mm outer diameter filter holder and wetting the filter with 100µl of Protosol (a strong base). Tissue (50µl) was added to the bottom of 16 x 125 mm test tubes and the reaction initiated by adding a solution (in final concentration) of 1.25 mM glutamic acid (with 0.125 mM tracer of 14C glutamic acid), 0.05 mM pyridoxal phosphate, 50 mM potassium phosphate buffer (pH 6.9), 0.2 mg/ml EDTA, and 5 mM ß-mercapto-ethanol. Immediately after the addition of this reaction mixture, the tubes were capped with the filter/filter holder assembly, vortexed briefly and incubated at 37° C for 60 minutes. The assay was stopped by injecting 100 ul of 15% trichloroacetic acid with a tuberculin syringe through the top of the filter holder. Tubes were stored overnight in a hood to ensure that all radioactive CO^2 was converted to carbonate on the filter paper. The filters were extracted with 2.5 ml Ready-Safe scintillation fluid (Beckman) and counted in a scintillation counter (5).

Choline acetyl transferase ChAT activity

Tissue was prepared as for the GAD assay and 40µl was added to 1.5 ml microcentrifuge tubes. The reaction was started by adding (in final concentration) 200 mM NaCl, 6 mM choline chloride, 50 mM sodium phosphate (pH 7.0), 0.075 mM eserine, 0.005% bovine serum albumin, and .25 mM acetyl CoA (containing a 0.025 mM tracer of 14C acetyl CoA). The tubes were incubated at 37°C for 20 minutes and stopped on ice. Samples were extracted with 1 ml of Kalignost solution (0.5% tetraphenylboron, 15% acetonitrile, in toluene) and vortexed vigorously. Samples were centrifuged for 5 minutes at 16,000 x g; the 0.8 ml of the top (non-aqueous) phase was placed in scintillation vials with 2 ml Ready-Safe scintillation fluid and counted in a scintillation counter.

Data reduction consisted of multiplying each enzymatic count, representing the activity of GAD or ChAT per gram wet weight of tissue, by the total wet weight comprising each hemispheric slice. This measure thus represents the absolute enzymatic activity per hemisphere and is the best method with which to compare the NMR spectroscopic estimates of neuronal loss (6).

RESULTS

In vivo NMR results

Figure 3.3 is a T1 weighted sagittal image along the mid-line of the rat brain. The line demonstrates the slice center for *in vivo* NMR spectroscopic investigation. Figure 3.4 is a T2 weighted MR image of a rat 4 months after kainic acid injection.

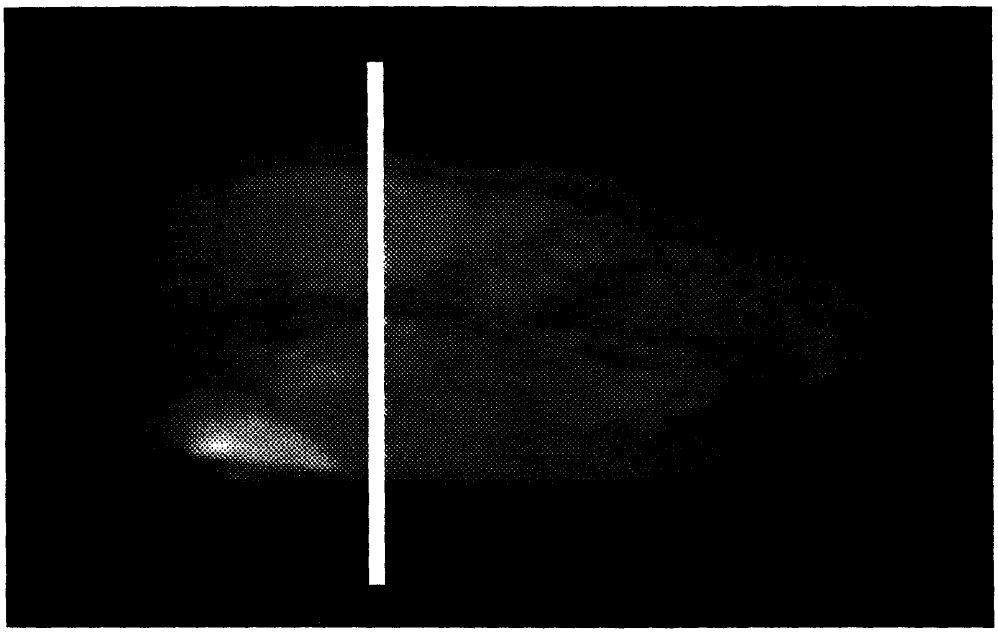

Figure 3.3 T1-weighted sagittal scout image of a rat. The white line represents the slice for chemical shift investigation

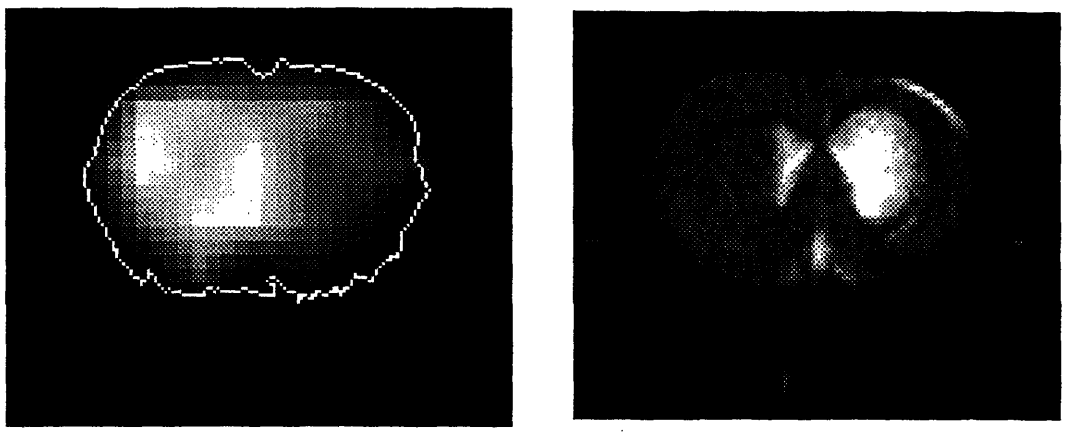

Figure 3.4 On the left is the NAA chemical shift image of a transverse slice through the brain of a rat lesioned in the right hemisphere with 2 μg of kainic acid. On the right is the standard T2 weighted MR image of the same animal obtained during the same imaging session.

Enlarged ventricles suggest severe atrophy and significant tissue loss consistent with kainic acid lesions at later time points (7). The image on the left is a chemical shift image of the NAA methyl moeiety superimposed over an outline of the brain derived from the MR image on the right. As is evident in the chemical shift image, there is substantial NAA loss in the affected right hemisphere. Using these NAA measurements, neuronal survival in the hemisphere with the lesion was 71 ± 1.6% of the contralateral (non-lesioned) hemisphere in the five rats examined.

Figure 3.5 is a morphometrically segmented image: the ventricular volume was subtracted from total hemispheric volume to provide a measure of atrophic progression and thus of residual brain parenchyma. The percentage of brain parenchyma remaining in the lesioned as compared to the non-lesioned hemisphere was found to be 80 ± 1.0% in the five rats examined. This demonstrated statistically significant differences ($p<0.05$) when compared to *in vivo* NAA measurements.

***In vitro* measurements**

Calibration curves were obtained during each high resolution experiment. An example is shown in Figure 3.6. Curves were made of 2.5, 5 and 10 mM NAA during each experiment for proper metabolite quantification. A high resolution *in vitro* spectrum from the lesioned hemisphere of a rat is shown in Figure 3.7.

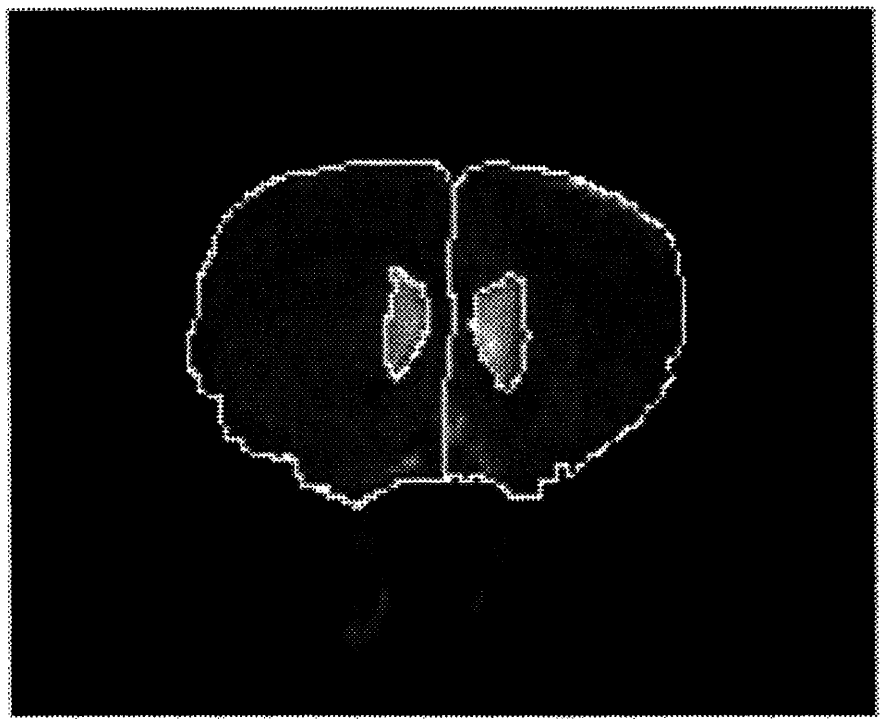

Figure 3.5 Morphometrically segmented T2-weighted image used to determine brain parenchymal volumes.

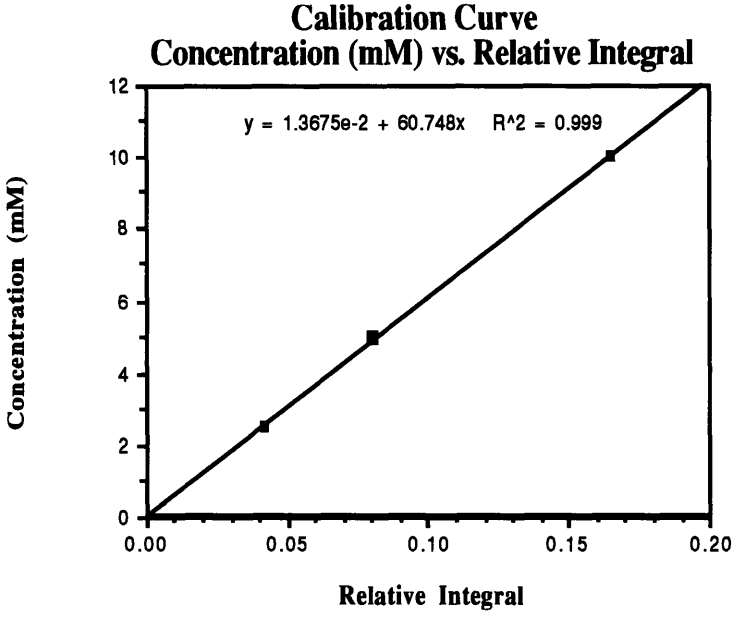

Figure 3.6 Typical calibration curve obtained during *in vitro* high resolution measurements of NAA.

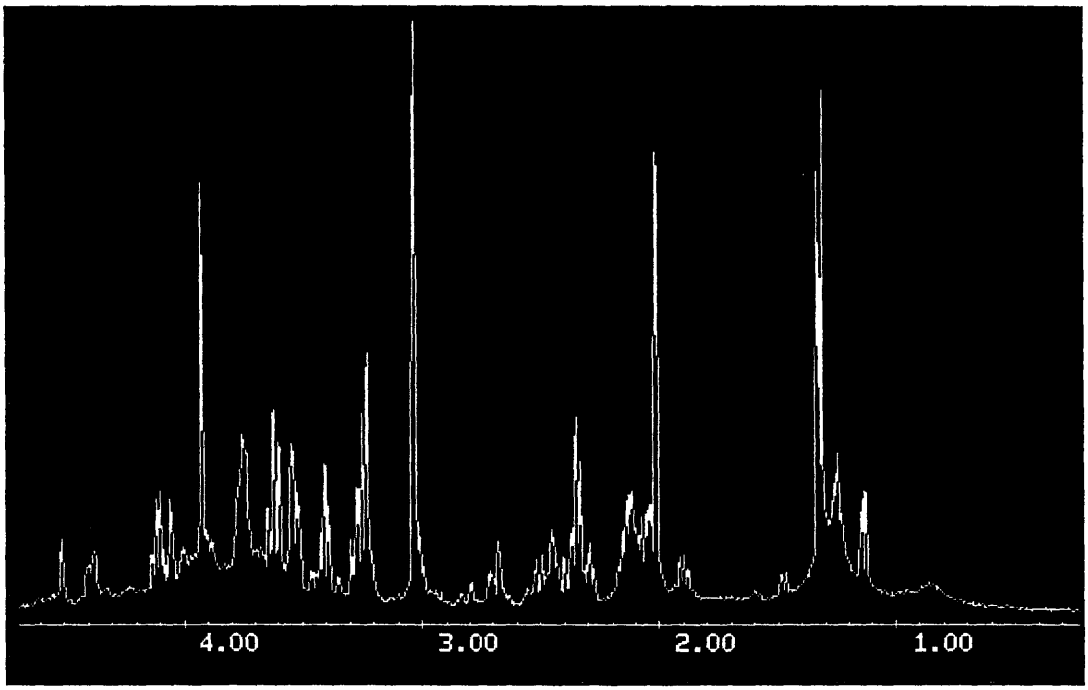

Figure 3.7 *In vitro* MR spectrum of aqueous phase of a rat brain extract.

The mean concentration of NAA within the non-lesioned hemisphere measured 6.5 ± 0.4 (μmol./g ww) for the five rats investigated. These values correlate well with published biochemical measurements of NAA (4.3 - 8 mmol./kg) (8).

The concentrations obtained were multiplied by the wet weight of the entire hemispheric slice to calculate measures of NAA/hemispheric slice. The percent of NAA remaining in the hemisphere with the lesion versus the contralateral hemisphere was found to be 73.8 ± 3.2 (mean ± s.e.m)

GAD and ChAT Assays

GAD and ChAT activities of the hemispheres with a lesion represented 72.1 ± 8.2 and 61.5 ± 5.8 percent of the contralateral hemisphere (mean ± s.e.m), respectively. A comparison of the MRI and NMR spectroscopic measurements with these enzymatic activities is shown in Figure 3.8 . No statistically significant differences were detected between the *in vivo* spectroscopy, *in vitro* spectroscopy and GAD activity measurements. However, the difference in relative ChAT activity approached statistically significance ($p<0.1$) when compared to these three measurements.

Percentage of Contralateral Hemisphere	
N-acetyl aspartate (NAA) *in vivo*	**71.0 ± 1.6**
Glutamate decarboxylase (GAD)	**72.1 ± 8.2**
Choline acetyltransferase (ChAT)	**61.5 ± 5.8**
N-acetyl aspartate (NAA) *in vitro*	**73.8 ± 3.2**
Morphometric analysis	**79.9 ± 1.0**

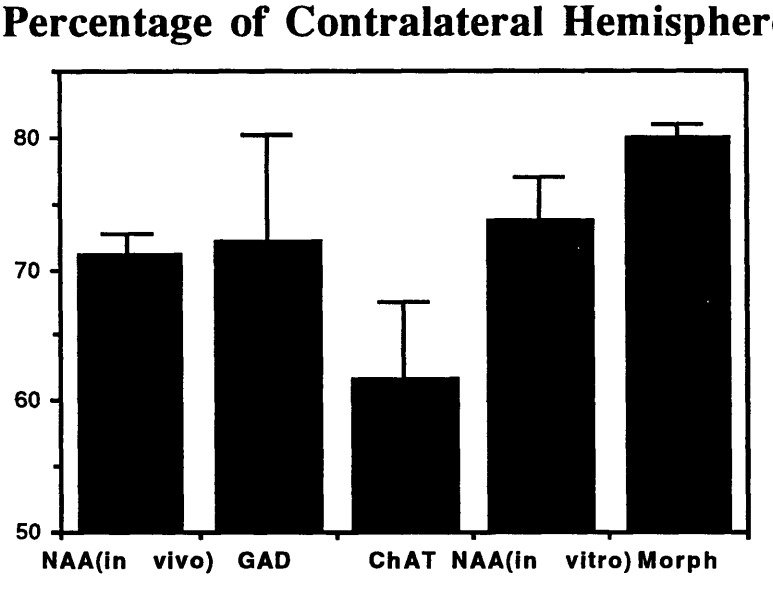

Figure 3.8 Depiction of percent neuronal content of the hemisphere with the kainate lesion relative to the contralateral hemisphere. Measures include *in vivo* NAA, ChAT activity, GAD activity,*in vitro* NAA and morphometric analysis.

DISCUSSION

The mean percentage of neuronal survival calculated with *in vivo* NAA measures (71±1.6%) correlates extremely well with the percentage of GAD survival measures (72.1±8.2%) ($p>0.87$) and *in vitro* spectroscopic measures (73.8±3.2%). The 10% discrepancy between ChAT and other markers of neuronal loss (GAD and NAA levels) may be explained by the known distribution of cholinergic and GABAergic neurons. GABAergic neurons are diffusely spread throughout the rat brain, while the activities of cholinergic neurons are markedly higher in the striatum. This is shown in Figure [gadchat dist]. Because GABAergic neurons are diffusely spread throughout the brain, GAD measurements more accurately represent the true global neuronal loss, while the greater ChAT decrement accurately reflects the relatively high activity of this enzyme in the striatum as compared to other brain regions. Since kainic acid was deposited in the right striatum, I would expect that the percentage of cholinergic neuron survival would be lower than that of GABAergic neuron survival within that hemisphere. NAA measurements, which include the entire hemisphere, should and do more closely correlate with the GABAergic neuron measurements. In fact, the ChAT ratios approached statistically significant differences when compared to either GAD or NAA *in vivo* measurements and were significant ($p<0.04$) when compared to NAA *in vitro* measurements. These enzymatic values (61.5 and 72.1 for GAD and ChAT, respectively) are consistent with previous studies on the neurochemical characteristics of striatal kainic acid lesions in rats (7).

The results of this investigation confirm the capability of chemical shift imaging to provide accurate quantification of metabolite quantity differences with spatial resolution capable of discriminating anatomical structures (9). The point spread function in this technique, although somewhat limited, is thus adequate to provide accurate and reproducible quantitative information about low concentration metabolites in the rat brain. Use of the higher resolution water image for anatomical reference improves the confidence of these measurements, reducing the error that may occur when trying to discriminate between hemispheres for these global assessments.

The ability of NMR spectroscopy to quantify metabolite concentrations accurately is constrained by the inherent T1 and T2 differences of the metabolites investigated. Recent evidence has demonstrated that edamatous lesions arising from focal brain pathologies show altered T1 and T2 relaxation times in cerebral metabolites. Differences in T1 and T2 can contribute to the error obtained within the measurements of percent neuronal loss. Expanding the signal intensity observed as a function of TE, TR, T2, and T1, the following relation is determined:

$$SI = SI_0(e^{-(TE/T2)})(1-2e^{-(TI/T1)}+e^{-(TR/T1)}) \quad [3.1]$$

To determine the accuracy (uncertainty due to systematic error) of the method in calculating percent neuronal survival, the following relation can be used:

$$\Delta SI \cong \frac{\partial SI}{\partial T2}(\Delta T2)+\frac{\partial SI}{\partial T1}(\Delta T1) \quad [3.2]$$

where

$$\frac{\partial SI}{\partial T2} = \left(1 - 2e^{(-TI/T1)} + e^{(-TR/T1)}\right)\left(-TE/T2^2\right)\left(e^{(-TE/T2)}\right)$$

$$\frac{\partial SI}{\partial T1} = \left(\frac{2e^{(-TE/T2)}}{T1^2}\left(TIe^{(-TI/T1)} - \frac{T\,\mathrm{Re}^{(-TR/T1)}}{2}\right)\right) \quad [3.3].$$

The *in vivo* data collection parameters used in this study may give rise to two types of systematic error. First, the TR employed prevented full recovery of the longitudinal magnetization. Second, the TE (272msec) was also long, making the pulse sequence susceptible to $T2^*$ effects. The following experimental parameters (TE=272msec, TR=2000msec, T1=1500msec, and T2=300msec) can be used to approximate the error of the method. Assuming a 10% change in the T1 and T2 of the sample, a maximum 2.6% change in the percent neuronal loss can be expected. This is well under the 10% of percent neuronal loss that was observed within the method and is approximately the standard error observed. Moreover, the empirical findings that *in vivo* CSI measurements of NAA were virtually equivalent to the *in vitro* MR measurements indicate that the changes in the T1 and T2 relaxation times of NAA (which may be expected to occur in the lesioned hemisphere) (10) are relatively small, and their effects well within the error of the *in vivo* measurements.

By using morphometric analysis of high resolution T2-weighted images as a measure of atrophy, statistically significant differences ($p<0.05$) were obtained between these measurments and those of neuronal loss estimated by using NAA as an *in vivo* neuronal marker. The combination of these differences and the lack of difference observed

between techniques utilizing NAA and enzymatic markers for neuronal loss suggest that NMR spectroscopic measurements are more sensitive to this loss than conventional MRI.

These data demonstrate the ability of chemical shift imaging to provide quantitative, spatially resolved images of neuronal loss in a striatal lesion rat model. These data indicate that NAA is an excellent marker for neuronal viability by comparison of %neuronal survival as measured by *in vivo* and *in vitro* NMR with established enzymatic measures of neuronal loss. These data also support the claim that *in vivo* CSI provides an index of neuronal loss comparable to classical biochemical assays. The implementation of quantitative proton spectroscopy or CSI techniques that utilize NAA as a neuronal marker can provide a quantitative, periodic assessment of the progression of neurodegeneration in patients suffering from neurodegenerative disease.

References

1. Schwarcz R, Coyle J. Striatal lesions with kainic acid: neurochemical characteristics. Brain Res 1977;127:235-249.

2. Beal MF, Brouillet E, Jenkins BG, et al. Neurochemical and histologic characterization of striatal excitotoxic lesions produced by the mitochondrial toxin 3-nitropropionic acid. J. Neurosci. 1993;13(10):4181-92.

3. Kennedy DN, Filipek PA, Caviness VS. Anatomic segmentation and volumetric calculations in nuclear magnetic resonance imaging. IEEE Trans. Med. Imaging 1989;8(1):1-7.

4. Nitsch R, Blusztajn J, Pittas A, Slack B, Growdon J, Wurtman R. Evidence for a membrane defect in Alzheimer disease brain. Proc Natl Acad Sci USA 1992;89:1671-1675.

5. Wilson S, Schrier B, Farber J, et al. Markers for gene expression in cultured cells from nervous system. Journal of Biological Chemistry 1972;247:3159-3160.

6. Bull G, Oderwald-Nowak B. Standardizaton of a radiochemical assay of choline acetyltransferase and a study of the activation of the enzyme in rabbit brain. Journal of Neurochemistry 1971;18:935-941.

7. Zaczek R, Schwarcz R, Coyle J. Long-term sequelae of striatal kainate lesion. Brain Res 1978;152:626-632.

8. Miyake M, Kakimoto Y, Sorimachi M. A gas chromatographic method for the determination of N-acetyl-L-aspartic acid, N-acetyl-alpha-aspartylglutamic acid and beta-citryl-L-glutamic acid and their distributions in the brain and other organs of various species of animals. Journal of Neurochem 1982;36:804-810.

9. Buxton R, Wismer G, TJ B, BR R. Quantitative proton chemical shift imaging. Magnetic Resonance in Medicine 1986;3:881-890.

10. Kamada K, Houkin K, Hida K, et al. Localized Proton Spectroscopy of Focal Brain Pathology in Humans: Significant Effects of Edema on Spin-Spin Relaxation Time. Magnetic Resonance in Medicine 1994;31(5):540.

Chapter 4

Animal model of Neuroprotection

After successfully demonstrating that *in vivo* nuclear magnetic resonance (NMR) spectroscopic measurements of N-acetyl aspartate (NAA) provide a valid measure of neuronal loss comparable to classical biochemical assays, it was necessary to assess NAA's sensitivity in determining subtle modulations of neuronal loss and protection within a neurodegenerative animal model. N-methyl-D-aspartic acid (NMDA), a synthetic analogue of glutamate, produces selective lesions upon unilateral instillation into the rat corpus striatum (1). Studies carried out both *in vivo* and *in vitro* demonstrate that competitive and noncompetitive antagonists of NMDA receptors protect against neuronal injury produced by NMDA (1-3). Most *in vivo* models of brain injury have relied on morphological or biochemical approaches to quantify the severity of

injury and efficacy of neuroprotective agents. Cell counts, histopathologic cross-sectional area measurements, activity of specific neuronal markers such as ChAT activity, measurement of disparities between NMDA injected and contralateral cerebral hemisphere weights, and neuron-specific immunoreactivity are often used to assess of neuronal injury (2, 4-6). Although these methods provide an accurate measure of neuronal loss, the measures obtained are at a single point in time and thus limit a dynamic assessment of neuronal degeneration and the long term potentiation of antagonists. Rapid and sensitive methods to quantify the *in vivo* neuroprotective effects of NMDA antagonists are needed.

NMR spectroscopic techniques were modified and applied to the kainic acid rat model to obtain a quantitative, non-invasive *in vivo* assessment of neuronal injury; these were then applied to a NMDA rat model that made use of a non-competitive, NMDA antagonist, MK-801 (7). Extant methods of chemical shift imaging (CSI), developed on a kainic acid model, were applied *in vivo* to Sprague-Dawley rats (some treated with MK-801 and NMDA and some with NMDA alone) to determine the sensitivity of NMR spectroscopic measurements of NAA as a quantitative indicator of neuronal loss. The measurements obtained were then compared with those determined through GAD and ChAT activity. The measures which demonstrated the smallest statistical deviance were then determined to be the most sensitive.

METHODS

Animal Model

Eighteen 250g Sprague-Dawley male rats (Charles River Farms) were anesthetized with either 42mg/kg pentobarbitol or 1ml/kg of a 10:1 solution of ketamine/rompun, and injected into the right corpus striatum (stereotactic coordinates: AP bregma, 3.0mm lateral, and 5mm ventral to bregma) with a dose of 250 nmol of NMDA (Sigma). NMDA was dissolved in NaOH and titrated to pH 7.4 with HCl. Volume of injection was made up with phosphate buffer in saline (pH 7.4). 250nmol of NMDA has been shown to produce lesions of moderate sizes as determined by histological and biochemical methods (1). MK-801(Sigma) has demonstrated neuroprotective effects as determined by these same methods. To test the capability of NMR spectroscopic measures of NAA to assess neuroprotection, six of these rats were given 4 mg/kg MK-801(Sigma) intraperitoneally (i.p.) 30 minutes prior to injection of the excitotoxin as a neuroprotective agent. The rats were kept warm (~40°C) by using a water heating blanket (Gaymar, Inc.) until they awakened. They were then given 1ml of lactate ringers and 5% dextrose subcutaneously each day for the first six days following injection.

Animal preparation and imaging

Prior to imaging, the rats were anesthetized using pentobarbital (50 mg/kg) and positioned horizontally in an air-tight, perspex cradle with gas lines; this apparatus encloses the radiofrequency coil. Anesthesia was maintained with a 1.5% halothane/1:1 oxygen:nitrous oxide mixture during imaging. All *in vivo* experiments were performed on a GE 4.7T

Omega system with a home-built, transmit/receive, bird-cage design ^1H coil tuned to 200.17MHz. The rat brain was positioned in the magnet isocenter by using high resolution, sagittal, T1-weighted imaging, while B_0 compensation was done with an automated OMEGA Compushim routine, which generally produces linewidths that range from 80-110 Hz across the rat cerebrum. Proton density and T2 weighted images (TR:TE=3000:40,80) were acquired of the rat brain to obtain eight contiguous, 2mm slices.

In vivo NMR spectroscopic measurments

The same methods employed to quantify neuronal loss in rats lesioned with kainic acid (see Figure 3.2 and methods for Chapter 2) were used to quantify neuronal loss as measured by NAA in this animal model. Typical CSI parameters included the following: fov = 35mm; TR:TE =2000:272; averages = 8; matrix = 16x16; slice thickness = 7mm; inversion time = 210ms; spectral width = 4000Hz; block size = 512; resulting in complete acquisition times of approximately 90min.

Prior to Fourier transformation, the data was zero filled to 32 steps in each spatial phase encoding dimension. This resulted in metabolite maps with a 32x32 matrix and a voxel volume of 8.4 mm^3. The data were processed by apodization with a sine multiplication in each dimension and subsequent 3D Fourier transformation. Metabolite images were constructed by extracting x and y planes from the 3D data sets. Data reduction for the *in vivo* studies included masking the NAA image onto an outline of a T2-weighted water image for anatomical reference, thereby using the higher resolution of the water image to discriminate between the hemispheres. Signal intensities representing the total NAA signal in each

hemispheric slice were then calculated (lesioned hemisphere divided by corresponding, contralateral non-lesioned hemisphere), resulting in a measure of neuronal survival.

Morphometric analysis was performed on the T2-weighted images by using an automated image segmentation program (8). Ventricular volumes were determined and subtracted from hemispheric volumes to obtain a measure of atrophic progression, and thus of residual brain parenchyma.

Enzymatic investigations

After imaging, the rats were sacrificed, the brain rapidly removed, and a slice of brain corresponding to the slice investigated *in vivo* dissected. Each brain slice was divided into two hemispheres and pulverized under liquid nitrogen. Approximately 50 mg of each pulverized hemisphere were removed for enzymatic activity measurements.

Enzymatic activity measurements

GAD and ChAT activity measurements were performed using the same methodology employed in the kainic acid rat model (see Chapter 2 GAD and ChAT activity measurements within Methods). Data reduction was performed by multiplying each enzymatic count that represented GAD or ChAT activity per gram wet weight of tissue by the total wet weight for each hemispheric slice. This measure thus represents the absolute enzymatic activity per hemisphere and is the best method with which to compare the NMR spectroscopic estimates of neuronal loss (9).

RESULTS

In vivo NMR results

Figure 4.1 and Figure 4.2 are T2-weighted images and chemical shift images of NAA representing rats lesioned with NMDA, treated and untreated with MK-801. In Figure 4.1, the T2-weighted image on the right shows evidence of tissue damage in the pyriform cortex and corpus striatum, consistent with the morphological features of rats striatally lesioned with NMDA (1). The image on the left is a chemical shift image of the NAA methyl moiety superimposed over an outline of the brain derived from the MR image on the right. As is evident in the chemical shift image, there is substantial NAA loss in the affected right hemisphere. By using these NAA measurements, neuronal survival in the lesioned hemisphere measured 88.6 ± 1.9% (mean ± s.e.m.) of the contralateral (non-lesioned) hemisphere in the twelve rats without prior MK-801 treatment and 93 ± 1.2% for those with prior MK-801 treatment.

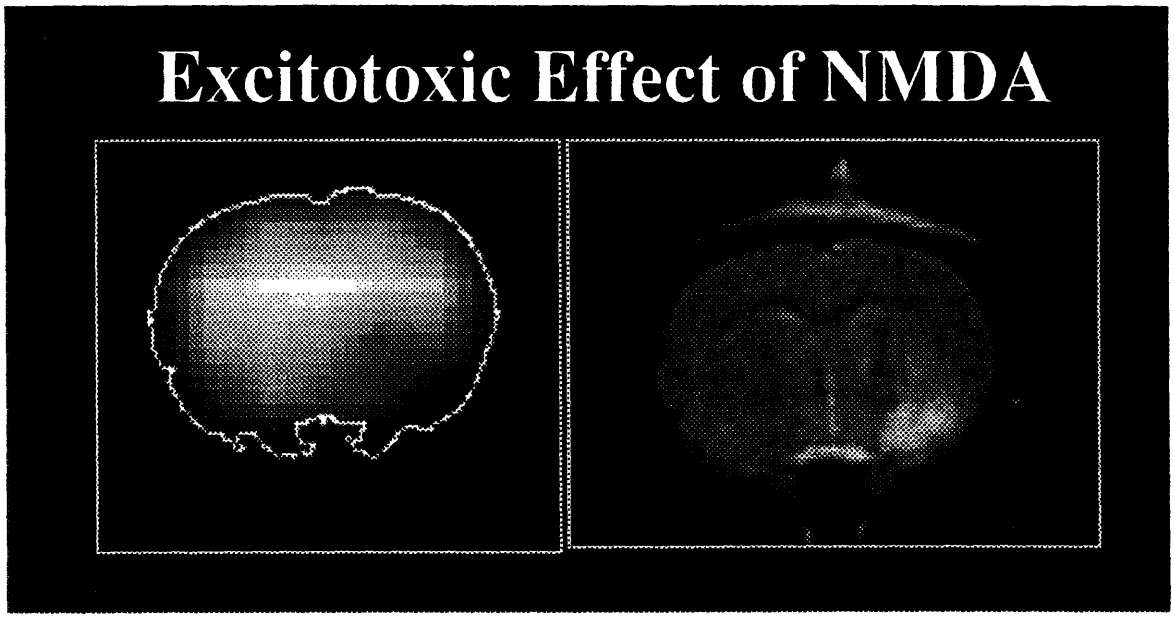

Figure 4.1 Chemical shift NAA image and corresponding T2-weighted image from rat lesioned with NMDA demonstrating the ability of CSI to spatially resolve the concordant neuronal damage associated with lesions visualized with T2-weighted images.

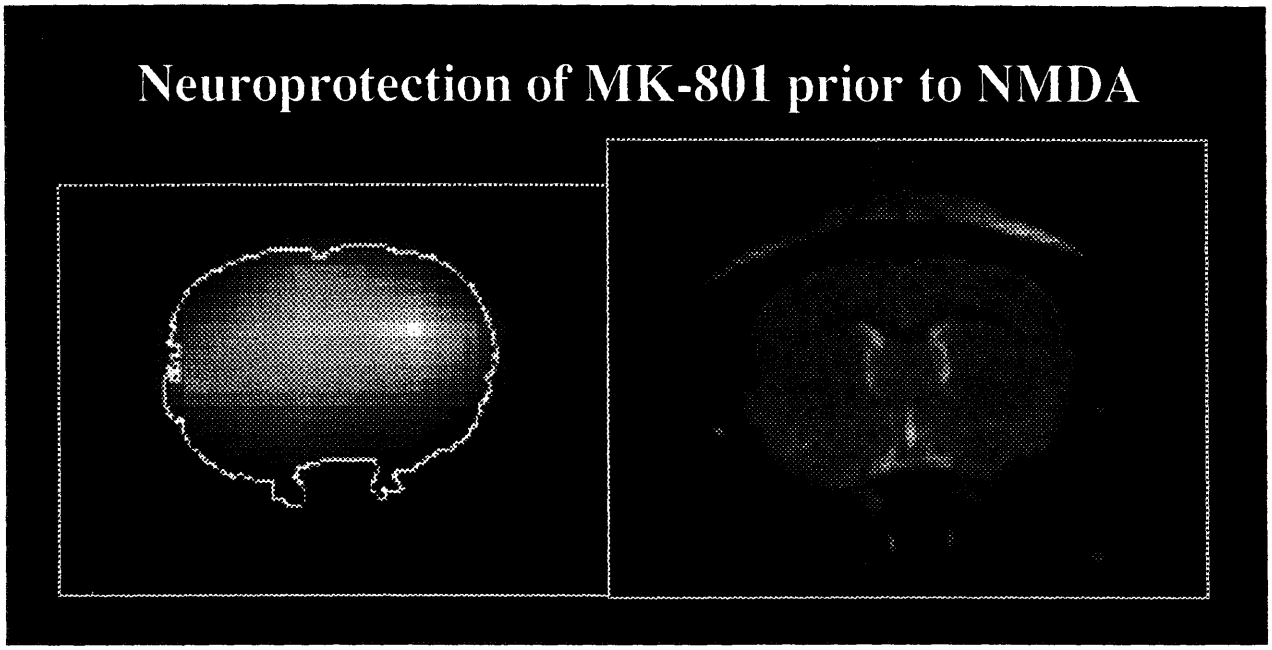

Figure 4.2 Chemical shift NAA image and corresponding T2-weighted image from a rat lesioned with NMDA pretreated with MK-801, demonstrating the capability of NMR imaging and spectroscopic measures to visualize the neuroprotection of MK-801.

Morphometric analysis consisted of subtracting ventricular volumes from total hemispheric volumes to provide a measure of atrophic progression and thus of residual brain parenchyma. The percentage of brain parenchyma remaining in the lesioned as compared to the non-lesioned hemisphere was found to be 92.9 ± 1.2% in the twelve rats lesioned with NMDA, and 93.1 ± 1.6%. in the six rats treated with MK-801 prior to instillation of NMDA. The measures of residual brain parenchyma, although demonstrating low variance, do not reveal evidence of neuroprotection from MK-801; a finding that is different from the measures of NAA *in vivo*. Further, Figure 4.3 shows a T2-weighted image and NAA chemical shift image of a rat, untreated with MK-801 prior to NMDA instillation, demonstrating NAA signal loss in the lesioned hemisphere. However, there is a lack of concordant damage within the T2-weighted image.

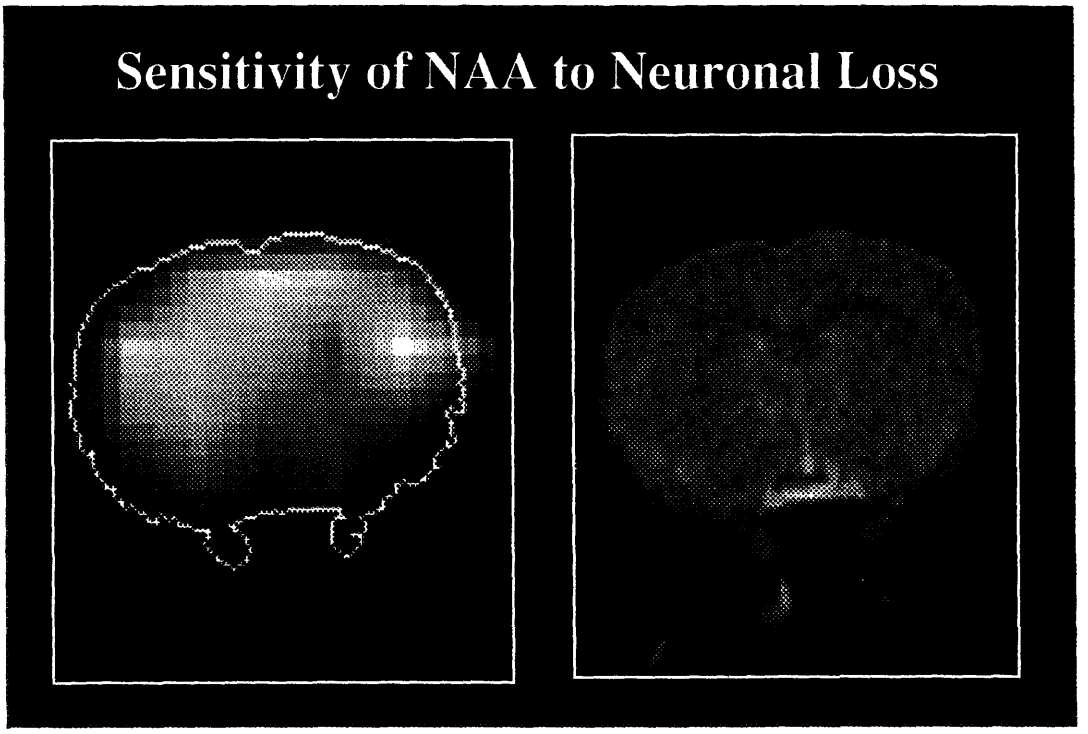

Figure 4.3 Chemical shift NAA image and T2-weighted water image of rat brain lesioned with NMDA. This demonstrates a lack of concordant discrepancy in signal within lesioned hemisphere.

GAD and ChAT Assays

GAD and ChAT activities of the lesioned hemispheres, without prior treatment with MK-801, represented 87.9 ± 7.9 and 71 ± 5.9 percent of the non-lesioned hemisphere (mean ± s.e.m), respectively. In the rats treated with MK-801 prior to NMDA instillation, however, GAD and ChAT activities measured 101 ± 7.6 and 92.2 ± 9.4 percent of the non-lesioned hemisphere, respectively. A comparison of the MRI and NMR spectroscopic measurements with these enzymatic activities is shown in Figure 4.4. No statistically significant differences were detected between the *in vivo* spectroscopy, *in vitro* spectroscopy and GAD activity measurements.

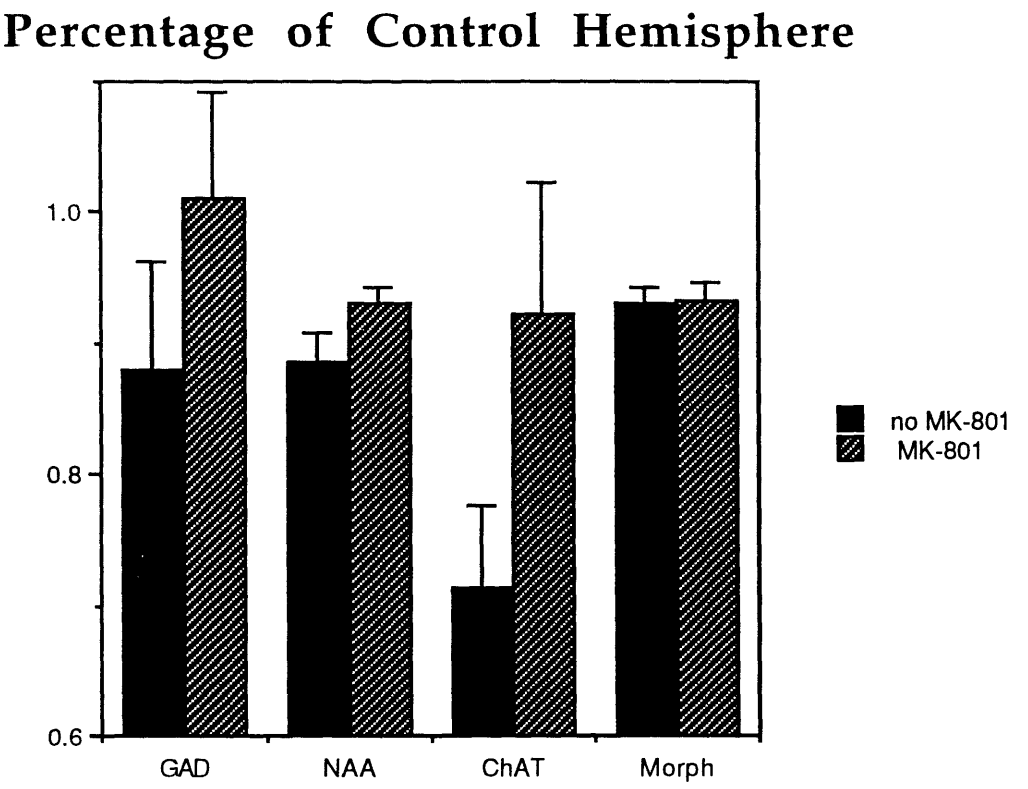

Figure 4.4 Summary of percent of contralateral hemisphere in the rat brain after direct kainic acid infusion assessed by *in vivo* NAA, ChAT activity, GAD activity, and morphometric analysis.

DISCUSSION

The mean percentage of neuronal survival calculated with *in vivo* NAA measures 88.6 ± 1.9% (mean ± s.e.m.) correlates extremely well with the percentage of GAD survival measures 87.9 ± 7.9% ($p > 0.93$, student's two tailed t-test) in rats lesioned with NMDA. This finding supports the previous work on rats lesioned with kainic acid which demonstrated similar correlations of *in vivo* and *in vitro* NMR spectroscopic measures of NAA with GAD activity. Moreover, the subsequent finding of a statistical difference ($p<0.05$) between GAD activity measurements with those measurements obtained from ChAT, corroborating previous results obtained from rats lesioned with kainic acid, is supported by the known distribution of cholinergic and GABAergic neurons. GABAergic neurons are diffusely spread throughout the rat brain, while the activities of cholinergic neurons are markedly higher in the striatum. The GAD activity measurements, therefore, should and do more closely represent the global neuronal loss occurring within the hemisphere. NAA measurements also demonstrated a statistically significant difference from ChAT measurements ($p < 0.05$). The combination of this difference with a lack of a difference between NAA measurements and GAD activity measurements further support the hypothesis that NAA measurements provide a valid index of neuronal loss.

MK-801 has been shown to protect neurons by its antagonistic effects on the NMDA receptor (1, 2). The results obtained from the NAA, GAD and ChAT activity measurements for the six rats treated with MK-801 prior to the instillation of NMDA suggested a corroboration of this

finding, while the results of the morphometric analysis of residual brain parenchymal volume did not. This morphometric finding is not supported by previous results (6). By using hemispheric, cross-sectional area measurements of Nissl stained slices, computer based histological image analysis was able to quantify 95 percent neuroprotection within a perinatal rat that had been injected with 1mg/kg MK-801 prior to instillation of 25nmol/0.5µl NMDA (6).

Neuroprotection assessed through NAA, GAD and ChAT activity measurements demonstrated a 5%, 12% and 22% level of protection, respectively. This was determined by taking the difference of percent survival measurements for each of the three methods. Although these differences in neuroprotection did not attain statistical significance, the NAA and ChAT measurements suggested trends ($p<.15$ and $p<.10$, respectively, as determined by student's two-tailed t-test comparing measurements with and without MK-801). A discrepency also existed in mean percent survival results, calculated as a ratio of lesioned over non-lesioned hemispheres, for NAA *in vivo* ($93 \pm 1.2\%$) and GAD activity ($101 \pm 7.5\%$) measurements. The 100 percent neuroprotection as determined by GAD activity is higher than that observed in other studies (2). Foster et al. report 93 ± 6.5 percent of control striatum using the same doses of NMDA and MK-801. The MK-801 was given 1hr. post-injection of NMDA in the Foster study, which may alter the results, but we speculate that it does not, because similar results have been obtained with MK-801 injection prior to other NMDA agonists (2). Nevertheless, the GAD activity measurements in this study are within the standard error of previous GAD activity

measurements and NAA measurements. This fact supports the use of NAA as a valid index for neuronal loss.

Statistically significant differences ($p<0.005$) were obtained between measurements using morphometric analysis and those of neuronal loss obtained by using NAA *in vivo* in rats with NMDA lesions. This finding corroborates previous results demonstrating statistically significant differences ($p<0.05$) between morphometric analysis and NAA measurements made *in vivo* in rats with kainic acid lesions. Morphometric analysis did not show a difference between animals treated with MK-801 and those untreated; there was 93% residual parenchyma in both cases. Although brain parenchymal volume measures suggest damage in both cases, the inability of morphometric analysis to indicate neuroprotection, while NAA, GAD and ChAT suggested statistical trends in assessing neuroprotection, suggests that imaging may be less sensitive to the process of neuronal damage than these other techniques. This hypothesis is supported by Figure 4.3, which demonstrates a lack of concordant damage in a rat exhibiting neuronal loss as demonstrated by NAA, GAD and ChAT.

These data indicate that NAA provides an excellent marker for neuronal decrement and suggest that *in vivo* CSI provides an index of neuronal loss that may be more sensitive than MRI to subtle changes in neuronal loss.

References

1. McDonald J, Silverstein F, Johnston M. Neurotoxicity of N-methyl-D-aspartate is markedly enhanced in the developing rat central nervous system. Brain Research 1988;459:200-203.

2. Foster A, Gill R, Kemp J, Woodruff G. Systemic administration of MK-801 prevents N-methyl-D-aspartate induced neuronal degeneration in rat brain. Neuroscience Letters 1987;76:307-311.

3. Choi D, Koh J, Peters S. Pharmacology of glutamate neurotoxicity in cortical cell culture: Attenuation by NMDA antagonists. Journal of Neuroscience 1988;8:185-196.

4. Coyle J, Schwarcz R. Lesion of striatal neurones with kainic acid provides a model for Huntington's chorea. Nature 1976;263(5574):244-246.

5. Beal M, Kowall N, Swartz K, Ferrante R, Martin J. Systemic approaches to modifying quinolinic acid striatal lesions in rats. Journal of Neuroscience 1988;8:3901-3908.

6. McDonald J, Roeser N, Silverstein F, Johnston M. Quantitative assessment of neuroprotection against NMDA-induced brain injury. Experimental Neurology 1989;106:289-296.

7. Wong E, Kemp J, Priestley T, Knight A, Woodruff G, Iversen L. The anticonvulsant MK-801 is a potent N-methyl-D-aspartate antagonist. Proceedings of the National Academy of Sciences 1986;83:7104-7108.

8. Kennedy DN, Filipek PA, Caviness VS. Anatomic segmentation and volumetric calculations in nuclear magnetic resonance imaging. IEEE Trans. Med. Imaging 1989;8(1):1-7.

9. Bull G, Oderwald-Nowak B. Standardizaton of a radiochemical assay of choline acetyltransferase and a study of the activation of the enzyme in rabbit brain. Journal of Neurochemistry 1971;18:935-941.

Chapter 5

Echo Planar Chemical Shift Imaging

Introduction

The previous work reported in this thesis has demonstrated that NMR spectroscopic measurements of neurodegeneration that use N-acetyl aspartate (NAA) as a neuronal marker provide a valid and sensitive index of neuronal loss that compares well with classical biochemical assays. This demonstration provides the foundation for the concluding objective of the present investigation: the development of novel, NMR spectrosopic techniques with which to assess neuronal loss in people suffering from neurodegenerative diseases.

Extant techniques for investigating the metabolic processes that underlie neurodegenerative disease processes are limited to *in vitro* biochemical assays (*e.g.* ChAT and GAD), localized, voxel NMR spectroscopy and single-slice, low spatial resolution CSI techniques.

Although localized NMR spectroscopy has been able to show concomitant decreases of NAA in neurodegenerative diseases, including Alzheimer's disease and the AIDS dementia complex (ADC) (1-6), the measurements remain focal, as shown in Figure 5.1 and thus limit the assessment of global patterns of degeneration that occur in these disease states. Moreover, although current CSI techniques provide a diffuse metabolic analysis, these techniques are limited to single slice techniques. A technique able to produce a high resolution, volumetric map of neuronal content could furnish important information about focal patterns of degeneration as well as global patterns of neuronal loss distal to lesion sites. Such a technique would be of great utility in assessing neurodegenerative disease processes that exhibit combined focal and diffuse neuronal loss. A principle goal of the last phase of this research was thus to develop CSI techniques able to acquire high spatial resolution, volumetric maps of neuronal content in reasonable imaging times.

While many methods of imaging spectral data have been proposed to date, no single method has yet demonstrated clear superiority. The methods that have been developed for chemical shift imaging, shown in Figure 5.2, can be categorized on the basis of how the spectral information is encoded: (1) Selective pulses (7-10). (2) Frequency encoding (11-15), and (3) Phase encoding (16-19)· By exciting the frequency to be imaged with a frequency-selective, narrow-band pulse, the selective pulse method can be used with standard imaging sequences to efficiently encode spatial dimensions. However, this

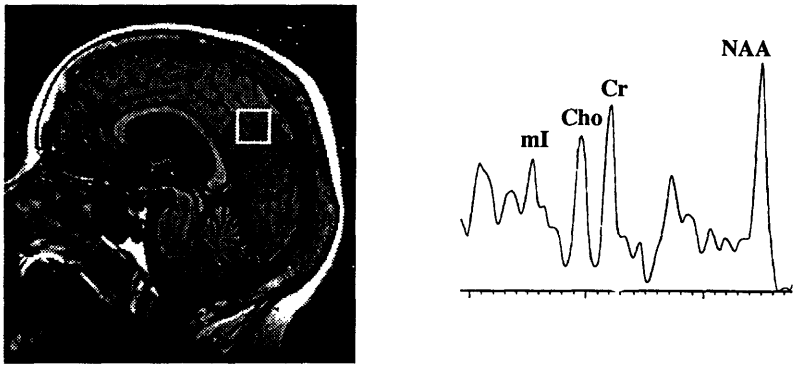

Figure 5.1 Localized ^{1}H magnetic resonance spectrum from a normal human volunteer

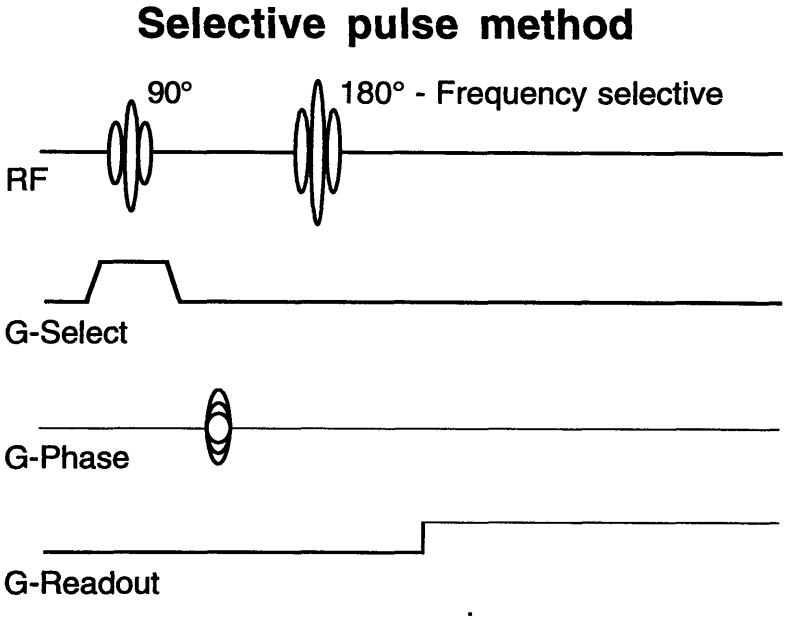

Figure 5.2a Conventional CSI sequence which combines narrow band frequency excitation with frequency and phase encoding for the spatial dimensions.

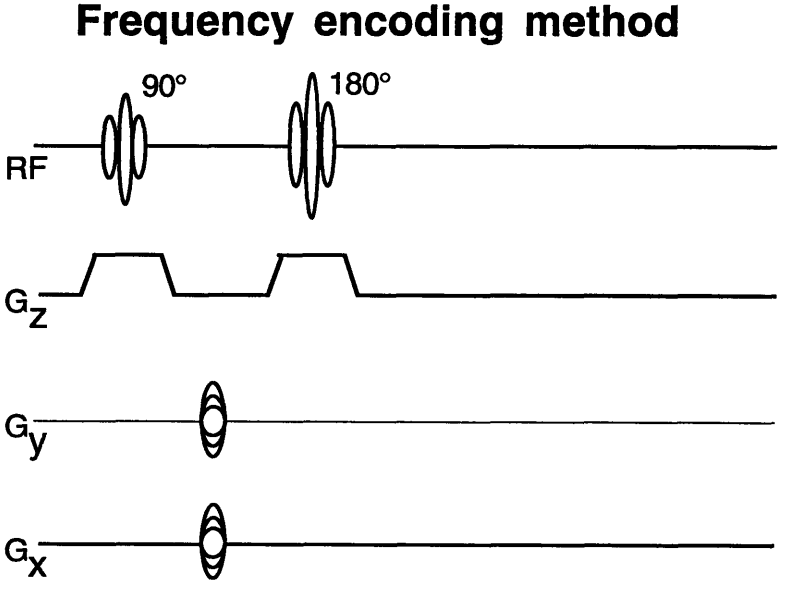

Figure 5.2b Conventional CSI sequence which combines frequency encoding of the frequency dimension with phase encoding for the spatial dimensions.

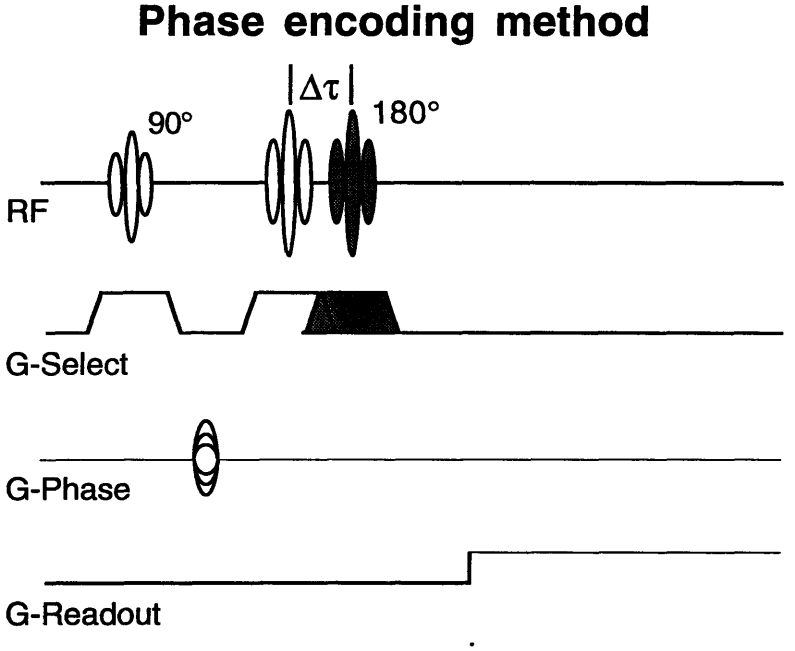

Figure 5.2c Conventional CSI sequence which combines phase encoding of the frequency dimension with frequency and phase encoding for the spatial dimensions.

method places severe constraints on the B_0 homogeneity: the variation of the field must be much less than the separation of the lines over the entire region being imaged. For this reason, it is not commonly utilized for quantitative applications. The frequency encoding method requires little prior knowledge of the spectrum and is, in principle, relatively insensitive to inhomogeneities in the field. However, since each spatial dimension must be phase encoded, imaging times per image can be long, leading to motion sensitivity as well as practical limitations on matrix size (typically to $<64^2$). Phase encode methods encode the chemical shift into the phase of the signal and can acquire high spatial resolution data efficiently through spatial frequency encoding, but are utilized less commonly than frequency encode methods, especially for metabolic work, because of their lower spectral resolution.

To date, the frequency encoding technique is the most commonly used for imaging spectral data, which requires that each spatial dimension be phase encoded (11, 12). This limitation becomes more pronounced when volumetric information is needed because of the time required to encode three spatial dimensions. Recently, groups have demonstrated techniques that combine multi-slice imaging with either conventional, phase-encoded CSI (20) or multi-echo CSI (21) to produce metabolite images over three to five slices of the brain. However, saturation effects and volume encoding time prevent CSI from providing contiguous slice, volumetric metabolic images.

The objective of the present research was to acquire rapidly the 3-D or 4-D data sets necessary for spectral characterization and high spatial resolution. For high concentration moieties such as water, high intrinsic SNR allows for high temporal resolution. For metabolite mapping, however, low intrinsic SNR precludes rapid imaging. Of equal concern, long acquisition times themselves become a critical, practical challenge. The high speed image acquisition sequences, such as echo planar imaging (EPI) (22) and RARE imaging (23), stand to significantly redefine chemical shift imaging because of their ability to explore spatial, spectral and temporal resolution tradeoffs. This derives from their ability to acquire individual images very rapidly, thus allowing a quick sampling of 3 or 4-D CSI data sets at high temporal and spatial resolution. The recent advent of Echo Planar Chemical Shift Imaging (EP CSI) (24, 25) offers a unique combination of echo planar imaging technology with phase encoded CSI. By sacrificing some spectral resolution, EP CSI can sample k-space rapidly and thereby produce metabolite maps with superior spatial resolution (<500μl voxel volumes). Unlike other conventional techniques, this approach lends itself easily to full 3D spatial encoding without a loss in temporal resolution because of the multiple number of excitations (NEX) required to obtain useful SNR. The experiments described in this work test the hypothesis that high speed imaging techniques offer significant advantages for at least some CSI applications.

The specific aim of this phase of research was to implement EP CSI on an *in vivo* GE Signa 1.5T human imager and to test the

hypothesis that EP CSI can provide volumetric maps of the distribution of NAA in the human brain. The goals of this work were therefore to evaluate the technique on phantoms of different millimolar concentration brain metabolites, to assess this technique in normal humans for producing high spatial resolution (≤ 6x6 mm) metabolite maps in reasonable imaging times, and to determine the technique's potential to provide information regarding the variation of neuronal content in the diseased brain.

Theory

EPI has been applied to chemical shift imaging (CSI) with limited successes (26, 27). EP CSI techniques successfully integrate the benefits of NMR spectroscopic encoding (16, 17) with EPI improvements in hardware and software. To acquire echo planar chemical shift images, an inversion recovery EPI sequence was modified to allow for multiple, sequential, temporal offsets of the 180° refocusing pulse. The chemical shift information, δ, is encoded in the initial phase of the spin-echo signal by changing the time period between the excitation and the 180 refocusing pulses at constant intervals ($\Delta\tau$). The signal intensity is a function of the signal phase and is governed by the following relation:

$$S_\tau(t) = \int \rho(x,\omega) e^{i\phi(x,\omega,\tau,t)} dx d\omega \quad [5.1]$$

where,

$$\phi = \gamma G_x x t + \omega(t - 2\tau) \quad [5.2].$$

and τ is the temporal offset of the 180° pulse. Replacing the signal phase expression [5.2] into [5.1], the following relation is obtained:

$$S_\tau(t) = \int \rho(x,\omega) e^{i\gamma G_x x t} e^{i\omega t} e^{-i\omega 2\tau} dx d\omega \quad [5.3]$$

By making the substitutions of equation [5.4] into equation [5.3].

$$\begin{aligned} k_x &= \gamma G_x t \\ k_\omega &= -2\tau \end{aligned} \quad [5.4]$$

the following expression is obtained.

$$S_\tau(k_x,k_\omega) = \int \rho(x,\omega) e^{ik_x(x+\omega/\gamma G_x)} e^{ik_\omega \omega} dx d\omega \quad [5.5]$$

Substitution of the following,

$$\begin{aligned} &\hat{x} = x + \omega/\gamma G_x \\ &\textit{where} \qquad [5.6] \\ &d\hat{x} = dx \end{aligned}$$

into equation [5.5], allows a more familiar expression relating the spin signal intensity to the Fourier transform of the spin density ρ.

$$S_\tau(k_{\hat{x}},k_\omega) = \int \rho\left(\hat{x} - \omega/\gamma G_x, \omega\right) e^{ik_x \hat{x}} e^{ik_\omega \omega} d\hat{x} d\omega \quad [5.7]$$

Equation [5.7] shows the relationship of the spin density ρ to the signal intensity S_τ. The spin density relationship in equation [5.7] demonstrates the chemical shift artifact observed in imaging through the translation by ($-\omega/\gamma G$) of the spin density as a function of chemical shift, ω.

Equation [5.7] relates the spin density and the signal intensity in a continuous case. Yet these signals are sampled discretely and because of this, these sampled signals must be transformed with a Discrete Fourier Transform (DFT) to obtain an image. After a 1DFT in the x-direction, the sampled signal as a function of the spin density ρ becomes:

$$S_\tau(x,k_\omega)=\int\rho\left(x-\omega/\gamma G\right)e^{ik_\omega\omega}d\omega \quad [5.8]$$

The DFT will only be treated in the chemical shift direction here, because the artifacts in the x and other spatial directions are well understood.

$$\hat{\rho}_n = image = \sum_{k=0}^{N-1} S_\tau(x,k_\omega)e^{-2\pi ink/N} \quad [5.9]$$

Substituting equation [5.8] into [5.9] produces the following equation:

$$\hat{\rho}_n = \int\rho(x-\omega/\gamma G)d\omega\sum_{k=0}^{N-1}e^{ik_\omega\omega}e^{-2\pi ink/N} \quad [5.10]$$

Yet, this relation can be simplified by substituting equation [5.4] into equation [5.10] and letting $\tau=(k/N)T_{max}$. Where T_{max} is the maximum temporal offset of the 180°pulse. These substitutions and simplifications result in the following expression:

$$\hat{\rho}_n = \int\rho(x-\omega/\gamma G)d\omega\sum_{k=0}^{N-1}e^{i\omega(-2k/NT_{max})}e^{-2\pi ink/N} \quad [5.11]$$

This simplifies to the following relationship through simple substitution.

$$\hat{\rho}_n = \int\rho(x-\omega/\gamma G)d\omega\sum_{k=0}^{N-1}e^{-2\pi ik/N(n+\frac{\omega}{\pi}T_{max})} \quad [5.12]$$

The term within the summation can be simplified through utilization of the power series relationship $\sum_{k=0}^{N-1}x^k=\frac{1-x^N}{1-x}$ to obtain the following equation.

$$\hat{\rho}_n = \int\rho(x-\omega/\gamma G)d\omega\frac{1-e^{-2\pi i(n+\frac{\omega}{\pi}T_{max})}}{1-e^{\frac{-2\pi i}{N}(n+\frac{\omega}{\pi}T_{max})}} \quad [5.13]$$

Recognizing that the spectral resolution in (rad/s) is given by the relation $\Delta\omega=(-\pi/T_{max})$, and simple algebraic manipulation of the expression allows the following simplification to occur.

$$\hat{\rho}_n = \int \rho(x - \omega/\gamma G) d\omega \frac{1 - e^{-2iT_{max}(\omega - n\Delta\omega)}}{1 - e^{\frac{-2iT_{max}}{N}(\omega - n\Delta\omega)}} \quad [5.14]$$

This F(ω–nΔω) is the point spread function associated with EP CSI. Simplification of F(ω–nΔω) results in the following expression.

$$F(\omega - n\Delta\omega) = e^{-iT_{max}(1-\frac{1}{N})(\omega - n\Delta\omega)} \left(\frac{Sin(T_{max}(\omega - n\Delta\omega))}{Sin\left(\frac{T_{max}}{N}(\omega - n\Delta\omega)\right)} \right) \quad [5.15]$$

The first exponential expression is a phase roll that results from asymmetric Discrete Fourier transformation with respect to the origin because the tau offsets are generally performed symmetrically about the null tau offset. This was not done in our treatment for mathematical simplicity, so the phase roll can be ignored. The second expression is the familiar Sinc-like function that is the point spread function resulting in the majority of magnetic resonance imaging because of truncated k-space sampling.

Figure 5.3 is an illustration of this function and demonstrates the distribution of signal intensity as a function of (ω–nΔω). The amplitude of the wings from the Sinc significantly distributes the signal from one particular frequency bin into adjacent frequency bins if it is not precisely on resonance. This spectral bleeding results because of the limited number of phase encode steps used to encode the chemical shift information. It hinders quantification because of the uncertainty of one particular frequency bin that contains all of its respective frequency.

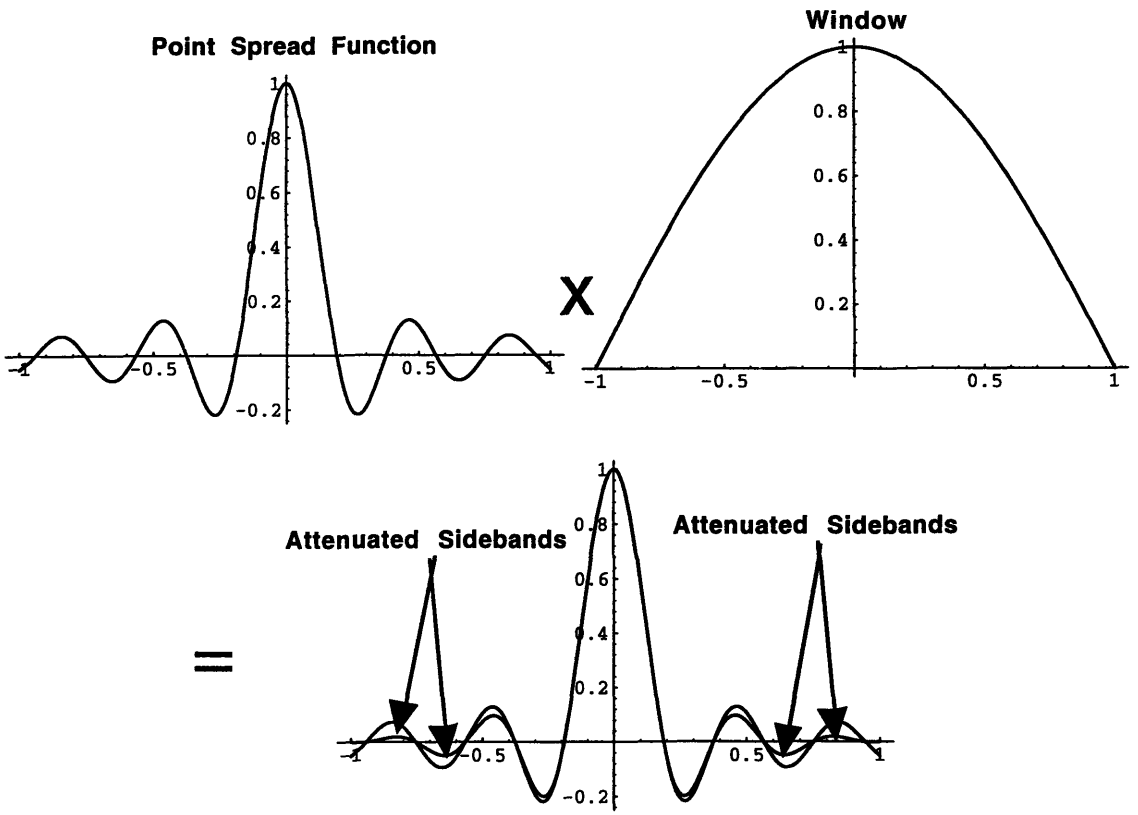

Figure 5.3 Illustrates the point spread function (psf) of the EP CSI technique and the effect of a Hanning window on the psf.

Spectral windowing, in particular, convolution with a Hamming window prior to Fourier Transformation, ameliorates this problem by attenuating the amplitude of the wings from the Sinc, at the sacrifice of some spectral resolution (33). Therefore, Hamming windowing will be incorporated prior to Fourier transformation in the EP CSI images.

Signal:Noise

Achieving a useful signal to noise ratio (SNR) is a significant limitation in CSI because of the low *in vivo* concentrations of metabolites within the central nervous system (~10,000 times lower than those found in fat and water). Extensive signal averaging and decreased spatial resolution are required to obtain images with useful SNR. For example, NAA has a concentration of ≤ 10mM *in vivo*, which translates to 30mM for the protons of the methyl group that resonate at 2.0 ppm. Comparing this to water (whose protons possess an *in vivo* concentration of ~ 80M), a 16 million fold increase in time would be required for equivalent SNR and spatial resolution, because of the second order relationship between signal averaging and SNR (28). Hence, depending on the particular biological application, in order to collect data in reasonable imaging times, one must accept lower SNR or sacrifice spatial resolution to increase the SNR per voxel.

To produce volumetric maps of neuronal content with high spatial resolution, EP CSI allows a unique tradeoff of decreased spectral resolution for improved spatial resolution with virtually no sacrifice in SNR as compared to conventional frequency encoded CSI (11). To

better understand the relationship between EP CSI and conventional CSI, a formal comparison of SNR is presented.

For an image of matrix size MxN, with effective pixel sizes of Δx and Δy in the spatial encode directions and a final signal bandwidth of Δf(Hz) (equivalent white-noise bandwidth of the base band processor filter), the signal-to-noise ratio becomes :

$$\Psi_{rms} = C\Delta x\Delta y\left(MN/\Delta f\right)^{1/2} \quad [5.16]$$

where C is a constant that incoporates the factors common to both imaging modalities,(*i.e.* η, K, μ_o, Q, ω_o, V_c, F_1 and k, defined above). A conventional CSI experiment with the following parameters, fov_x = fov_y = 20 cm, M = N= 64 pts in each spatial dimension, producing $\Delta x=\Delta y$= 3.125mm spatial resolution and Δf = 1kHz with 64 points in the spectral dimension, will produce an SNR of 6.25C in 4096s of imaging time, assuming a repetition rate of 1 second. Ignoring T1 and T2 effects for the present, a similar comparison can be made for the EP CSI experiment. The rapid sampling required to traverse k-space rapidly limits the bandwidth to 200kHz, while hardware limitations constrain the fov in the read-out direction to 40 cm with EPI. Therefore, a symmetric (40cm) fov will be maintained as above, and 128 lines will be encoded in both directions to maintain the same pixel dimensions. This is done without a sacrifice in time because spatial encoding is rapid with EP CSI. By using 64τ offsets at τ =1ms to phase encode the chemical shift information and maintain the same spectral resolution for both techniques, one obtains a SNR of ~0.6 in 64s ignoring T1 and T2 effects. This translates to an SNR of 6.4C in the same 4096 seconds

of signal averaging. Hence, the two methods have comparable SNR in the same averaging time, based on a comparison of imaging methods alone, and ignoring T1 and T2 effects for the present.

Methods

To acquire echo planar chemical shift imaging (EP CSI) data, an echo planar (EPI) spin echo imaging sequence was modified to allow multiple, sequential (τ) offsets of the 180° refocusing pulse. This sequence, shown in Figure 5.4, is essentially an echo planar version of the CSI technique first described by Sepponen (16, 17). In this technique, each rf excitation is fully encoded in two spatial directions with an echo planar acquisition. The k-space traversal of this sequence is shown in Figure 5.5. The 180° pulse is moved temporally on sequential acquisitions to encode the chemical shift into the phase of the signal. This produces a phase shift (ϕ) which results from signals that are spectrally off-resonance by the amount $f=\phi/2\tau$, where τ is the temporal offset of the 180° pulse. The spectral frequency resolution, Δf, is determined by the maximum relative displacement of the 180° pulse, $\Delta f=1/2|\tau max - \tau min| = 16Hz$ and the spectral width is thus $f=1/2\Delta\tau$.

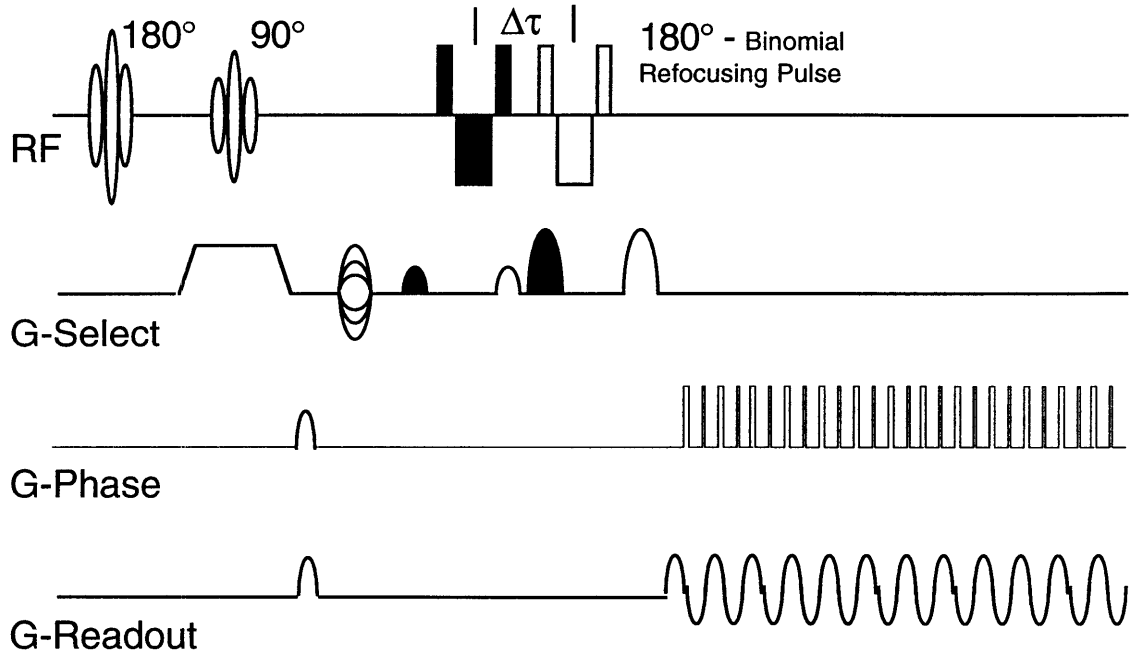

Figure 5.4 EP CSI sequence which combines phase encoding of the frequency dimension and z direction with echo planar imaging for encoding the x and y spatial dimensions.

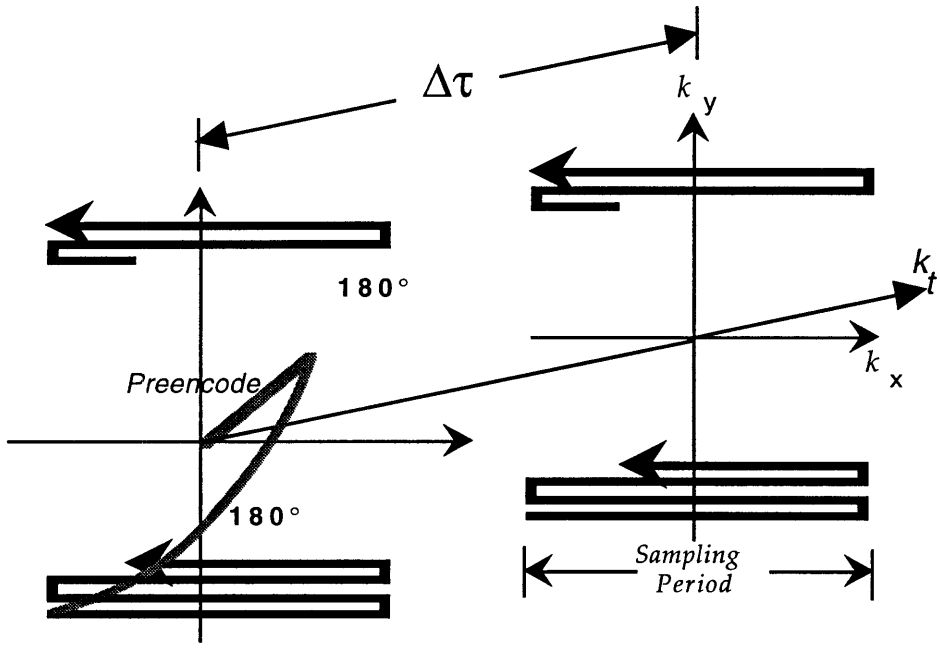

Figure 5.5 K-space trajectory of EP CSI sequence. Each 180° pulse encodes the chemical shift into the phase of the signal and encodes a full image by an EPI acquisition.

Water/lipid suppression:

The protons from water are in a concentration of 80M within the brain, while the protons of cerebral brain metabolites are in physiological concentrations of ≤ 30mM. This discrepancy in concentration is ≥ 2000 and is impossible for most analog-to-digital converters to resolve. Moreover, inadequate water suppression allows spectral contamination of the water resonance's Lorentzian wings into surrounding moieties. Therefore, adequate water suppression must be provided when attempting to perform proton CSI. A frequency-selective, binomial 1$\underline{4}$6$\underline{4}$1, 180° pulse was used to provide water suppression for EP CSI (29). This pulse is B_0 insensitive, with less than a 1% change in suppression in a range ±1/4 ppm around the peak of interest; close to the transmitter frequency it is insensitive to small variations in B_1. At the carrier frequency, the net flip angle is zero, irrespective of the rf field, while at small frequency offsets the compensation responsible for the flatness of the null is largely unaffected by expected changes in B_1. This pulse has been optimized for maximal excitation of the methyl protons of NAA resonating at 2.0ppm. Figure 5.6 demonstrates the analytical suppression characteristics of the binomial (1$\underline{2}$1) and (1$\underline{4}$6$\underline{4}$1) pulses obtained from calculations done by Hore et. al. (29). Alongside this is a plot of the signal amplitude as a function of frequency offset that represents the empirical suppression characteristics of the (1$\underline{4}$6$\underline{4}$1) pulse.

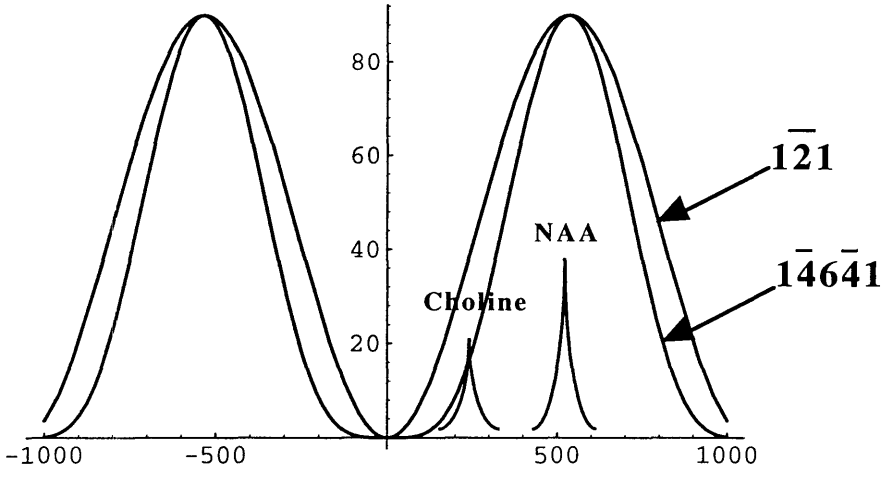

Figure 5.6a Analytical suppression characteristics of 121 and 14641 binomial pulse.

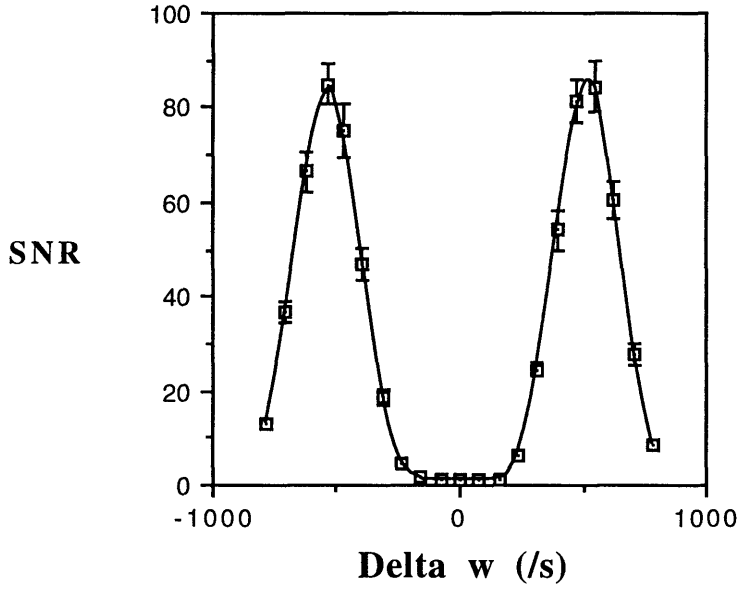

Figure 5.6b Empirical suppression characteristics of 14641 binomial pulse.

The signal caused by extraneous lipids that originate from the scalp also pose a significant problem in CSI. This signal is a multi-resonant waveform that predominates in the 1.5ppm region. The resonances are an inconvenience because their concentration is 100-1000 times greater than that of the metabolites of interest, and their short T2's broaden their resonances to overlap with resonances of interest (i.e. NAA and lactate). To achieve adequate suppression of this resonance, an inversion recovery technique was implemented to exploit the large T1 difference between lipids (~250ms) and metabolites (≥ 1400 ms) (30-32). The signal intensity of NAA and fat can be simulated as a function of TI, TR, and TE is given by the following relationship.

$$SI = SI_0\left(1 - 2e^{-TI/T1} + e^{-TR/T1}\right)\left(e^{-TE/T2}\right) \quad [5.17]$$

The residual signal intensity as a function of inversion time for NAA and lipids is shown in Figure 5.7. Although there is a sacrifice in SNR concomitant with inversion recovery techniques (~30%), the imaging of NAA, which is chemically close (<1/2 ppm) to fat, makes this loss necessary.

Volumetric encoding

To provide volumetric coverage, phase encoding in the z-direction has been included as shown in Figure 5.4. To reduce truncation artifacts in the z-encode direction from limited sampling, the number of z-encode steps was doubled (16 encoding steps for human applications), while the maximum amplitude of the

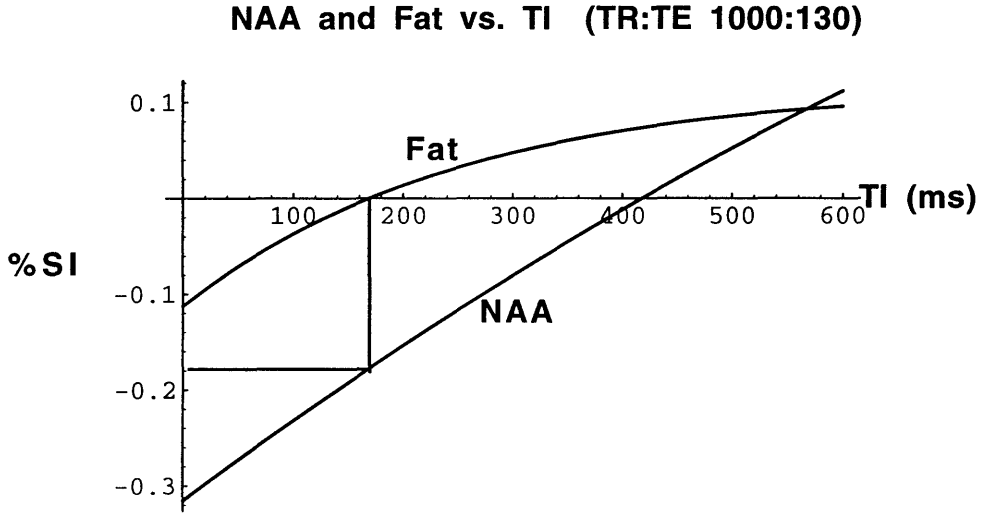

Figure 5.7 Analytical graph demonstrating the residual signal intensity as a function of inversion time for NAA and lipids.

z encoding gradient in that direction was reduced by a factor of two prior to imaging. This preserves the effective slice thickness for the chemical shift images and provides a 2x oversampling scheme within the volume being excited, while reducing possible Gibbs ringing (33) and wrap-around artifact by discrete Fourier transformation of limited encoding steps.

B0 compensation

B_0 compensation was performed by an automated shimming algorithm that fits $\Delta B_0(r)$, measured as a phase difference between asymmetric spin echoes, to a truncated orthonormal basis of spherical harmonics, and re-adjusts the shims to compensate for the calculated offset for each harmonic (34). This is done prior to each investigation by shimming on nine slices surrounding the slice of interest. Two sets of multislice images, 40cm x 40cm in size, with a data matrix size of 128x128, TE/TR 80/3000, and a slice thickness of 15mm, are acquired with the EP CSI sequence. No solvent suppression is performed during this phase of the experiment, but extraneous lipids are suppressed with pre-saturation techniques.(35) A symmetric and an asymmetric data set are taken with the refocusing pulse offset by 2.2ms (τ). A frequency map f(r) is then computed in each pixel using:

$$f(r) = \frac{1}{4\pi\tau} \arctan\left[\frac{S_a(r)}{S_b(r)}\right] \quad [5.18]$$

where τ is the echo offset, and $S_a(r)$ and $S_b(r)$ are the complex signal values from the paired images a and b at spatial location r (36). With τ=2.2ms, the lipid signal advances an extra 2π radians, thereby

providing a signal that supplies accurate B_0 information and is free from fat-water interference (37). f(r) is then fit to a constant plus the four controllable shims (z1,z2,x,y) by using a least-squares fit. The magnitude data of the signal in each pixel is used as a weighting for the chi-square value of the fitted coefficients. Because the frequency is computed from the phase of the MR image, the standard deviation σ at each pixel is approximately equal to the inverse of the magnitude. The shims are then adjusted and the process is reiterated until convergence is attained. This usually takes 2 or 3 iterations (34).

Imaging Protocol

Imaging was performed by using a resonant gradient system (ANMR Systems Inc.) retrofitted to a GE Signa 1.5 Tesla whole body system. Imaging protocols consisted of T1-weighted sagittal localizers (TR/TE:600/16). Shimming was performed by using the automated shimming algorithm and parameters as detailed above, followed by EP CSI. Lipid suppression was performed by tweaking the inversion time TI= ~160±10ms until minimization of lipid signal was attained. This was done by measuring a region of interest in the scalp after one excitation. The EP CSI sequence utilized the following parameters: TE/TR = 130/1000ms; τ offset = -17.6 to 16.5 ms in 1.1ms $\Delta\tau$ increments resulting in a 500Hz spectral width; 128x128 matrix with 40cm x 40cm FOV (3x3mm voxel size) and 10 cm slab thickness encoded with 16 phase encode steps (over 20 cm z-encode field of view, resulting in 2x oversampling). Complete 4-D CSI data acquisition times were 34 and 68min for NEX=64 and 128.

The images were reconstructed by a Hamming windowed 3DFT through the x,y, and δ dimensions. NAA maps were then generated by spectral averaging the spectral bins of 2.0±1/4ppm, because of imperfections in B_0 compensation.

Results

Phantom experiments

Figure 5.8 demonstrates the application of EP CSI to simple phantom systems of fat and water. Neither lipid nor solvent suppression was utilized in this experiment. CSI data was filtered in 3 dimensions prior to Fourier transformation, resulting in 6mm in-plane resolution. SNR values measured ~320:1 for fat and ~2000:1 for water.

To assess the capability of EP CSI to produce chemical shift images of metabolites possessing *in vivo* concentrations, phantoms of NAA and choline at 10mM concentrations, doped with Gadolinium to shorten the T1 to ~250 ms, were investigated. Because lipid suppression was not required, the inversion pulse was not utilized in this experiment. The parameters of the experiment were as outlined above, with the following changes: TE/TR = 115ms/ 500ms; 15mm slice thickness; NEX = 64 and 16 resulted in imaging times of ~17 and ~4min, respectively. Figure 5.9a demonstrates the application of EP CSI on phantoms of NAA and choline.

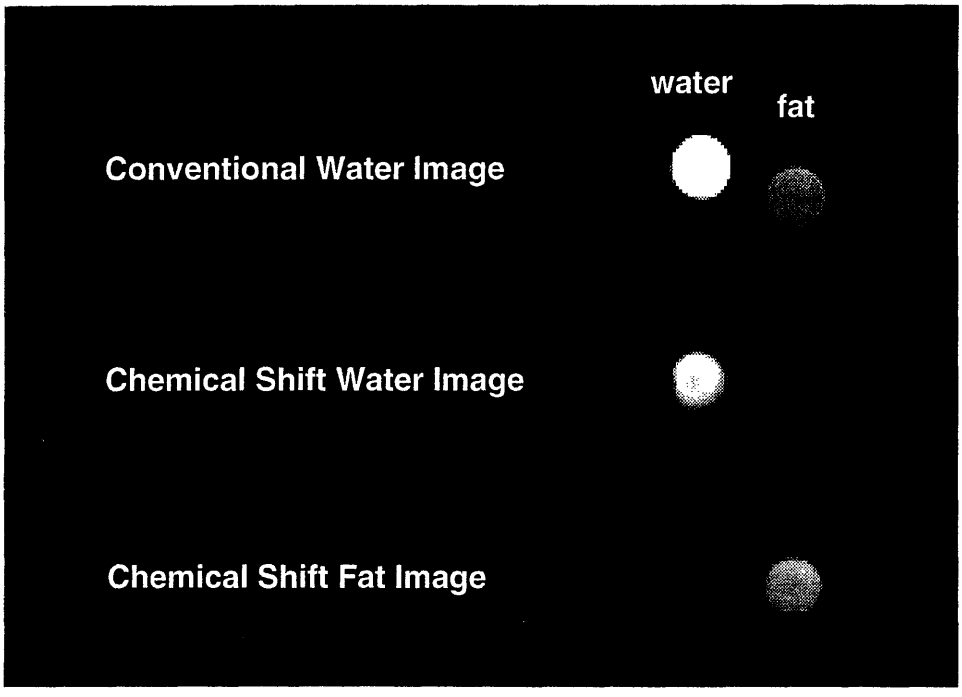

Figure 5.8 EP CSI experiment depicting the capability of EP CSI to adequately separate different chemical shifts by phase encoding the frequency into the phase of the signal. Imaging parameters remained as outlined before, except for the following changes: TE/TR = 115ms/3 s; 10mm slice thickness; and NEX = 1. Complete 3-D CSI data acquisition times were 192 seconds.

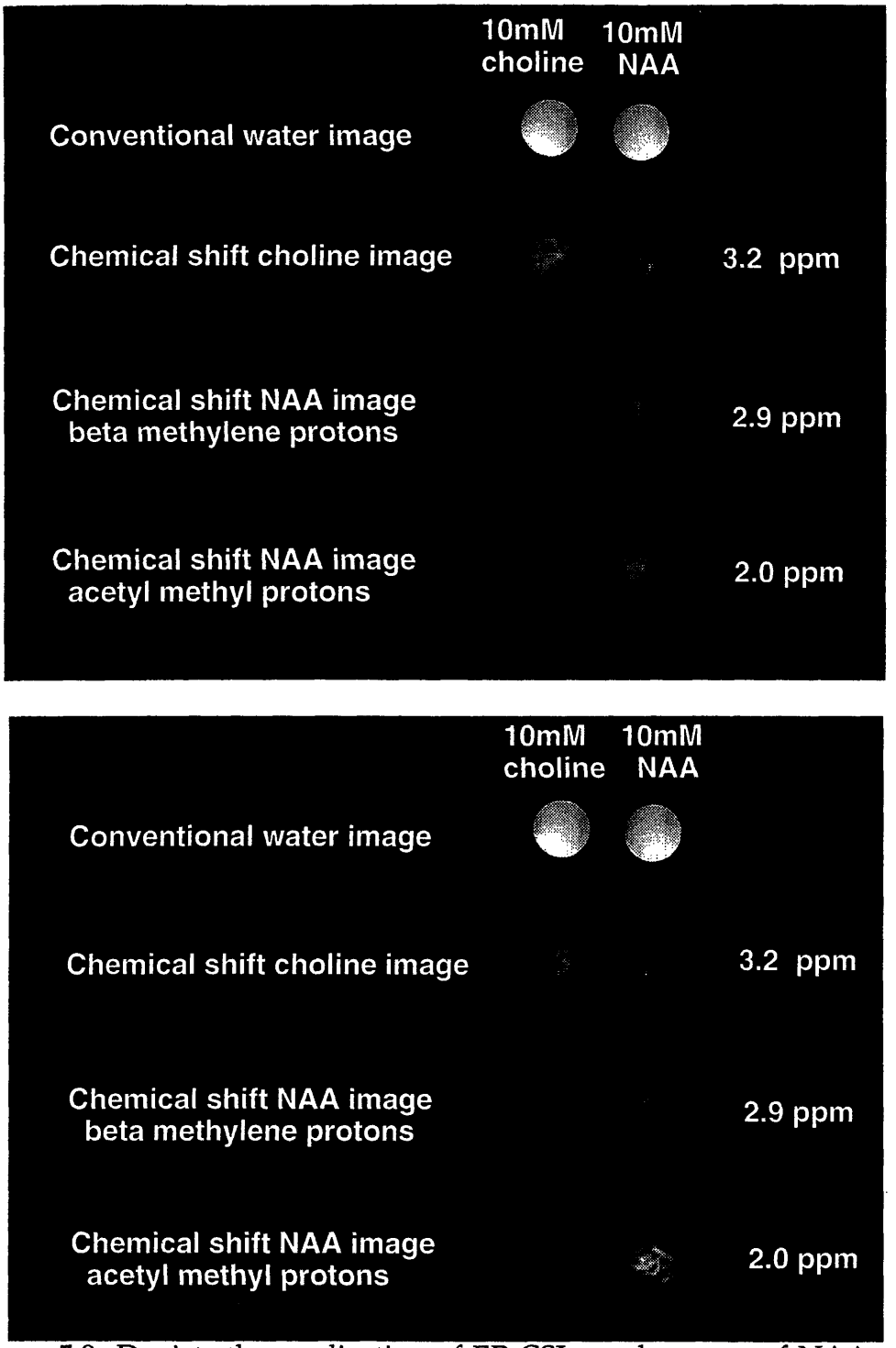

Figure 5.9 Depicts the application of EP CSI on phantoms of NAA and choline with 10mM concentrations. The top figure (a) shows images with NEX=64 and the bottom images (b) show images with NEX=16.

SNR values measured ~9:1 for NAA (2.0ppm), ~7:1 for NAA (2.9ppm), and 11:1 for choline (3.2ppm)for NEX=128. The binomial (1$\underline{4}$6$\underline{4}$1) was optimized for resonances occurring at 2.6ppm (133 Hz off resonance) to allow for comparable excitation of both choline and NAA. The close proximity of the beta methylene protons of NAA to the optimal frequency results in the high SNR of this resonance. Figure 5.9b shows this same experiment performed with NEX=16, reducing the imaging time to ~4min. SNR values are ~5:1 for NAA(2.0ppm) and ~4:1 for NAA(3.0ppm) and 6:1 for choline(3.2ppm).

Human Experiments

Figure 5.10 represents metabolite maps obtained from a normal volunteer investigated with a 15mm slice thickness and no spatial encoding in the z direction. In this case, a (1$\underline{2}$1) binomial sequence provided better suppression, (as determined by region of interest analysis during tweaking of lipid and water suppression prior to acquisition), than the (1$\underline{4}$6$\underline{4}$1) and was optimized for the NAA(2.0ppm) resonance. Parameters were as illustrated in methodology. Complete 3-D CSI data acquisition times were 34 minutes with NEX=64 and 68 minutes for NEX=128. A Hamming window was again applied in all three dimensions prior to Fourier transformation to minimize truncation artifacts and improve signal to noise at the expense of some spatial resolution. Figure 5.10 shows a T2 weighted Echo Planar water image for anatomical reference alongside the NAA metabolite maps, (2.0ppm ± 1/4ppm), shown without spatial averaging for true 3x3mm in-plane voxels (NEX=64 -5b, NEX=128 -5c).

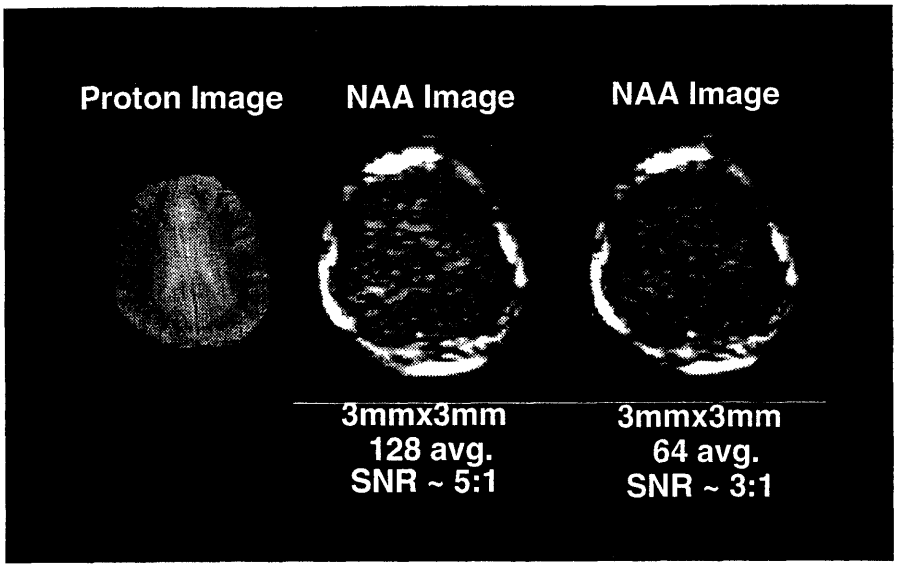

Figure 5.10 T2-weighted and EP CSI NAA maps from one slice of a normal human volunteer. TE/TR = 130/1000ms; TI= ~160ms for lipid suppression; t offset = -17.6 to 16.5 ms in 1.1ms $\Delta\tau$ increments resulting in a 500Hz spectral width; 128x128 matrix with 40cm x 40cm FOV (3x3mm voxel size)

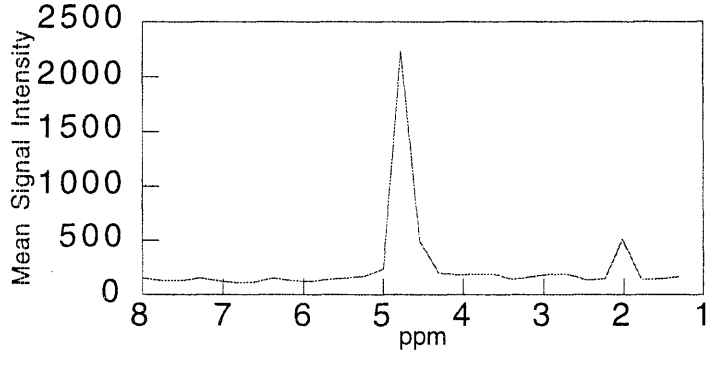

Figure 5.11 Spectrum from an 8ml. region of interest within the slice.

A spectrum obtained from a 8ml region of interest within the brain is displayed below in Figure 5.11. SNR in the NAA image measured ~5:1 for NEX=128 at 3x3mm resolution. Water and extraneous lipid were efficaciously suppressed by factors of 1000 and 20, respectively.

Figure 5.12 demonstrates the first efforts to produce volumetric neuronal maps of the brain. In this case, a 10cm slab was excited with 5 phase encodes in the z-direction, producing an effective slice thickness of ~20mm. These results demonstrate metabolite images from two slices corresponding to the NAA protons at 2.0 ppm, shown along with theirconcordant water images and a spectrum from an 8ml. region of interest taken from the cortex. Images from NAA, choline and creatine, and a fat image with no signal contamination within the brain parenchyma are shown as well. SNR measured ~ 8:1 for NAA. Because of the increase in effective slice thickness, water and lipids were not as efficaciously suppressed (approximately a factor of 100 and 10, respectively).

Figure 5.13 is a sagittal image along the mid-line of a healthy, young adult volunteer. The slab in white (12cm) demonstrates the slab that is excited for the EP CSI experiments. Figure 5.14 shows the volumetric map of NAA and residual water produced using EP CSI. CS images were processed using a Hamming window in 2 spatial dimensions (x and y) and in the spectral dimension (δ), resulting in 6x6x15mm spatial resolution. SNR measured ~5:1 for NAA from an 8ml region of interest within the parietal lobe of the center slice.

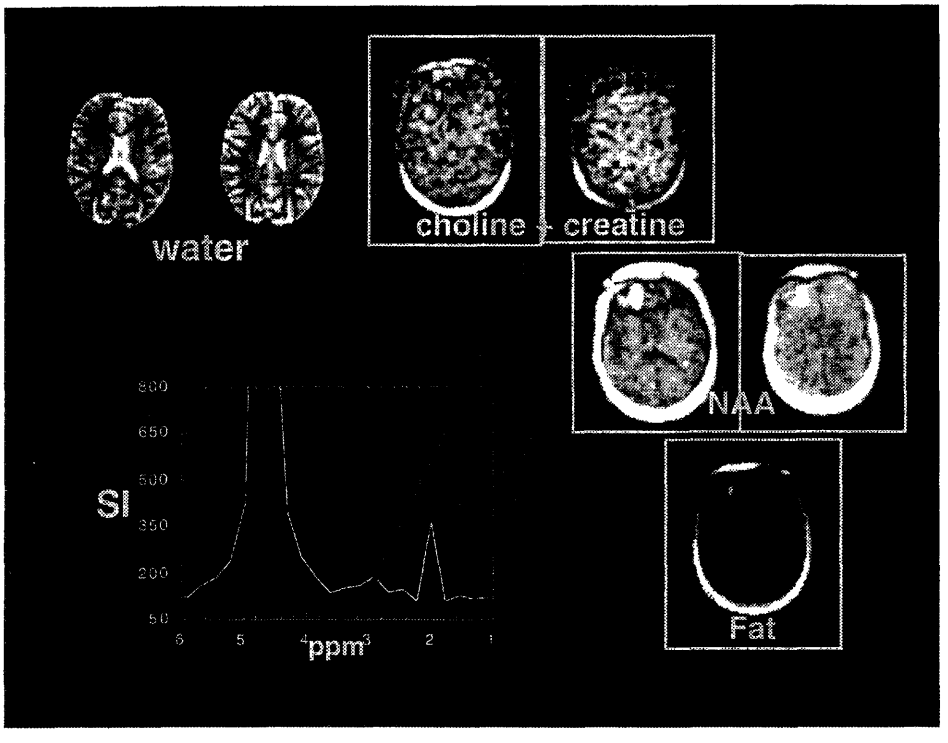

Figure 5.12 Shows water images and metabolic images (NAA and choline/creatine) from two slices within the brain of a normal human volunteer acquired with the EP CSI sequence.

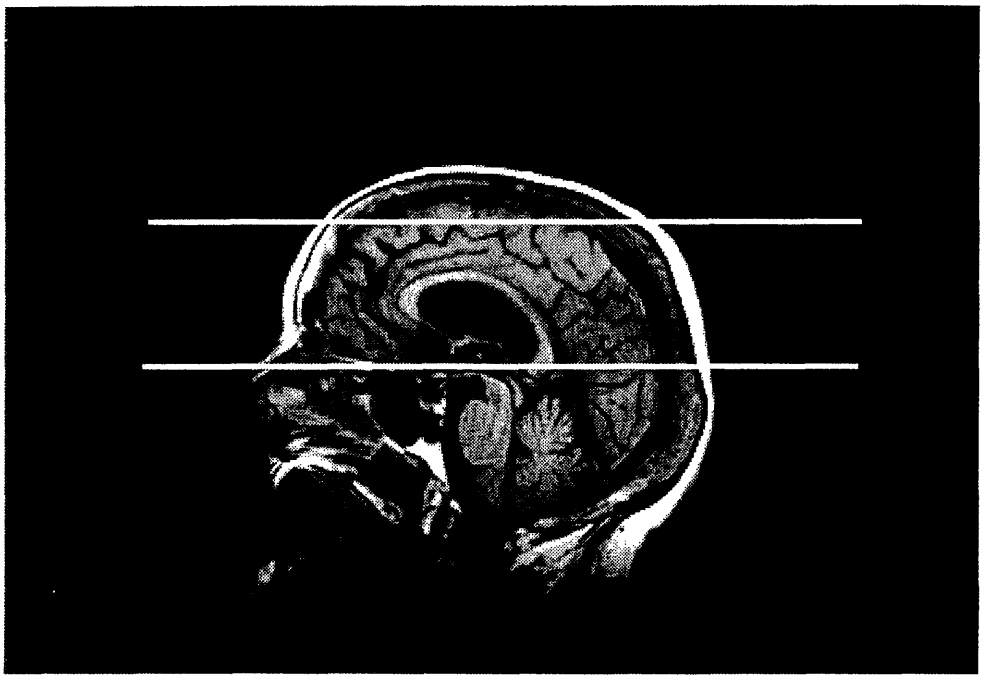

Figure 5.13 Shows the 10cm slice that is excited for 4D acquisition using 2x oversampling in the z-encoding direction concomitant with EP CSI.

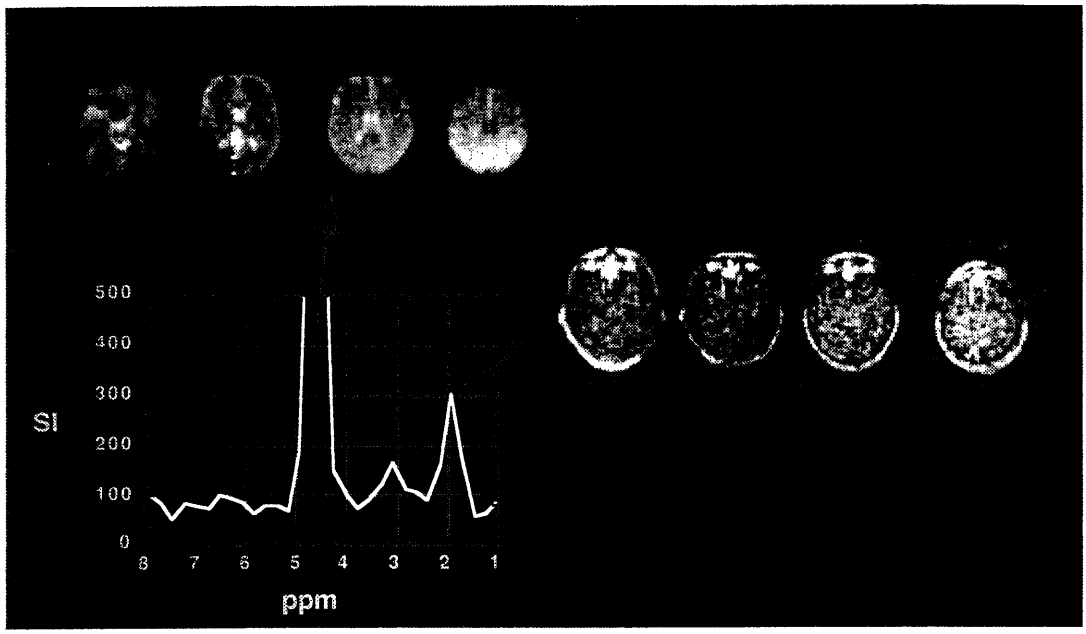

Figure 5.14 Residual water and NAA maps from four 15mm contiguous slices of a normal human volunteer. Parameters included: 8cm slab thickness with 16 phase encodes in the z direction; a 2x oversampling scheme was employed resulting in 10mm effective slice thickness for each chemical shift image; TE/TR = 130/1000ms; TI= ~160ms for lipid suppression; τ offset = -17.6 to 16.5 ms in 1.1ms $\Delta\tau$ increments resulting in a 500Hz spectral width; 128x128 matrix with 40cm x 40cm FOV (3x3mm voxel size); total acquisition time = 68min.

Discussion

The data demonstrate that EP CSI can produce high spatial resolution metabolite maps within reasonable imaging times. By combining EPI's ability to traverse k-space rapidly through the use of a technique that encodes the chemical shift information into the phase of the signal, EP CSI is capable of producing chemical shift images *in vitro* for simple phantom systems and *in vivo* for cerebral metabolites. Figure 5.8 demonstrates that adequate spectral resolution is achieved by encoding the chemical shift into the phase of the signal. Figure 5.9 illustrates that EP CSI can produce chemical shift images of cerebral metabolites (*i.e.* NAA and choline) that possess *in vivo* relevant concentrations of ≤ 10mM with SNR measurements of ~9:1 for NAA methyl moiety at 2.0ppm. This finding shows that the signal averaging required to produce adequate SNR was not burdened by any possible deleterious phase incoherences between acquisitions. The Hamming window used prior to processing aided, but did not eliminate, all truncation artifacts in the chemical shift dimension. The spectral resolution is clearly capable of discriminating the major resonances that appear at longer echo times (≤ 100ms).

Figure 5.10 demonstrates the first efforts of EP CSI to acquire *in vivo* chemical shift images of the distribution of NAA within one slice of a normal human. The images in the middle and right are echo planar metabolic images representing the distribution of the 2.0ppm NAA resonance. Lipid signal is observed in the scalp region within the NAA image. This is due to insufficient lipid suppression and

overlapping signal arising from the shoulders of the lipid resonance. Although this indicates some of the spectral resolution limitations of the technique, its superior spatial resolution is demonstrated by the absence of a spatial overlap of the lipid signal into the brain parenchyma. This eliminates the need for box-like excitations and allows for full cortical excitation and discrimination. SNR measurments of ~5:1 for NEX=128 (68min) and ~3:1 for NEX = 64 (34min).

To compare these SNR measurements to theoretical measurements, the SNR of NAA after one excitation was extrapolated from measured values of water (~270:1 for 3x3x10mm and 128x64 acquisition matrix) in our EPI instrument. Taking the concentration differences (~80M protons for water and ~30mM protons for NAA) into account, the SNR was determined to be ~(0.2:1) for NAA after one excitation. This value was used to estimate the SNR of NAA using the following equation:

$$SI = SI_0\left(1 - 2e^{-TI/T1} + e^{-TR/T1}\right)\left(e^{-TE/T2}\right) \quad [5.19]$$

Figure 5.15 shows SNR estimates for 68, 34, and 17min. of signal averaging assuming full excitation of the NAA signal at each repetition. The SNR of (~5:1) agrees well with the theoretical estimates (~6:1) assuming a $(2)^{1/2}$ increase with spatial windowing and a linear increase of SNR with slice thickness.

Figure 5.11 is a spectrum from a 5ml ROI acquired through the right hemisphere. It illustrates the good level of water suppression achieved by the binomial pulse. The NAA peak at 2 ppm is clearly

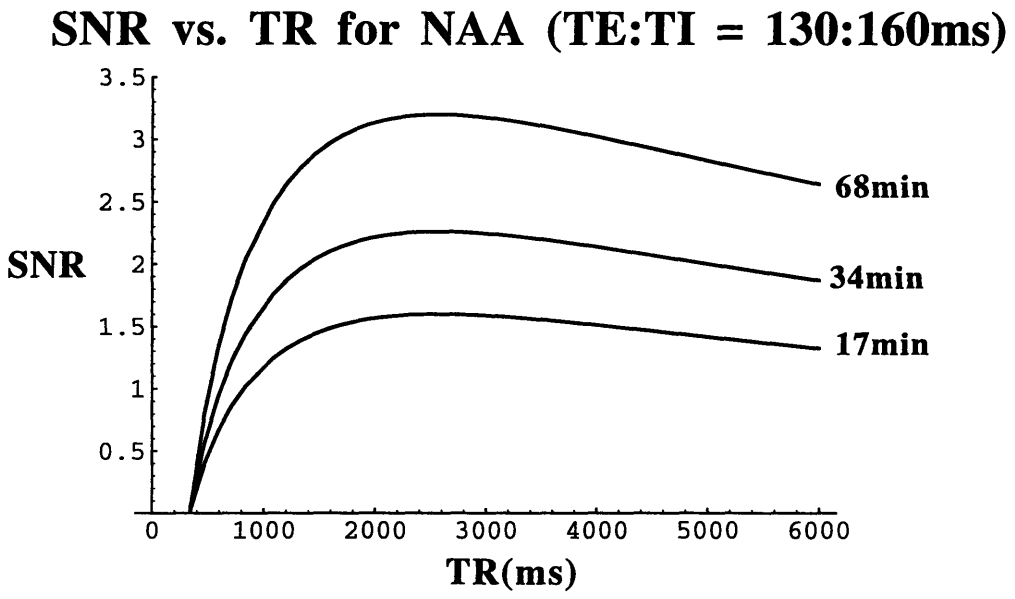

Figure 5.15 Analytical simulation of SNR vs. TR for EP CSI with inversion recovery and the parameters TE:TI = 130:160ms.

visible, with suggestions of other peaks existing in the 2.5-3.5ppm range. Moreover, there is no lipid resonance within the spectrum which demonstrates the ability of this technique to spatially separate the spectral frequencies.

Figure 5.12 demonstrates the first efforts in this research to obtain volumetric maps of the distribution of NAA within the human brain. In the case of Figure 5.12, a slab of ~10cm was excited with 5 z-encodes to produce an effective slice thickness of ~20mm. The results show metabolite images from two slices of the 3D set. A NAA image with improved SNR, achieved through the increased effective slice thickness, is clearly resolved. An image showing the distribution of choline/creatine, with SNR limited by the suppression bandwidth of the binomial, is also clearly resolved. A fat image, with no signal contamination in the parenchyma, demonstrates that the spectral resolution, although limited, can clearly resolve major peaks in the proton spectrum that are visible at longer echo times. The region of signal intensity increase within the frontal lobes of the NAA image can be attributed to the retro-orbital fat that that rings through in the z-direction as a result of limited z-encoding.

Figure 5.14 demonstrates the most recent efforts in this study to obtain volumetric maps of neuronal content within the human brain. Here, a 120cm slab was excited and encoded with a 2x oversampling scheme to produce eight, 15mm slices across the cerebrum. The figure shows four slices, encompassing the cerebrum, which represent the NAA and water peaks, along with a spectrum from a 8ml voxel within

the the parietal lobe of the center slice. The SNR measures ~5:1 and agrees well with theoretically calculated results. The 2x oversampling, which increases the number of z-encodes to 16, ameliorates the spatial smearing along the z encoding direction.

The data, although demonstrating the feasibility of the technique, reaffirms an SNR limitation caused by encoding the spatial dimensions at 3x3mm. This limitation becomes pronounced when accurate comparisons of neuronal loss are to be made with high statistical confidence. To discern accurately the neuronal loss within one voxel of the brain (encoded at 3x3x15mm), the probability of one comparison is multiplied by the number of comparisons made. This is known as a Bonferonni statistical correction. Hence, the probability of one voxel being statistically different ($p<.05$) from the rest of the pixels within the brain is a function of the SNR and the number of pixels being compared. If $P(z=z_0)$ is the statistical confidence that we desire and z is the z-score of the data, then this expression becomes

$$P(z=z_0)=\frac{1}{\sqrt{2\pi\sigma^2}}\int_{z_0}^{\infty} e^{-z^2/2\sigma^2}dz \quad [5.20]$$

This simplifies to

$$P(z=z_0)=\frac{1}{z_0}e^{-z_0^2/2} \quad [5.21]$$

when $z_0>1$. Assuming that the brain contains approximately 15,000 (3x3x10) voxels and that the probability of detecting a change in the absolute content of NAA will be at the 0.05 confidence level, then z_0 becomes approximately 4.5. Therefore, to discern statistically ≥10% loss in one voxel of the EP CSI images as they are presently taken, the EP CSI images must contain a SNR of ≥45:1 per voxel. Presently, our

method attains SNR values of ~5:1, from images that are spatially encoded at 3x3mm spatial resolution and smoothed to 6x6mm. Therefore, to be statistically confident ($p<0.05$) that 10% difference measurements in NAA per voxel are true, the images should be spatially encoded at 9x9x15mm at 1.5T given the present limitations. On the other hand, regions of interest>3ml. (15x15x15mm) must be taken to obtain the same 10% discrimination in absolute NAA with a statistical confidence of 0.05. It is therefore more prudent to encode at larger voxel sizes than taking regions of interest. This is because of the $(2)^{1/2}$ loss in SNR inherent with spatial smoothing.

From the data presented above, we can estimate SNR improvements through simple modifications of our existing pulse sequence. As demonstrated in Figure 5.16, an SNR improvement of ~40% can be expected by eliminating the STIR inversion. This can be accomplished by using other lipid suppression methods. We can take advantage of the fact that NAA possesses a long T2 (≥300ms), and perform multiple-echo acquisitions with this technique for improved SNR. For example, the implementation of a four echo Carr-Purcell-Meigboom-Gill (CPMG) type sequence (23), would be expected to provide an additional ~50% improvement in SNR for NAA. The residual SNR of each echo of a four echo experiment is demonstrated analytically in Figure 5.17. Increases in field strength would significantly improve the SNR. At 3.0T the combination of all of these improvements should allow us to produce high spatial resolution (6x6x10mm) NAA maps with SNR ~30:1 (per 360μl voxel) in imaging

times of approximately ten minutes. This will ensure that measurement differences of neuronal loss ≥15% may be made on a voxel per voxel basis with a statistical confidence of >95% ($p<0.05$).

EP CSI offers certain theoretical advantages that are not available in other conventional techniques. The superior spatial resolution (3mm in-plane) of EP CSI results from its rapid traversal through k-space. The ability to sample a complete 3-D CSI data matrix in as little as 30 seconds allows improvements in metabolite SNR to be translated directly into decreased CSI imaging time. This feature, in particular, distinguishes EP CSI from more conventional approaches. Moreover, in-plane motion can be theoretically corrected easily by reregistration of the images prior to Fourier transformation because each pulse acquires a complete two dimensional image. Finally, the chemical

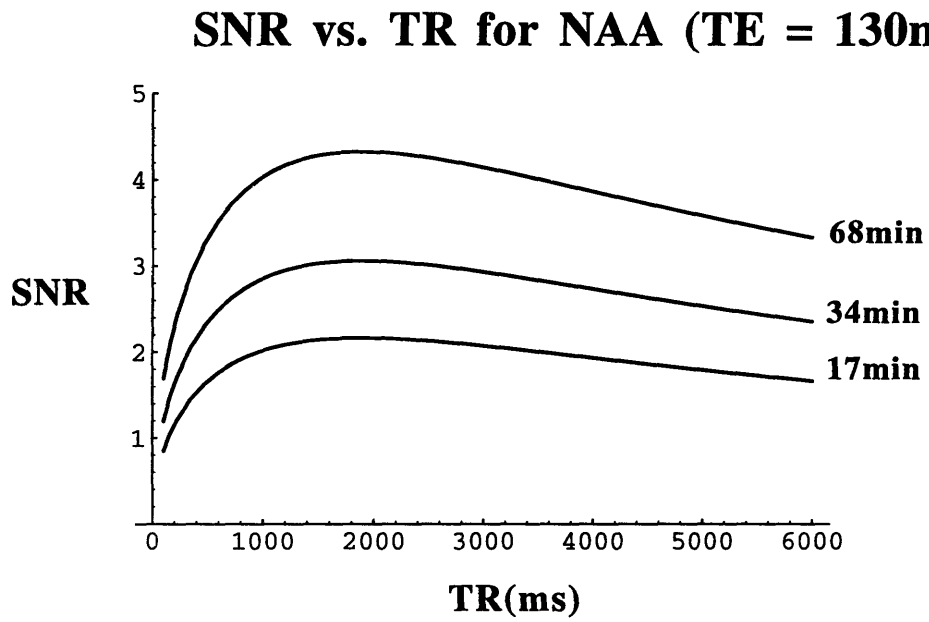

Figure 5.16 Analytical simulation of SNR vs. TR for EP CSI without inversion recovery and the parameters TE = 130ms.

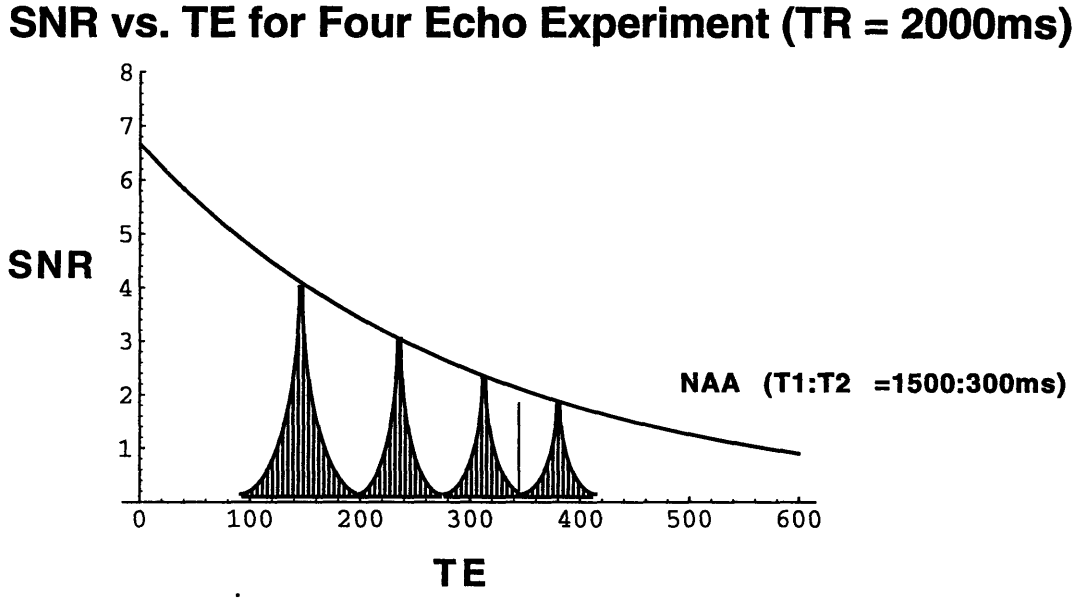

Figure 5.17 Analytical simulation of SNR vs. TE for EP CSI without inversion recovery and TE = 130ms illustrating the residual signal intensity of each echo in a four echo experiment.

shift artifacts seen in standard EPI can be circumvented by using this technique to directly correct for fat-water pixel shifts utilizing the discrete frequency representation of the data.

A robust echo planar chemical shift imaging method has been developed and applied in studies of normal human volunteers. This method has produced chemical shift images of NAA with spatial resolution that is superior to both existing MRI and PET techniques. Since multiple NEX acquisitions are required to produce useful metabolite SNR, volumetric encoding is capable without a sacrifice in temporal resolution. Alternative modes of lipid suppression, multiple echo acquisitions, and increases in field strength will decrease imaging times to 10 minutes or less and make it feasible to acquire high resolution, volumetric maps of neuronal function routinely, as part of a comprehensive functional imaging examination.

References

1. Menon D, Ainsworth J, Cox I, et al. Proton MR spectroscopy of the brain in AIDS dementia complex. J Comput Assist Tomogr 1992;16:538-42.

2. Miller B, Moats R, Shonk T, Ernst R, Woolley S, Ross B. In vivo abnormalities of cerebral myo-inositol and n-acetyl residues in Alzheimer disease. Radiology 1992;.

3. Miller B, Moats R, Shonk T, Ernst T, Woolley S, Ross B. Alzheimer disease: depiction of increased cerebral myo-inositol with proton MR spectroscopy. Radiology 1993;187(2):433-437.

4. Jarvik J, Lenkinski R, Grossman R, Gomori J, Schnall M, Frank I. Proton MR spectroscopy of HIV-infected patients: characterization of abnormalities with imaging and clinical correlation. Radiology 1993;186:739-744.

5. Kreis R, Ernst T, Ross B. Development of the human brain: in vivo quantification of metabolite and water content with proton magnetic resonance spectroscopy. Magn Reson Med 1993;30(4):424-437.

6. Chong W, Paley M, Wilkinson I, et al. Localised Cerebral Proton MR Spectroscopy in HIV infection and AIDS. AJNR 1994;15:21-25.

7. Rosen B, Wedeen V, Brady T. Selective saturation proton NMR imaging. J Comput Assist Tomogr 1984;8:813-818.

8. Bottomley P, Foster T, Leve W. In vivo nuclear magnetic resonance chemical shift imaging by selective irradiation. Proc Natl Acad Sci USA 1984;81:6856-6860.

9. Haase A, Frahm J, Hanicke W, Matthaei D. 1H-NMR chemical shift selective (CHESS) imaging. Phys Med Biol 1985;30:341-344.

10. Joseph P. A spin echo chemical shift MR imaging technique. J Comput Assist Tomogr 1985;9:651-658.

11. Brown T, Kincaid B, Ugurbil K. NMR chemical shift imaging in three dimensions. Proc Natl Acad Sci USA 1982;79:3523-3526.

12. Pykett I, Rosen B. Nuclear magnetic resonance: in-vivo proton chemical shift imaging. Radiology 1983;149:197-201.

13. Maudsley A, Hilal S, Perman W, Simon H. Spatially resolved high resolution spectroscopy by "four dimensional" NMR. J Magn Reson 1983;51:147-152.

14. Hall L, Rajanayagam V, Sukumar S. Chemical-shift-resolved tomography using four-dimensional FT imaging. J Magn Reson 1985;61:188-191.

15. Satoh K, Kose K, Inouye T, Yasuoka H. Chemical shift imaging by spin-echo modified Fourier method. J Appl Phys 1985;57:2174-2181.

16. Dixon W. Simple proton spectroscopic imaging. Radiology 1984;153:189-194.

17. Sepponen R, Sipponen J, Tanttu J. A method for chemical shift imaging: demonstration of bone marrow involvement with proton chemical shift imaging. J Comput Assist Tomogr 1984;8:585-587.

18. Manassan Y, Navon G. A constant gradient experiment for chemical-shift imaging. J Magn Reson 1985;61:363-370.

19. Martin J, Wade C. Chemical shift encoding in NMR images. J Magn Reson 1985;61:153-157.

20. Moonen C, Van Zijl P, Gillen J, Sobering G. Multi-slice proton spectroscopic imaging of the human brain. Eleventh Annual Meeting of the Society of Magnetic Resonance in Medicine. , 1992: 931.

21. Duyn J, Moonen C. Fast proton spectroscopic imaging of human brain using multiple spin-echoes. Magn. Reson. Med. 1993;30:409-414.

22. Mansfield P. Multi-planar image formation using NMR spin echos. J. Physics 1977;C10:L55-L58.

23. Hennig J, Nauerth A, Freidberg H. RARE imaging: a fast imaging method for clinical MR. Magn. Reson. Med 1986;3:823-833.

24. Guimaraes A, Hoppel B, Weisskoff R, Rosen B, Gonzalez R. Echo Planar Chemical Shift Imaging. Eleventh Annual Meeting of the Society of Magnetic Resonance in Medicine. Berlin: , 1992: 3925.

25. Guimaraes A, Baker J, Weisskoff R, Rosen B, Gonzalez R. Echo Planar Metabolic Imaging of Brain. Twelfth Annual Meeting of the Society of Magnetic Resonance in Medicine. New York: , 1993: .

26. Mansfield P. Spatial mapping of the chemical shift in NMR. Magnetic Resonance in Medicine 1984;1984:370-386.

27. Webb P, Spielman D, Macovski A. A fast spectroscopic imaging method using a blipped phase encode gradient. Magnetic Resonance in Medicine 1989;12:306-315.

28. Hoult D, Richards R. The signal-to-noise ratio of the nuclear magnetic resonance experiment. Journal of Magnetic Resonance 1976;24:71-85.

29. Hore P. Solvent suppression in fourier transform nuclear magnetic resonance. Journal of Magnetic Resonance 1983;55:283-300.

30. Bydder G, Young I. MR Imaging: Clinical Use of the Inversion Recovery Sequence. J. Comput Assist Tomogr 1984;9:659-675.

31. Eland B, Kennedy D, Moore J, Thulborn K, Rosen B. Quantitative in vivo lactate imaging. Seventh Annual Meeting of the Society of Magnetic Resonance in Medicine. San Francisco: , 1988: 818.

32. Spielman D, Brosnan T, Glover G, Macovski A. Inversion recovery methods for lipid suppression in 1H brain spectroscopic imaging. Tenth Annual Meeting of the Society of Magnetic Resonance in Medicine. San Francisco: , 1991: .

33. Oppenheim A, Schafer R. Discrete-Time Signal Processing. (Second ed.) Englewood cliffs, NJ: Prentice-Hall, Inc, 1989:880.

34. Reese T, Davis T, Weisskoff R. Automated shimming at 1.5T using echo-planar image frequency maps. Twelfth Annual Proceedings of the Society of Magnetic Resonance in Medicine. New York: 1993: .

35. Weisskoff R. Improved hard-pulse sequences for frequency-selective presaturation in magnetic resonance. Journal of Magnetic Resonance 1990;86:170-175.

36. Prammer M, Hasselgrove J, Shinnar M, Leigh J. A new approach to automatic shimming. J. Magn. Reon. 1988;77:40-52.

37. Schneider E, Glover G. Rapid in vivo proton shimming. Magn Reson Med 1991;18:335-347.

Chapter 6

Thesis Summary

The primary objectives of the investigations described in this thesis were to design and implement experiments to verify the utility of NAA as a NMR neuronal marker and to develop novel CSI techniques for determining neuronal content volumetrically by employing this marker in patients suffering from neurodegenerative diseases. Neurodegenerative diseases range from acute insults, such as stroke, hypoglycemia, trauma, and epilepsy, to chronic neurodegenerative states, such as Huntington's disease, acquired immunodeficiency syndrome (AIDS) dementia complex, amyotrophic lateral sclerosis, and Alzheimer's disease (1). The morbity and mortality associated with these clinical manifestations have served as the rationale for the development of quantitative methods with which to study neurodegenerative progression.

In recent work, excitatory amino acids, including glutamate and aspartate, have been implicated to some degree in the neuronally degenerative processes associated with many neurologic disorders. Where neurodegeneration is caused by glutamatergic neurotoxicity, a troubling conundrum exists in understanding the temporal dynamics that relate the neurotoxic action of glutamate to age-related neurodegenerative disorders. The dynamics of glutamate-gated ion channels occur in milliseconds, while neurodegenerative diseases usually occur gradually. Compelling evidence has been demonstrated in a number of neurodegenerative disorders that suggests a coupling between glutamatergic neurotoxicity and oxidative stress, with a host of ionic and/or enzymatic mediators linking them. However, current techniques for investigating and quantifying the neuronal loss observed after induced neurochemical insult in animal models and accompanying neurodegenerative disorders in patients remains *in vitro*.

Nuclear magnetic resonance (NMR) methods have the potential to provide a non-invasive, quantitative, temporal index of neuronal loss that can be applied to both *in vivo* models and studies of patients suffering from neurodegenerative diseases. To date, NMR spectroscopic methods have utilized the neuron-specific metabolite N-acetyl aspartate to study decreases in neuronal loss that occur subsequent to neurodegenerative diseases. Quantitative NMR spectroscopic studies of the putative, concordant decrease of NAA in neurodegenerative disease are expected to provide an *in vivo* measure

of neuronal loss, a hypothesis which has already been incorporated in several useful, recent patient studies of neurodegenerative disease (2-6). Although significant data concerning the validity of NAA as a neuronal marker in NMR spectroscopic studies have been obtained, the core of this work has remained *in vitro* (7), and the ability of NAA to provide quantitative measures of neuronal loss has not yet been validated. An initial specific aim of this research was therefore to verify the utility and assess the validity and sensitivity of NAA as an *in vivo* NMR spectroscopic marker for neuronal loss in animal models of neurodegeneration utilizing glutamatergic neurotoxins.

Validation of NAA as a NMR neuronal marker

The hypothesis that NAA may serve as a NMR spectroscopic measure of neuronal content was assessed by modifying extant CSI techniques for the purpose of quantifying NAA *in vivo* in a neurodegenerative rat model. These NMR spectroscopic measurements of NAA loss were then compared to *in vitro* NMR spectroscopic measures and enzymatic measures of GABAergic (glutamate decarboxylase [GAD]) and cholinergic (choline acetyl transferase [ChAT]) presynaptic activity.

In the first set of experiments, kainic acid, an analogue of glutamate that exhibits potent excitotoxic properties, was instilled in the right corpus striatum of five rats. The lesions so produced were examined to determine whether a significant difference existed between the amount of NAA found in the injured and contralateral brain hemispheres and to assess the correlation of any such differences

between enzymatic and *in vitro* NMR spectroscopic measurements. The existence of a correlation between these *in vivo* and *in vitro* measures of NAA with GAD and ChAT activites within the same animal would further support the hypothesis that NAA can provide a quantitative *in vivo* measure of neuronal loss. Figure 6.1 is a T2-weighted image and NAA chemical shift image of a rat that has a kainic acid lesion and demonstrates the capability of CSI to resolve this. Hemispheres lesioned with kainic acid were compared to contralateral hemispheres to obtain measures of the percent neuronal survival. The mean percentage of neuronal survival calculated with *in vivo* NAA measures (71±1.6%) correlated extremely well with the percentage of GAD survival measures (72.1±8.2%) ($p>0.87$) and *in vitro* spectroscopic measures (73.8±3.2%). Moreover, by using morphometric analysis of high resolution T2-weighted images as a measure of atrophy, statistically significant differences ($p<0.05$) were obtained between these measurements and those of putative neuronal loss obtained by using NAA as an *in vivo* neuronal marker. This data is summarized in Figure 6.2. The combination of these differences and the lack of difference observed between techniques utilizing NAA and traditional neuronal enzymatic markers for neuronal loss ($p>0.87$), suggest that NMR spectroscopic measurements are more sensitive to this loss than conventional MRI and unequivocally demonstrate that NAA is a valid neuronal marker with the capability of providing accurate assessments of neuronal loss *in vivo*.

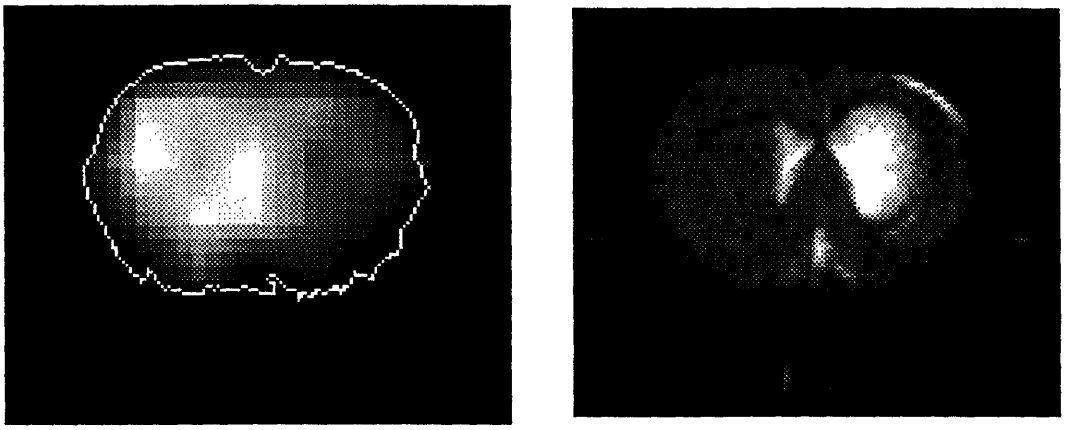

Figure 6.1 On the left is the NAA chemical shift image of a transverse slice through the brain of a rat lesioned in the right hemisphere with 2 μg of kainic acid. On the right is the standard T2 weighted MR image of the same animal obtained during the same imaging session.

Percentage of Contralateral Hemisphere	
N-acetyl aspartate (NAA) *in vivo*	**71.0 ± 1.6**
Glutamate decarboxylase (GAD)	**72.1 ± 8.2**
Choline acetyltransferase (ChAT)	**61.5 ± 5.8**
N-acetyl aspartate (NAA) *in vitro*	**73.8 ± 3.2**
Morphometric analysis	**79.9 ± 1.0**

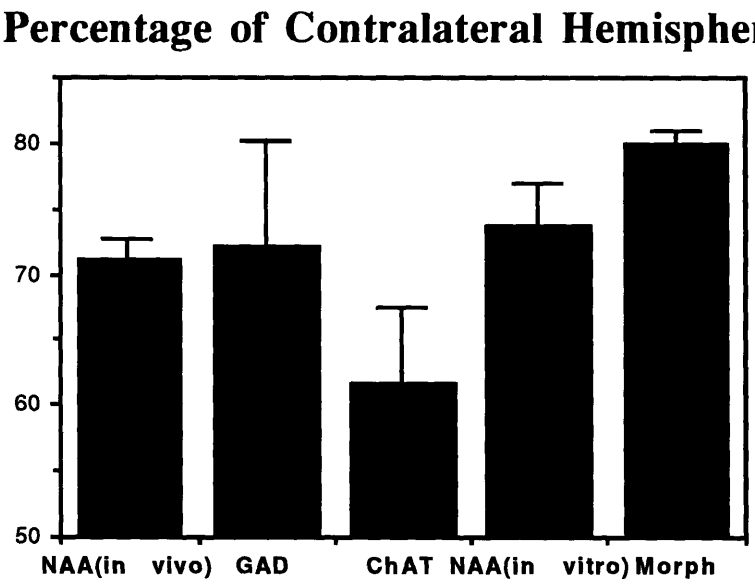

Figure 6.2 Depicts percent neuronal content of the hemisphere with the kainate lesion relative to the contralateral hemisphere. Measures include *in vivo* NAA, ChAT activity, GAD activity,*in vitro* NAA and morphometric analysis.

Assessing Sensitivity of NAA as a neuronal marker

To assess the sensitivity of NAA in determining subtle modulations of neuronal loss, methods developed on a kainic acid model were applied to an excitotoxic system able to demonstrate evidence of excitotoxicity (through NMDA) and of neuroprotection (through the action of antagonists, in particular MK-801). NMR spectroscopy was applied *in vivo* to eighteen Sprague-Dawley rats, six treated with MK-801 and NMDA, and twelve with NMDA alone, to determine the sensitivity of NMR spectroscopic measurements of NAA as a quantitative indicator of neuronal loss. The measurements obtained were then compared with those determined through GAD and ChAT activity.

Figure 6.3 shows a NAA chemical shift and T2-weighted image of a rat injured with NMDA, while Figure 6.4 shows a rat that has had MK-801 prior to NMDA instillation. These figures illustrate the capability of CSI to spatially resolve the neuronal loss or lack thereof in an animal model of neurodegeneration and neuroprotection. The mean percentage of neuronal survival calculated with *in vivo* NAA measures, 88.6 ± 1.9% (mean ± s.e.m.), correlates extremely well with the percentage of GAD survival measures, 87.9 ± 7.9% ($p > 0.93$, student's two tailed t-test), in rats injured by NMDA instillation. This finding supports the previous work on rats lesioned with kainic acid which demonstrated similar correlations of *in vivo* and *in vitro* NMR spectroscopic measures of NAA with GAD activity. Moreover, the subsequent finding of a statistical difference ($p<0.05$) between GAD and

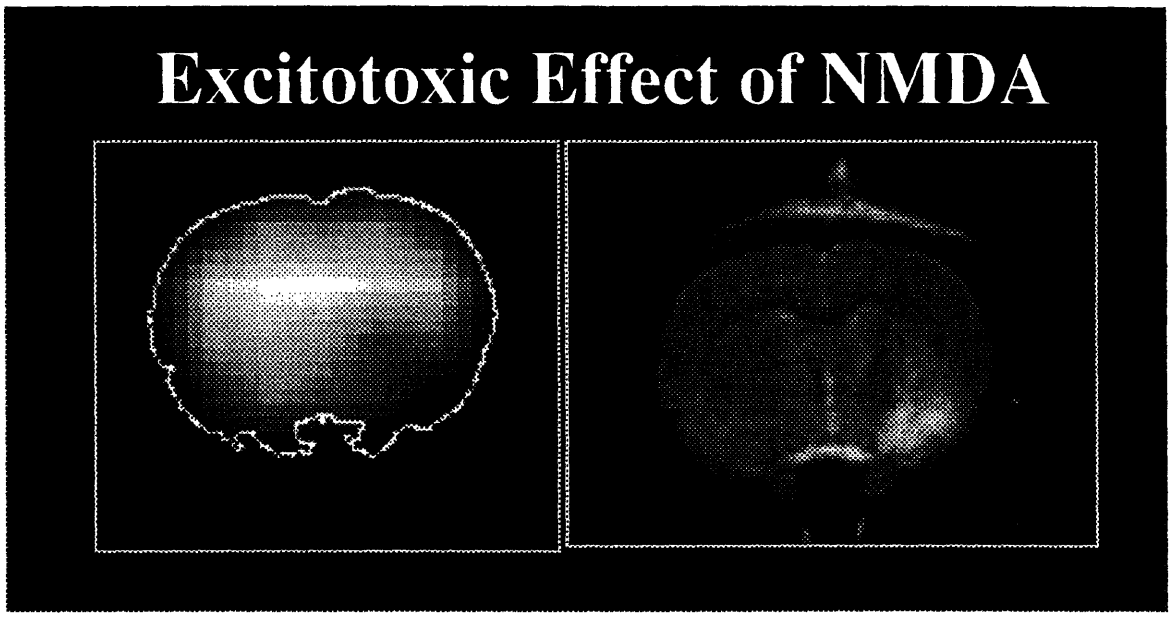

Figure 6.3 Chemical shift NAA image and corresponding T2-weighted image from rat lesioned with NMDA demonstrating the ability of CSI to spatially resolve the concordant neuronal damage associated with lesions visualized with T2-weighted images.

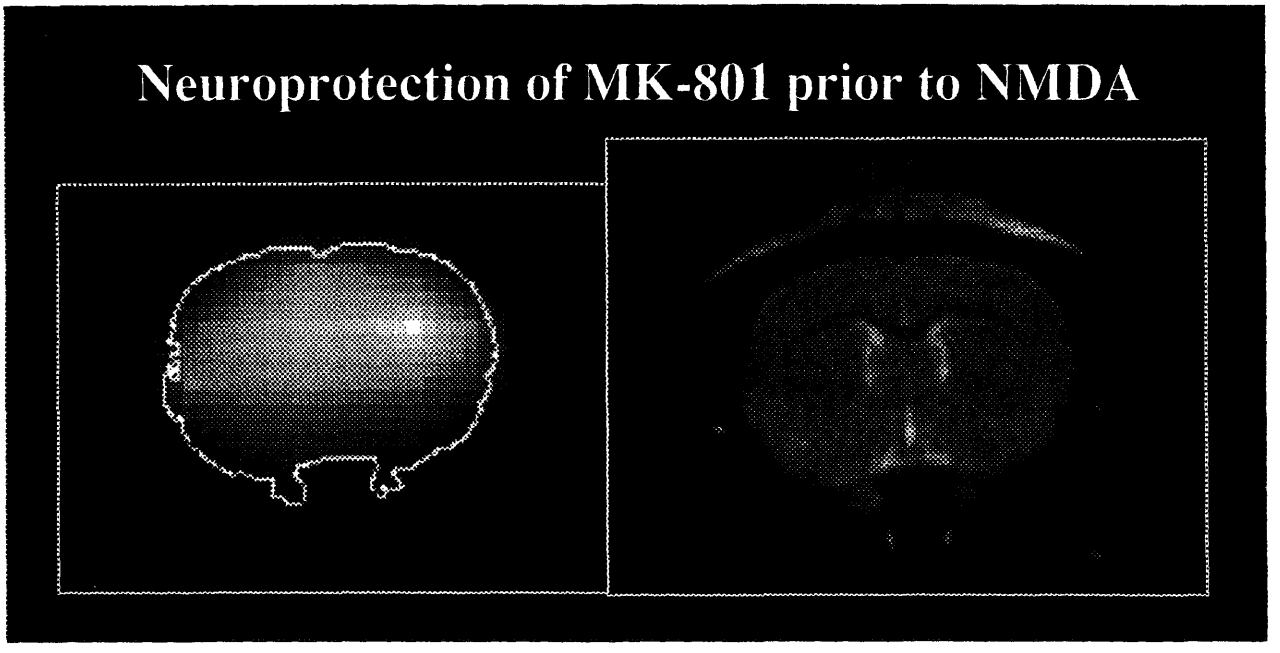

Figure 6.4 Chemical shift NAA image and corresponding T2-weighted image from a rat lesioned with NMDA pretreated with MK-801, demonstrating the capability of NMR imaging and spectroscopic measures to visualize the neuroprotection of MK-801.

ChAT activity measurements (corroborating previous results obtained from rats injured with kainic acid) is supported by the known distribution of cholinergic and GABAergic neurons. GABAergic neurons are diffusely spread throughout the rat brain, while the activities of cholinergic neurons are markedly higher in the striatum. The GAD activity measurements, therefore, should and did more closely represent the global neuronal loss occurring within the hemisphere. NAA measurements also demonstrated a statistically significant difference from ChAT measurements ($p < 0.05$). The combination of this difference with a lack of a difference between NAA measurements and GAD activity measurements further support the hypothesis that NAA measurements provide a valid index of neuronal loss.

MK-801 has been shown to protect neurons by its antagonistic effects on the NMDA receptor (8, 9). The results obtained from the NAA, GAD and ChAT activity measurements for the six rats treated with MK-801 prior to the instillation of NMDA suggested a corroboration of this finding, while the results of the morphometric analysis of residual brain parenchymal volume did not. This was determined by taking the difference of percent survival measurements for each of the three methods. Neuroprotection assessed through NAA, GAD and ChAT activity measurements demonstrated a 5%, 12% and 22% level of protection, respectively. This was determined by taking the difference of percent survival measurements for each of the three methods. Although these differences did not attain statistical

significance, the NAA and ChAT measurements suggested trends ($p<.15$ and $p<.10$, respectively). A discrepency also existed in mean percent survival results, calculated as a ratio of injured to contralateral hemisphere, for NAA *in vivo* (93 ± 1.2%) and GAD activity (101 ± 7.5%) measurements. Although this mean percent differs, it is well within the standard error of GAD activity and NAA measurements. This fact supports the use of NAA as a valid index for neuronal loss.

Statistically significant differences ($p<0.005$) were obtained between measurements using morphometric analysis and those of neuronal loss obtained by using NAA *in vivo* in rats with NMDA lesions. This finding corroborates previous results demonstrating statistically significant differences ($p<0.05$) between morphometric analysis and NAA measurements made *in vivo* in rats with kainic acid lesions. Morphometric analysis did not show a difference between animals treated with MK-801 and those untreated; there was 93% residual parenchyma in both cases. Although brain parenchymal volume measures suggest damage in both cases, the inability of morphometric analysis to indicate neuroprotection, while NAA, GAD and ChAT suggested statistical trends in assessing neuroprotection, suggests that imaging may be less sensitive to the process of neuronal damage than these other techniques. This hypothesis is supported by Figure 6.5, which demonstrates a lack of concordant damage in a rat exhibiting neuronal loss as demonstrated by NAA, GAD and ChAT.

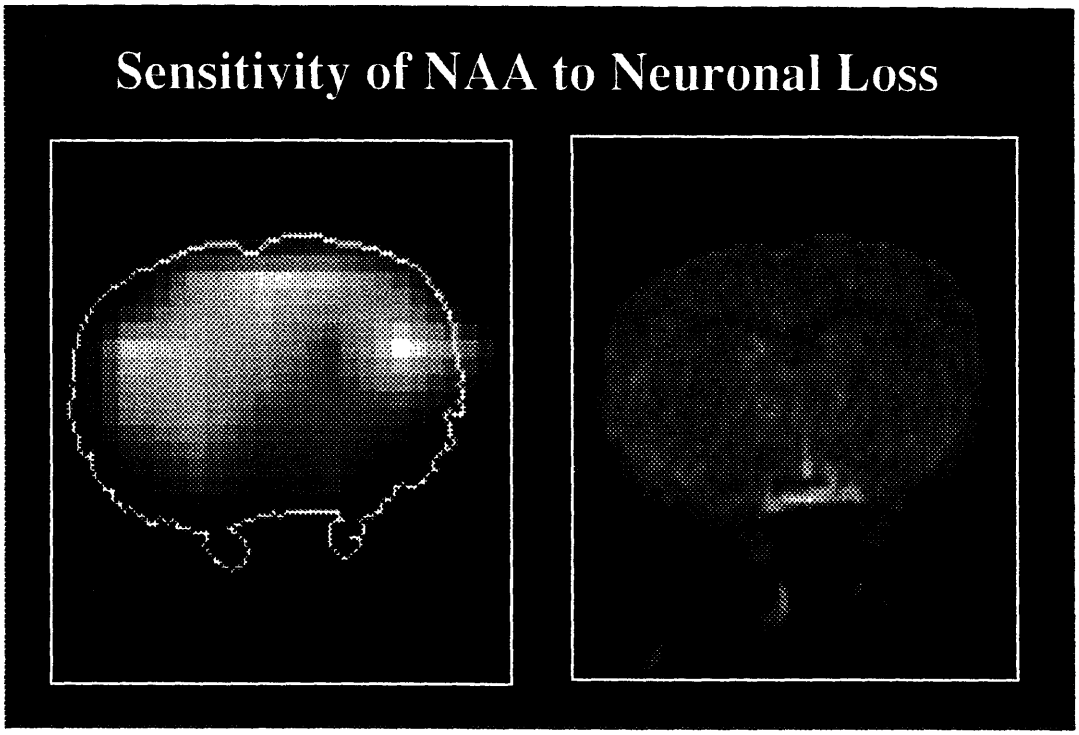

Figure 6.5 Chemical shift NAA image and T2-weighted water image of rat brain lesioned with NMDA. This demonstrates a lack of concordant discrepancy in signal within lesioned hemisphere.

These data, summarized in Figure 6.6, demonstrate the ability of chemical shift imaging to provide quantitative, spatially resolved images of neuronal loss in a striatal lesion rat model. By comparing the percentage of neuronal survival measured by *in vivo* NMR with established enzymatic measures of neuronal loss, these data indicate that NAA provides an excellent marker for neuronal content. They also support the claim that *in vivo* CSI provides an index of neuronal loss that may be more sensitive than water imaging. The implementation of quantitative proton spectroscopy or CSI techniques that utilize NAA as a neuronal marker can provide a quantitative, periodic assessment of the progression of neurodegeneration in patients suffering from neurodegenerative disease.

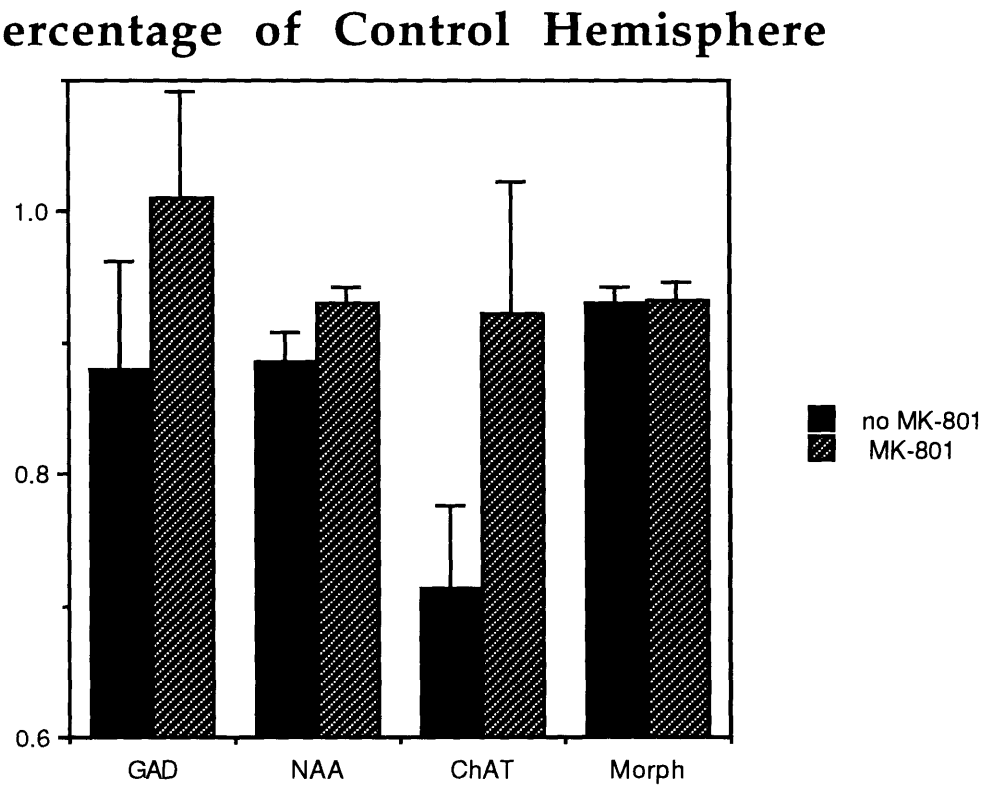

Figure 6.6 Summary of percent of contralateral hemisphere in the rat brain after direct kainic acid infusion assessed by *in vivo* NAA, ChAT activity, GAD activity, and morphometric analysis.

Volumetric Echo Planar Chemical Shift Imaging

The ability of NAA to provide a valid and sensitive marker for NMR spectroscopic measures of neuronal loss has provided a foundation for the development of novel approaches to map the neuronal distribution of the human brain volumetrically. These techniques may offer a non-invasive, quantitative means of furnishing information regarding the progression of neurodegeneration in patients. Extant techniques for investigating the metabolic processes that underlie neurodegenerative disease processes are limited to *in vitro* biochemical assays (*e.g.* ChAT and GAD) and localized, voxel NMR spectroscopy. Although localized NMR spectroscopy has been able to show concomitant decreases of NAA in neurodegenerative diseases, including Alzheimer's disease and the AIDS dementia complex (ADC) (2-4, 6, 10, 11) the measurements remain focal and thus limit the assessment of global patterns of degeneration that occur in these disease states. A technique able to produce a high resolution, volumetric map of neuronal content could furnish important information about focal patterns of degeneration as well as global patterns of neuronal loss distal to lesion sites. Such a technique would be of great utility in assessing neurodegenerative disease processes that exhibit combined focal and diffuse neuronal loss.

A principle goal of the last phase of this research involved the development of a novel approach to chemical shift imaging (CSI) that made use of echo planar imaging's (EPI) capability to traverse k-space rapidly for improvements in spatial resolution and volume coverage.

This new approach is here termed echo planar chemical shift imaging (EP CSI).

EP CSI offers a unique combination of echo planar imaging technology with phase encoded CSI. By sacrificing some spectral resolution, EP CSI can sample k-space rapidly and thereby produce metabolite maps with superior spatial resolution (<500μl voxel volumes). Unlike other conventional techniques, this approach lends itself easily to full 3D spatial encoding without a loss in temporal resolution because of the multiple NEX required to obtain useful SNR. To acquire echo planar chemical shift imaging (EP CSI) data, an echo planar (EPI) spin echo imaging sequence was modified to allow multiple, sequential τ offsets of the 180° refocusing pulse. In this technique, shown in Figure 6.7, each rf excitation is fully encoded in two spatial directions with an echo planar acquisition. The 180° pulse is moved temporally on sequential acquisitions to encode the chemical shift into the phase of the signal. A phase shift (ϕ) results, caused by signals that are spectrally off-resonance by the amount $f=\phi/2\tau$, where τ is the temporal offset of the 180° pulse. The spectral frequency resolution, Δf, is determined by the maximum relative displacement of the 180° pulse, $\Delta f=1/2\,|\tau max - \tau min| = 16Hz$, and the spectral width is thus $f=1/2\Delta\tau$.

Water and lipid suppression are provided to ameliorate the analog-to-digital converter difficulties that arise from the concentration of these two moieities being three to four orders of magnitude greater

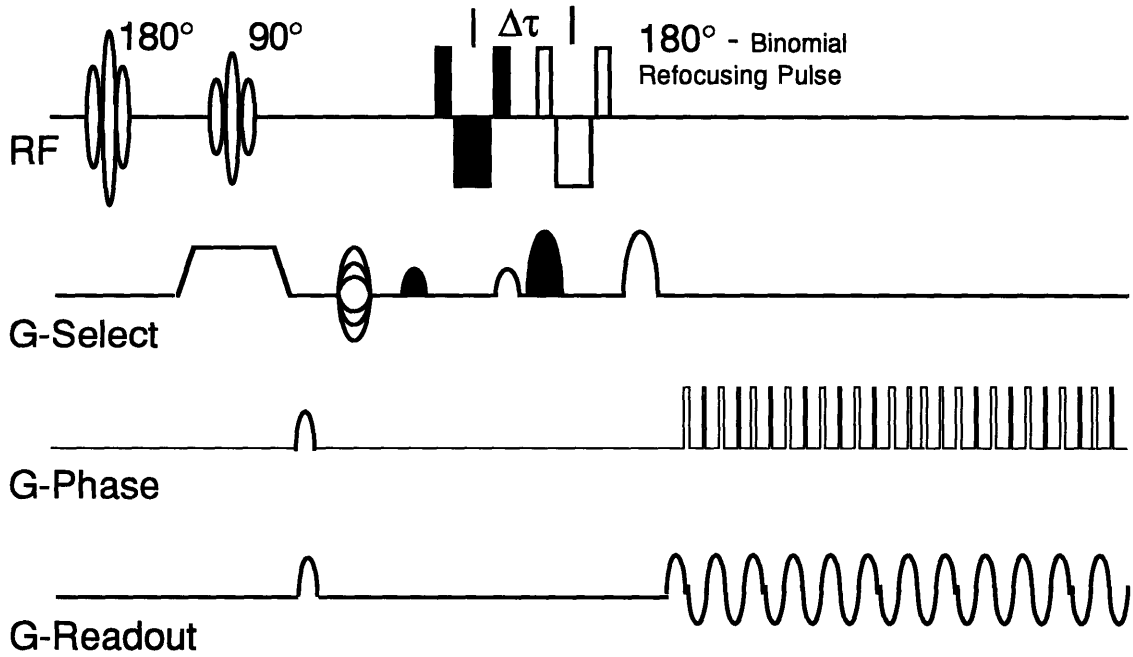

Figure 6.7 EP CSI sequence which combines phase encoding of the frequency dimension and z direction with echo planar imaging for encoding the x and y spatial dimensions.

than that of NAA. A frequency-selective, binomial 1$\underline{4}\underline{6}\underline{4}$1, 180° pulse is used to provide water suppression for EP CSI, while an inversion recovery scheme is used to null the extraneous lipid signal in EP CSI. B0 compensation is provided by an automated shimming algorithm to improve water and lipid suppression, in addition to improving SNR. The images are reconstructed by a Hamming windowed 3DFT through the x,y, and δ dimensions. The Hamming window is applied to τ offset data prior to Fourier transformation to minimize Gibbs ringing from limited chemical shift encoding steps and in the x and y dimensions to improve SNR (12). NAA maps are then generated by spectral averaging the spectral bins of 2.0±1/4ppm, because of imperfections in B_0 compensation.

EP CSI possesses the capability to encode the chemical shift into the phase of the signal by resolving the fat and water frequencies without spectral contamination in phantoms of fat and water. The Hamming window used prior to Fourier transformation (FT) was integral to the amelioration of spectral leakage and contamination from limited sampling in the spectral dimension. Further, EP CSI, when applied to phantoms of cerebral metabolites (*i.e.* NAA and choline) possessing *in vivo* concentrations, can produce chemical shift images, shown in Figure 6.8, with SNR comparable to estimated values of concentrations $\leq$ 10mM. This finding shows that the signal averaging required to produce adequate SNR was not burdened by any possible deleterious phase incoherences between acquisitions.

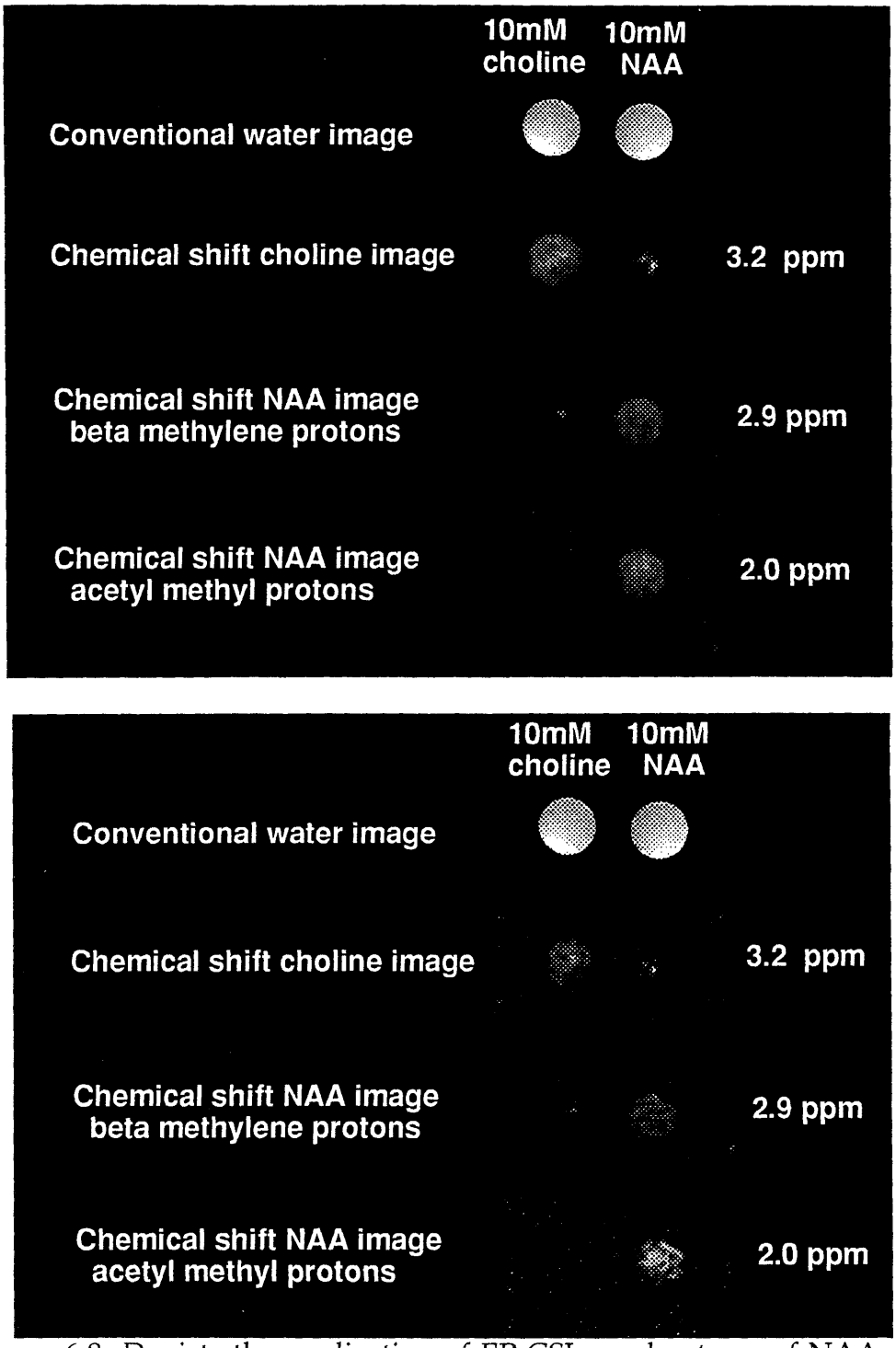

Figure 6.8 Depicts the application of EP CSI on phantoms of NAA and choline with 10mM concentrations. The top figure (a) shows images with NEX=128 and the bottom images (b) show images with NEX=64.

Moreover, the spectral resolution, although limited, is capable of discriminating the major resonances that appear at longer echo times ($\leq$ 100ms).

EP CSI was used to produce single slice and volumetric maps of the distribution of NAA in normal human volunteers. Acquisitions were obtained in 34 and 68 minutes at an SNR that agrees well with theoretical estimates. In the preliminary *in vivo* investigations a one slice variant of the 4D EP CSI technique produced a high spatial resolution map of the distribution of NAA within a young, normal volunteer. The result of this investigation demonstrated *in vivo* chemical shift images of the distribution of NAA possessing SNR measurements of approximately 5:1 for NEX=128 (68min) and 3:1 for NEX = 64 (34min). Anatomical features within the images demonstrated ventricular discrimination and spectral, but not spatial, overlap of extraneous lipid signal. This spectral contamination indicated some of the spectral resolution limitations of the technique, but reinforced its superior spatial resolution.

Volume encoding allowed maps of the distribution of NAA within 40-60mm of the normal human cerebrum to be produced. In the first volumetric series of experiments, a slab of ~10cm was excited with 5 z-encodes to produce an effective slice thickness of ~20mm. The results showed metabolite images from two slices of the 3D set. A NAA image with improved SNR, achieved through the increased effective slice thickness, was clearly resolved, while an image showing the distribution of choline/creatine, with SNR limited by the

suppression bandwidth of the binomial, was also clearly resolved. A fat image, with no signal contamination in the parenchyma, demonstrated that the spectral resolution, although limited, can clearly resolve major peaks in the proton spectrum that are visible at longer echo times.

The most recent efforts at volume encoding were performed with a 120cm slab excitation and encoded with a 2x oversampling scheme to produce eight, 15mm slices across the cerebrum. Four slices, encompassing the cerebrum and representing the NAA and residual water peaks, are shown in Figure 6.9. The SNR measured approximately 5:1 from the 8ml voxel, which agrees well with estimated results. The 2x oversampling, which increased the number of z-encodes to 16, ameliorated the spatial smearing along the z encoding direction.

The *in vivo* EP CSI data demonstrated the feasability of the technique, but reaffirmed a SNR limitation caused by encoding the spatial dimensions at 3x3mm. From the data above, SNR improvements can be estimated based on simple modifications of our existing pulse sequence. By simulating the SNR vs TR for the NAA resonance with and without inversion recovery, an SNR improvement of ~40% can be estimated concomitant to the elimination of the STIR inversion with the implementation of novel lipid suppression methods. Further, because NAA possesses a long T2 (≥300ms), the implementation of multiple-echo acquisitions with this technique is also feasible.

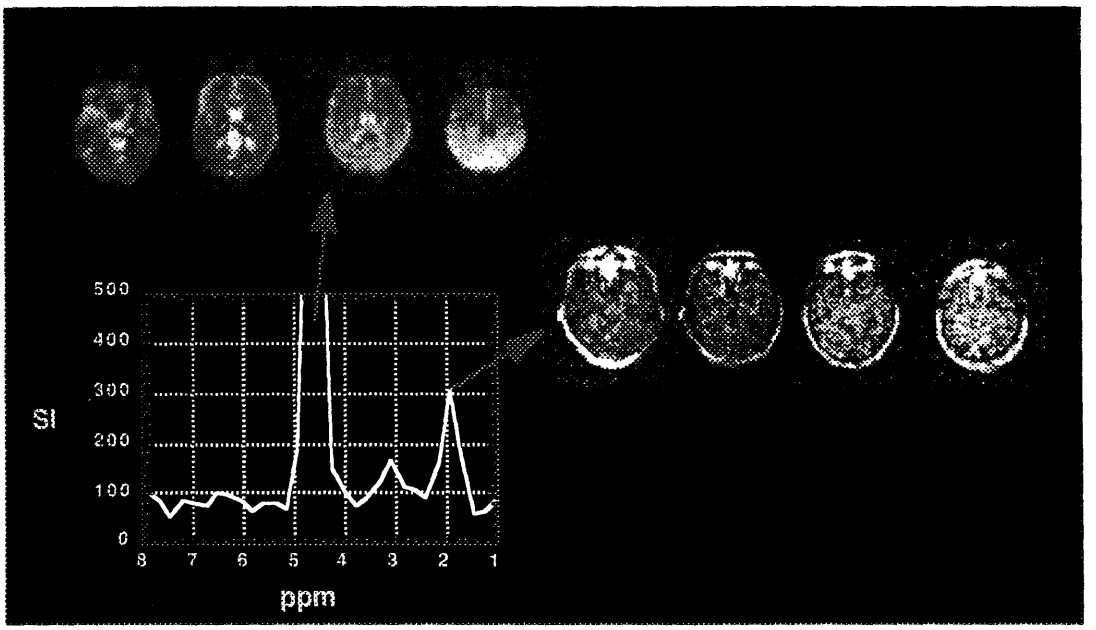

Figure 6.9 Residual water and NAA maps from four 15mm contiguous slices of a normal human volunteer.

For instance, the implementation of a four echo CPMG should provide an additional ~50% improvement in SNR for NAA. Increases in field strength will also increase the SNR. At 3.0T the combination of all of these improvements should allow us to produce high spatial resolution (6x6x10mm) NAA maps with SNR ~30:1 (per 360μl voxel) in imaging times of approximately ten minutes. This will ensure that measurement differences of neuronal loss ≥15% may be made on a voxel per voxel basis with a statistical confidence of >95% ($p<0.05$).

A robust echo planar chemical shift imaging method has been developed and applied in studies of normal human volunteers. This method has produced chemical shift images of NAA with spatial resolution that is superior to both existing MRI and PET techniques. Since multiple NEX acquisitions are required to produce useful metabolite SNR, volumetric encoding is possible without a sacrifice in temporal resolution. Full 3D spatial encoding has provided volumetric images in the same time, something previously unattained within clinically relevant time periods.

Conclusions

The data presented in this thesis demonstrate the ability of chemical shift imaging to provide quantitative, spatially resolved images of neuronal loss in a striatal lesion rat model. By comparing the percentage of neuronal survival measured by *in vivo* NMR with established enzymatic measures of neuronal loss, these data indicate that NAA provides an excellent marker for neuronal content. They also support the claim that *in vivo* CSI provides an index of neuronal

loss that may be more sensitive than classical biochemical assays. These facts have served as the foundation for the successful development of volumetric CSI techniques (EP CSI). EP CSI exploits the rapid traversal of k-space inherent in EPI to allow a slight decrease in spectral in order to improve spatial (and possibly temporal) resolution. Future optimizations will decrease imaging times to 10 minutes or less and make it feasible to acquire high resolution, volumetric maps of neuronal content routinely, as part of a comprehensive functional imaging examination. The implementation of EP CSI techniques that utilize NAA as a neuronal marker is therefore expected to provide means for a volumetric, periodic assessment of the progression of neurodegeneration. This technique has the capability to furnish information, presently unavailable, that could elucidate treatment strategies and improve the condition of patients suffering from neurodegenerative disease.

References

1. Lipton S, Rosenberg P. Excitatory amino acids as a final common pathway for neurologic disorders. New England Journal of Medicine 1994;330(9):613-622.

2. Miller B, Moats R, Shonk T, Ernst R, Woolley S, Ross B. In vivo abnormalities of cerebral myo-inositol and n-acetyl residues in Alzheimer disease. Radiology 1992;.

3. Kreis R, Ernst T, Ross B. Development of the human brain: in vivo quantification of metabolite and water content with proton magnetic resonance spectroscopy. Magn Reson Med 1993;30(4):424-437.

4. Jarvik J, Lenkinski R, Grossman R, Gomori J, Schnall M, Frank I. Proton MR spectroscopy of HIV-infected patients: characterization of abnormalities with imaging and clinical correlation. Radiology 1993;186:739-744.

5. Gideon P, Henriksen O. In vivo relaxation of N-acetyl-aspartate, creatine plus phosphocreatine, and choline containing compounds during the course of brain infarction: a proton MRS study. Magn Reson Imaging 1992;10:983-988.

6. Chong W, Paley M, Wilkinson I, et al. Localised Cerebral Proton MR Spectroscopy in HIV infection and AIDS. AJNR 1994;15:21-25.

7. Urenjak J, Williams SR, Gadian DG, Noble M. Proton nuclear magnetic resonance spectroscopy unambiguously identifies different neural cell types. J. Neurosci. 1993;13(3):981-989.

8. Foster A, Gill R, Kemp J, Woodruff G. Systemic administration of MK-801 prevents N-methyl-D-aspartate induced neuronal degeneration in rat brain. Neuroscience Letters 1987;76:307-311.

9. McDonald J, Silverstein F, Johnston M. Neurotoxicity of N-methyl-D-aspartate is markedly enhanced in the developing rat central nervous system. Brain Research 1988;459:200-203.

10. Menon D, Ainsworth J, Cox I, et al. Proton MR spectroscopy of the brain in AIDS dementia complex. J Comput Assist Tomogr 1992;16:538-42.

11. Miller B, Moats R, Shonk T, Ernst T, Woolley S, Ross B. Alzheimer disease: depiction of increased cerebral myo-inositol with proton MR spectroscopy. Radiology 1993;187(2):433-437.

12. Miyake M, Kakimoto Y. N-acetyl-L-aspartic acid, N-acetyl-α-aspartylglutamic acid and β-citryl-l-glutamic acid in different brain regions and spinal cords of rat and guinea pig. Journal of Neurochemistry 1981;37:1064-1067.